PHYSICS TEXTBOOK

Samuel S.M. Wong

WILEY-VCH

Introductory Nuclear Physics

Second Edition

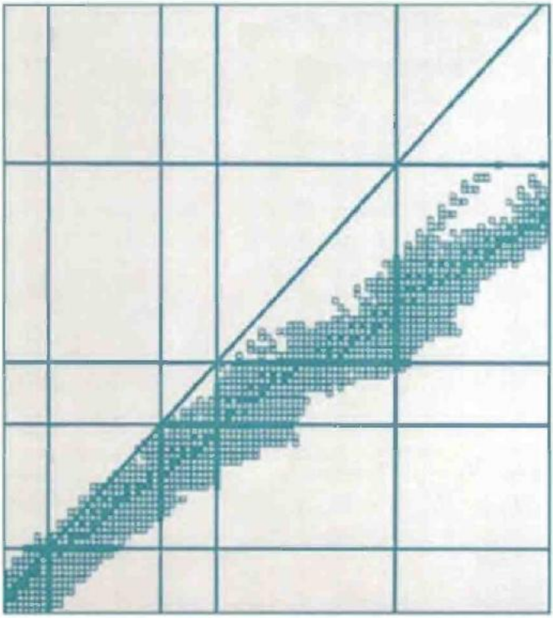

Introductory Nuclear Physics

SECOND EDITION

SAMUEL S.M. WONG

Introductory Nuclear Physics

Introductory Nuclear Physics

SECOND EDITION

SAMUEL S.M. WONG

All books published by Wiley-VCH are carefully produced.
Nevertheless, authors, editors, and publisher do not warrant the information contained in these books, including this book, to be free of errors. Readers are advised to keep in mind that statements, data, illustrations, procedural details or other items may inadvertently be inaccurate.

Library of Congress Card No.:
Applied for

British Library Cataloging-in-Publication Data:

[redacted]

Contents

Useful Constants viii

Preface to the Second Edition ix

Preface to the First Edition xi

1 Introduction 1

[redacted]

4 **Bulk Properties of Nuclei** **105**
- 4-1 Electron Scattering Form Factor 105
- 4-2 Charge Radius and Charge Density 109
- 4-3 Nucleon Form Factor 113
- 4-4 High-Energy Lepton Scattering 115
- 4-5 Matter Density and Charge Density 119
- 4-6 Nuclear Shape and Electromagnetic Moments 124
- 4-7 Magnetic Dipole Moment of Odd Nuclei 129

[redacted]

Problems 315

9 Nuclei under Extreme Conditions 317
9-1 Overview of Heavy-Ion Reactions 317
9-2 High-Spin States in Nuclei 326
9-3 Phase Transition and Quark-Gluon Plasma 340
Problems 353

10 Nuclear Astrophysics 355

[redacted]

Useful Constants

Quantity	Symbol	Value			
Universal constants:					
fine structure constant	$\alpha = \frac{e^2}{[4\pi\epsilon_0]\hbar c}$	1/137.0359895(61)			
Planck's constant	h	$6.6260755(40) \times 10^{-34}$	J-s	4.135669×10^{-21}	MeV-s
(reduced)	$\hbar = \frac{h}{2\pi}$	$1.05457266(63) \times 10^{-34}$	J-s	$6.5821220 \times 10^{-22}$	MeV-s
	$\hbar c$			197.327053(59)	MeV-fm
speed of light	c	299792458	m/s		
unit of charge	e	$1.60217733(49) \times 10^{-19}$	C	$4.8032068 \times 10^{-10}$	esu

Conversion of units:

[redacted]

Preface to the Second Edition

In the half dozen years or so since the first publication of *Introductory Nuclear Physics*, there have been several new developments and changes in the emphasis in the field. This, together with the enthusiastic feedback from colleagues and students, makes it imperative to publish a new edition.

For an active topic of research, a textbook cannot stay static. There are large areas that are basic and well established. These form the core of the first edition and they have stayed more or less the same. At the same time, the students should be made

[redacted]

Preface to the First Edition

Nuclear physics is a subject basic to the curriculum of modern physics. There are several good reasons for this to be so. First and foremost is the intrinsic interest of the subject itself: The study of atomic nuclei has historically given us many of the first insights into modern physics. Furthermore, the potential of future discoveries remains very promising. Second, nuclear physics is closely associated with several other active branches of research: particle physics, in terms of the large overlap of interests in fundamental interactions and symmetries, and condensed matter physics,

[redacted]

One result of adhering to this philosophy is that very few of the excellent papers of my colleagues have been cited. I have also had some difficulty in selecting standard textbooks for reference in subjects such as quantum mechanics, classical mechanics, electromagnetism, and statistical mechanics. Here, I have relied purely on my own biases without guidance from a general philosophy, as I have done with papers.

One decision that had to be made concerns the system of units used for equations involving electromagnetism. The Système International (SI) or meter-kilogram-second (mks) system would have been the more correct choice since essentially all students

[redacted]

Chapter 1

Introduction

Nuclear physics is the study of atomic nuclei. From deuteron to uranium, there are almost 1700 species that occur naturally on earth. In addition, large numbers of others are created in the laboratory and in the interior of stars. The main force responsible for

[redacted]

The existence of the nucleus as the small central part of an atom was first proposed by Rutherford in 1911. Later, in 1920, the radii of a few heavy nuclei were measured by Chadwick and were found to be of the order of 10^{-14} m, much smaller than the order of 10^{-10} m for atomic radii. The experiments involve scattering α-particles, obtained from radioactive elements, off such heavy elements as copper, silver, and gold, and the measured cross sections were found to be different from values expected of the Rutherford formula for Coulomb scattering off point charges.

The building blocks of nuclei are neutrons and protons, two aspects, or quantum

[redacted]

Table 1-1: Fundamental interactions.

Interaction	Field quantum	Range (m)	Relative strength	Typical cross section (m^2)	Typical time scale (s)
Strong	Gluon	10^{-15}	1	10^{-30}	10^{-23}
Weak	$W^{\pm}, Z^0$	10^{-18}	10^{-5}	10^{-44}	10^{-8}

[redacted]

electrons and positrons are found to have a continuous spectrum of energy up to some maximum value known as the end-point energy. This seemed, on the surface, to violate energy conservation, as there is a definite energy difference ΔE between the parent and daughter nuclei. If the final state of the decay involves only two particles, an electron and the much more massive daughter nucleus, the kinetic energy of the electron is essentially fixed and completely specified by conservation of energy and momentum in the reaction. A continuous distribution of electron kinetic energy violates this simple argument. The neutrino was proposed by Pauli in 1931 and used by Fermi in 1933 to

[redacted]

the structure of nuclei, and how nuclei interact with each other and with other subatomic particles. These three questions are, to a large extent, related with each other. Furthermore, their interests are not necessarily confined to nuclear physics alone.

Nuclear force. One may argue that, since nuclear force is only one aspect of the strong interaction between quarks, all we need to do is to understand quantum chromodynamics (QCD), the theory for strong interaction. This is, however, not the complete picture. Nuclear interaction operates at the low-energy extreme of QCD where the interaction

[redacted]

interaction is not well known. In fact, the interaction between nucleons bound in nuclei can be somewhat different and, perhaps, even simpler than nucleon-nucleon interaction in general. For this reason, an important part of nuclear structure studies involves effective potentials between bound nucleons. A second difficulty is the Hilbert space that must be used to obtain a solution. In principle, the dimension is infinite. To reduce the problem to a tractable one, sever truncations are necessary. It is possible to compensate in part the errors introduced in making the calculation within a restricted space by adjusting, or "renormalizing," the interaction. We shall see in Chapter 7 that

[redacted]

part of modern physics, nuclear phenomena can give and have given deep insight in understanding physics. The possibility is only limited by our imagination.

1-3 General Properties of Nuclei

The intense activity in the last century has resulted in a large body of knowledge on nuclear physics. We shall summarize in this section some of the general properties that are basic to the subject.

[redacted]

Table 1-2: Known elements.

Z	Symbol	Name	Z	Symbol	Name	Z	Symbol	Name
1	H	Hydrogen	39	Y	Yttrium	77	Ir	Iridium
2	He	Helium	40	Zr	Zirconium	78	Pt	Platinum
3	Li	Lithium	41	Nb	Niobium	79	Au	Gold
4	Be	Beryllium	42	Mo	Molybdenum	80	Hg	Mercury

[redacted]

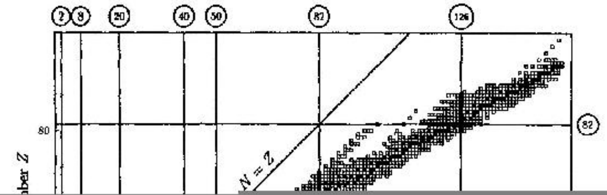

[redacted]

most stable nucleus for a given nucleon number. The binding energy, $E_B(Z,N)$, is the amount it takes to remove all Z protons and N neutrons from the nucleus and is given by the mass difference between the nucleus and the sum of those of the (free) nucleons that make up the nucleus,

$$E_B(Z,N) = \Big\{ZM_{\rm H} + NM_n - M(Z,N)\Big\}c^2 \tag{1-1}$$

Here $M(Z,N)$ is the mass of the neutral atom, $M_{\rm H}$ is the mass of a hydrogen atom, and M_n is the mass of a free neutron. It is conventional to use neutral atoms as the

[redacted]

viewed as if they are made of α-particles. The fact that their average binding energies per nucleon are larger than their neighbors implies that nucleons like to form α-particle clusters in nuclei. This can be seen quantitatively by looking at the values for nuclei, with $2 \leq A \leq 25$, shown in Table 1-3. For the $4n$ nuclei, the difference between the total binding energy and the sum of those for n α-particles is also given:

$$\Delta E \equiv E_B(N, Z) - nE_B(^4\text{He})$$

For $n = 2$, we find that the value is negative, showing that ^{8}Be is unstable with respect

[redacted]

Nuclear radius and nuclear density. In addition to binding energy, the general trend of nuclear size shows also a simple dependence on nucleon number. For the most part, the nuclear radius is given by

$$R = r_0 A^{1/3} \tag{1-2}$$

with $r_0 = 1.2$ fm (1 fm, or femtometer, equals 10^{-15} m). This means that the volume is linearly proportional to A and that the nucleons are not compressed in size in spite of the large forces acting between them. In fact, one has to go to some extreme situations,

[redacted]

hand, tries to keep the shape spherical so that the short-range attraction can be more effective. Since nuclear forces are stronger, light nuclei on the whole are spherical. However, once we go to intermediate values of A and beyond, the saturation property cuts off further increase in the binding energy per nucleon with increasing A due to nuclear force. As a result, slight deformation can actually increase the binding energy by decreasing the Coulomb contribution.

Density of excited states. The binding energy defined in Eq. (1-1) is only that for

[redacted]

be stored in an excited nucleus under certain conditions, only the smooth part of the spectrum is of primary importance.

A second consequence because of interaction is a shift in the energy scale by some amount Δ. Since excitation energy is measured from the ground state, any change to the latter produces a constant shift of the whole spectrum. In general, interaction tends to lower the ground state energy from the value given by a noninteracting model. Because of such a change in the energy scale, the level-density formula in many applications takes on the form

$$\rho_A(E) = \frac{1}{12a^{1/4}(E-\Delta)^{5/4}}\, e^{2\sqrt{a(E-\Delta)}} \qquad (1\text{-}5)$$

[redacted]

Table 1-4: De Broglie wavelengths of γ-ray, electron, and proton.

Energy (MeV)	Wavelength (fm)		
	Photon	Electron	Proton
0.1	1.2×10^4	3701	90
0.5	2.5×10^3	1421	40
1	1.2×10^3	872	29

[redacted]

Reaction types. The usual type of final state we wish to deal with in a reaction is two body. In other words, before the reaction, we have a projectile particle a incident on a target particle A. After the reaction, a particle b is scattered away, leaving behind a residual particle B. The reaction may be represented in either one of the following two ways:

$$A(a,b)B \qquad \text{or} \qquad a + A \longrightarrow b + B$$

For example, if a proton incidents on a ^{48}Ca target and a neutron is observed to emerge from the reaction, the residual nucleus is ^{48}Sc. The reaction may be written as

[redacted]

Coulomb scattering where the target nucleus is raised to an excited state by electromagnetic interaction, the inverse of electromagnetic decay. As another example, the reaction

$$\nu_e + {}^{37}\mathrm{Cl} \rightarrow e^- + {}^{37}\mathrm{Ar}$$

is the inverse of β^--decay of ^{37}Ar and is used in detecting solar neutrinos.

When two nuclei interact, it is possible to transfer one or more nucleons between them. For example, if a deuteron is incident on a ^{16}O target, the loosely bound neutron in the projectile may be attracted by the target nucleus and becomes attached to it as

[redacted]

reasonable choice, as it is essentially half the distance between the centers of the two ions when they are just in contact with each other.

1-4 Commonly Used Units and Constants

In atomic nuclei, we are dealing with length scales that are extremely small and time scales that are extremely short, compared with standard measures in daily life. Instead of the meter, a more suitable unit of length, as we have seen earlier, is the femtometer,

[redacted]

where multiplication by 931.49432 converts the quantity from atomic mass units to energy units in MeV. For a hydrogen atom, the mass excess is

$$\Delta(H) = (1.007276470 - 1) \times 931.49432 + 0.51110 = 7.2891 \text{ MeV}$$

and for a free neutron,

$$\Delta(n) = (1.008664904 - 1) \times 931.49432 = 8.0713 \text{ MeV}$$

Given the mass excess of a nucleus, the binding energy in Eq. (1-1) may be expressed

[redacted]

The formula is in cgs units if the factor in square brackets is ignored and in SI units when the factor is included. To avoid any dependence on the system of electromagnetic units adopted, we can make use of the fine structure constant

$$\alpha = \left[\frac{1}{4\pi\epsilon_0}\right]\frac{e^2}{\hbar c} \approx \frac{1}{137}$$

to replace factors in Eq. (1-6) that depend on the system adopted. Thus, we can write

[redacted]

Chapter 2

Nucleon Structure

All nuclei are made of neutrons and protons, the two lightest members of the baryon family. Nucleons are, however, not elementary particles. Partly for this reason, a sig-

[redacted]

the lightest members of the hadron family: nucleons, which make up all the nuclei, and pions, which constitute the main carriers of nuclear force. There are six different kinds, or *flavors*, of quarks: u (up), d (down), c (charm), s (strange), t (top), and b (beauty, or bottom). These six particles may be arranged according to their masses into three pairs, with one member of each pair having a charge $\frac{2}{3}e$ and the other $-\frac{1}{3}e$, as shown in Table 2-1.

Table 2-1: Quarks and leptons.

it is a few electron-volts or less, although much larger values for the upper limit have also been reported. For the other two types of neutrinos, only the upper limits of their masses are known: $m_{\nu_\mu} < 0.25$ MeV and $m_{\nu_\tau} < 70$ MeV.

In nuclear physics, leptons make their presence felt through nuclear β decay and other weak transitions. In general, only electrons and electron neutrinos are involved; occasionally muons may enter, such as in the case of a muonic atom where a muon replaces one of the electrons in the atom. Because of its larger mass and its more recent discovery, the τ-lepton has yet to enter nuclear physics studies.

To conserve charge, the charged lepton on the right-hand side must be a positron with $L = -1$. However, the reaction is not observed to take place. On the other hand, the reaction

$$\overline{\nu}_e + p \rightarrow e^+ + n \tag{2-4}$$

is observed. This establishes that ν_e and $\overline{\nu}_e$ are two different particles as well as confirms that the lepton number is conserved (see §5-6 for more detail). In fact, the conservation of leptons (i.e., that leptons cannot be created or annihilated except in pairs each one consisting of a lepton and an antilepton) is a fundamental conservation law, not too

[redacted]

concerned with this possibility and we shall take the baryon number to be conserved in all the reactions of interest to us.

There is no conservation law for the number of mesons. If there is enough energy available, they can decay into other mesons, baryon and antibaryon pairs, lepton and antilepton pairs, or γ-rays. The lightest members of the meson family are the pions with rest mass around 140 MeV/c^2. It is stable on the time scale of strong interaction, as it cannot decay into another hadron. However, through weak interactions, charged pions decay predominantly to muons,

[redacted]

antiquark, a new quark, heavier than u, d, and s, the three known at the time, must be postulated in order to understand this new meson. This is the c-, or charm, quark, having a mass far greater than those of u, d, and s. The existence of the c-quark was subsequently confirmed by other experiments, including the discovery of excited states of J/ψ. The birth of the c-quark prompted the search for even heavier quarks. In this way, the presence of a b-quark was found in the Υ-meson at 10 GeV. The mass of the t-quark has only been measured recently [97]. At the same time, one may also wonder whether there is a fourth generation of quarks beyond the three known ones.

[redacted]

Similarly, the quark wave function of a neutron is

$$|\,n\,\rangle = |\,udd\,\rangle \tag{2-10}$$

so that the total charge of a neutron in units of e is $\frac{2}{3} - \frac{1}{3} - \frac{1}{3} = 0$. Nuclear physics is usually not concerned with any of the heavier baryons, except perhaps for Δ- and Λ-particles. This comes because we are normally dealing with very low-energy phenomena, a few giga-electron-volts per nucleon or less. As a result, there is usually inadequate energy to excite nucleons to become heavier baryons.

[redacted]

If protons and neutrons are considered as identical particles, we need a new label to distinguish between them. For this purpose, the concept of *isospin* is introduced. Since there are only two possible states for a nucleon, the proton state and the neutron state, we can assign isospin $t = \frac{1}{2}$ to a nucleon, based on the analogy that a spin-$\frac{1}{2}$ system can have two different substates. The two nucleons are distinguished by $t_0 = \pm\frac{1}{2}$, the expectation value of the third component of isospin operator $\boldsymbol{t}$. It is a matter of convention whether we consider the $|t=\frac{1}{2}, t_0=+\frac{1}{2}\rangle$ state to be a proton state and the $|t=\frac{1}{2}, t_0=-\frac{1}{2}\rangle$ state to be a neutron state, or the other way around. Both conventions

[redacted]

where the subscript t, which we shall omit in the future unless required for reasons of clarity, identifies that the column matrices are for isospin. Using the convention that a proton has $t_0 = +\frac{1}{2}$ and a neutron has $t_0 = -\frac{1}{2}$, we can relate the *charge number* Q, electric charge in units of e, for a nucleon to t_0,

$$Q = t_0 + \tfrac{1}{2}$$

When we extend the concept of isospin to antiparticles and to systems of several nucleons, the relation between Q and t_0 depends also on A, the number of baryons in the

[redacted]

The definition used here for τ_+ and τ_- is the more general form used in textbooks and differs slightly from the convention for spherical tensor operators given in §A-2.

For nuclei made of several nucleons, isospin operators may be constructed out of the single-nucleon operators I, τ_1, τ_2, and τ_0 $(= \tau_3)$. For example,

$$T_0 = \frac{1}{2}\sum_{i=1}^{A} \tau_0(i) \tag{2-22}$$

where $\tau_0(i)$ acts only on the isospin wave function of the ith nucleon.

[redacted]

proton, the antiproton $\bar{p}$ must also have $t = \frac{1}{2}$. The third component of isospin for a proton is $t_0 = +\frac{1}{2}$ by the convention we have adopted. For an isoscalar system, the sum of the third components of isospin for all the quantities involved must also be zero. From this, we conclude that $t_0 = -\frac{1}{2}$ for an antiproton, the opposite in sign from that for its particle.

We see that the relation between charge number Q and the third component of isospin given by Eq. (2-17) applies to antiparticles as well. For an antiproton, the baryon number $A = -1$, and we obtain the correct result of $Q = -1$ from Eq. (2-17)

[redacted]

find that, under charge conjugation,

$$\begin{aligned} |p\rangle &\xrightarrow[C]{} (-1)^{1/2+1/2}|\bar{p}\rangle = -|\bar{p}\rangle \\ |n\rangle &\xrightarrow[C]{} (-1)^{1/2-1/2}|\bar{n}\rangle = +|\bar{n}\rangle \end{aligned} \tag{2-26}$$

The same considerations apply to other particles as well. For example, since a u-quark has isospin ranks $(t, t_0) = (\frac{1}{2}, +\frac{1}{2})$ and a d-quark has ranks $(\frac{1}{2}, -\frac{1}{2})$, the transformations to their antiparticles under charge conjugation are

[redacted]

$t_0 = +\frac{1}{2}$ to a u-quark and $t_0 = -\frac{1}{2}$ to a d-quark. The relation between charge number Q and t_0 is still given by Eq. (2-17), when we note that a quark has baryon number $A = \frac{1}{3}$, from the fact that it takes three quarks to make a baryon.

More formally, we can write the $\boldsymbol{\tau}_{\pm}$ operator for a nucleon as the sum of isospin-raising or isospin-lowering operators acting on each one of the three quarks,

$$\boldsymbol{\tau}_{\pm}(\text{nucleon}) \longrightarrow \sum_{i=1}^{3} \tau_{\pm}(q_i)$$

[redacted]

However, for the antiquarks,

$$\tau_+|\bar{u}\rangle = -|\bar{d}\rangle \tag{2-33}$$

The additional negative sign comes from the symmetry requirement under charge conjugation, as discussed in the previous section.

The normalization factor N in Eq. (2-31) may be determined using Eq. (2-21). Since $|\pi^-\rangle$ is a $t = 1$, $t_0 = -1$ system,

$$\tau_+|1,-1\rangle = \sqrt{2}\,|1,0\rangle$$

[redacted]

possible energy states. To obtain other mesons, we must either introduce excitations in the quark-antiquark system or invoke s- and other more massive quarks. We shall return to this point later.

Other quarks. Let us examine briefly the isospin of the other quarks, c, s, t, and b and their antiparticles. It is perhaps tempting to assume that each one of the remaining two pairs forms also an isospin doublet. This, however, is not the case. As can be seen from Table 2-2, these four quarks are isoscalar particles. Two questions are raised

[redacted]

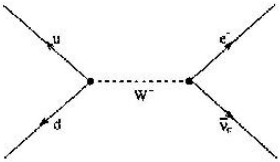
u
d
W⁻
e⁻
$\bar{\nu}_e$

[redacted]

B is used with $B = -1$ for a b-quark and $B = +1$ for a $\bar{b}$-quark (and $B = 0$ for all other quarks). Thus, for example, a hadron with n c-quarks has $C = n$ and a hadron with m b-quarks has $B = -m$. Whether a quark or an antiquark of a given flavor should take on the positive sign for the quantum number representing that flavor is somewhat arbitrary. The convention described here is the one commonly used and satisfies the relation between Q and t_0 given in Eq. (2-37).

Earlier, we saw the long lifetime of kaons as an example of strangeness conservation. Similarly, long lifetimes of the order 10^{-13} s are observed for the analogous situation of

[redacted]

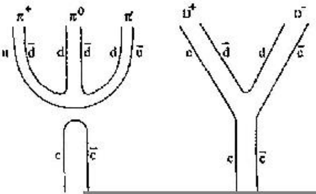
π^+
π^0
π^-
u
$\bar{d}$
d
$\bar{d}$
d
$\bar{u}$
c
$\bar{c}$
D^+
D^-
c
$\bar{d}$
d
$\bar{c}$
c
$\bar{c}$

[redacted]

all hadrons must be colorless objects: The color degree of freedom of the constituents inside a hadron must somehow neutralize each other. For mesons, this is easy to achieve, as an antiquark must have the opposite color for a quark. For baryons made of three identical quarks, such as Δ^{++}, the different colors cancel by being antisymmetric with respect to each other.

In nuclear physics, we are usually not involved explicitly with the color degree of freedom. However, the Δ-particle is important. It was discovered by Fermi and Anderson in 1949 as a resonance in π^{+}-scattering off protons at pion kinetic energy

[redacted]

Mesons and pseudoscalar mesons. Let us start with the simpler case of mesons. Although mesons can be made with any number of quark-antiquark ($q\bar{q}$)-pairs, most of the observed ones may be understood by considering only a single ($q\bar{q}$)-pair. A simple quark model of mesons, therefore, involves a quark and an antiquark moving with respect to each other with orbital angular momentum $\boldsymbol{\ell}$. The total angular momentum, or spin, of the system is $\boldsymbol{J} = \boldsymbol{\ell} + \boldsymbol{S}$, where $\boldsymbol{S} = \boldsymbol{s}_q + \boldsymbol{s}_{\bar{q}}$ is the sum of the intrinsic spins of the quark and the antiquark. Since $s_q = s_{\bar{q}} = \frac{1}{2}$, the possible value of S for a $q\bar{q}$-system is either 0 (singlet state) or 1 (triplet state). As for the spatial part of the wave function,

[redacted]

as an irreducible representation of the SU_3 group, special unitary group of dimension 3. Mathematically the transformation is very similar to, for instance, a rotation of the spatial coordinate axes by some Euler angles. The various components of a spherical tensor of a given rank, e.g., spherical harmonics $Y_{\ell m}(\theta, \phi)$, differing only in the values of m, are modified because of the rotation. However, the relation between different components of $Y_{\ell m}(\theta, \phi)$ is such that, in the rotated system, the new $Y_{\ell m}(\theta, \phi)$ can always be expressed in terms of the spherical harmonics of the same order ℓ in the old system, as shown in §A-2. In group theoretical language, the $2\ell + 1$ spherical harmonics

[redacted]

Cabibbo angle,

$$\eta = \eta_8 \cos\theta + \eta_0 \sin\theta \qquad \eta' = -\eta_8 \sin\theta + \eta_0 \cos\theta$$

For the pseudoscalar mesons, the value is $\theta \simeq 10°$.

Vector mesons. Instead of $S = 0$, the total intrinsic spin of the quark-antiquark pair in a meson may be coupled to $S = 1$. For $\ell = 0$, the spin of the pions produced is now $J = 1$. The parity, however, remains negative. Similar to the pseudoscalar mesons,

[redacted]

8×10^{-23} s ($\Gamma = 8.5$ MeV). As we shall see later, both ρ- and ω-mesons play special roles in the interaction between nucleons.

Baryons. With three flavors, we can construct a total of $3 \times 3 \times 3 = 27$ baryons for a given set of (ℓ, S)-values. They can be classified according to their SU_3(flavor) symmetries into four groups consisting of 10, 8, 8, and 1 members. The group of 10 baryons (decuplet) is completely symmetric under a transformation in flavor, and the group of one baryon (singlet) is completely antisymmetric. The other two groups,

[redacted]

other three members of the isospin quartet, Δ^+, Δ^0, and Δ^-, may be obtained using the isospin-lowering operator τ_- on $|\Delta^{++}\rangle$, in the same way as we have done earlier in obtaining the pion wave functions. With each application of the τ_--operator, one of the u-quarks is changed into a d-quark. This gives us the correct isospin structure of all four members of the Δ. However, unlike the pion case where two nonidentical fermions are involved, a quark and an antiquark, we are dealing here with three identical particles. In addition to isospin coupling, we must also ensure proper symmetry between the quarks under a permutation between any two of them.

[redacted]

To simplify the notation, we shall write the same equation in a shorthand form,

$$|\Delta^{+}\rangle = \frac{1}{\sqrt{3}}\Big\{|duu\rangle + |udu\rangle + |uud\rangle\Big\}$$

where it is implied that the first symbol in each term is for quark number 1, the second one for number 2, and the third one for number 3. In cases where we wish only to indicate the quark content of a hadron without displaying the permutation symmetry explicitly, the notation can be shortened further to (uud), for example, as done in Fig. 2-6.

For $S = -3$ there is only one possibility,

$$|\Omega^-\rangle = |\,sss\,\rangle$$

Although it is an isoscalar particle, and consequently $t_0 = 0$, it is a charged particle. This can be seen from Eq. (2-37). Since the baryon number is $A = 1$ and strangeness $S = -3$, the charge number of the particle is -1. The same result can also be obtained from the fact that each s-quark carries a charge $-\frac{1}{3}e$. The particle therefore carries one unit of negative charge and, hence, the negative sign in the superscript.

[redacted]

the symmetry in flavor of the quark wave function, it does not constitute an independent degree of freedom in fixing the wave function.

So far we have not explicitly put in the intrinsic spin part of the wave function. An example will be given later for the nucleon wave function. Here, we shall simply state the result that $J^\pi = \frac{1}{2}^+$ for the Λ_1-baryon.

Since the SU_3(flavor) symmetry is not an exact one, the observed strangeness $S = -1$, isoscalar, $J^\pi = \frac{1}{2}^+$ particle Λ is a mixture of $|\Lambda_1\rangle$ and $|\Lambda_8\rangle$, the latter being a member of the $J^\pi = \frac{1}{2}^+$ baryon octet. This is similar to the admixture in pseudoscalar

[redacted]

choice is complicated by the fact that the final system is a mixture of total spin $\frac{3}{2}$ and $\frac{1}{2}$. To project out the desired $S = \frac{1}{2}$ part, a linear combination must be taken of the two possibilities, $\{(q_1q_2)_{1,1}(q_3)_{1/2,-1/2}\}$ and $\{(q_1q_2)_{1,0}(q_3)_{1/2,+1/2}\}$, where the first of the two subscripts indicates S and the second the value of its third component.

The combined symmetry of the spin and flavor parts of the wave function may be determined after assigning a flavor to each one of the quarks involved, subject to the condition that, for a proton, each term must consist of two u-quarks and one d-quark. Let us start by giving the first two quarks different flavors. Equation (2-44) becomes

[redacted]

obtaining the wave functions, such as charge number, spin, isospin, and strangeness, the magnetic dipole moment is one we can use to test our model. We shall only deal with members of the baryon octet given in Fig. 2-7, as more are known about them.

The magnetic dipole moment of a baryon comes from two sources, the intrinsic dipole moments of the constituent quarks and the orbital motion of the quarks. For the baryon octet of interest here, all the members have $J^\pi = \frac{1}{2}^+$. In the simple model adopted in the previous section for our discussion, the three quarks are symmetric in the spatial parts of their wave functions, with relative motion $\ell = 0$. As a result,

[redacted]

given by the number of quarks of each flavor in each one of the two possible spin orientations. For a proton, we can count the numbers of $u\uparrow$, $u\downarrow$, $d\uparrow$, and $d\downarrow$ explicitly using the wave function given earlier in Eq. (2-46). The results are simply the sums of the squares of the coefficients in the wave function for each one of the four possible combinations of flavor and spin orientations: $\frac{5}{3}$ for the number of u-quarks with spin up, $\frac{1}{3}$ for the number of u-quarks with spin down, $\frac{1}{3}$ for the number of d-quarks with spin up, and $\frac{2}{3}$ for the number of d-quarks with spin down. The net contribution from u-quarks to the proton magnetic dipole moment is then $\frac{5}{3} - \frac{1}{3} = \frac{4}{3}$, and that from

[redacted]

must have very similar quark wave functions, except for the replacement of d with s. Hence, the magnetic dipole moment of the Σ^+-baryon is given by

$$\mu_{\Sigma^+} = \tfrac{4}{3}\mu_u - \tfrac{1}{3}\mu_s$$

Similarly, the quark content of Σ^- is (dds). Comparing it with a neutron, we find that the expression for the magnetic dipole moment of a Σ^--baryon is the same except that, in the place of u-quarks in a neutron, we have the contributions from s-quarks. This gives us the result

[redacted]

The spins of these two quarks cannot be both up, as such an arrangement will be antisymmetric under the simultaneous exchange of spin and flavor. The only possibility is therefore

$$\begin{aligned}|(t,t_0)=(0,0);(s,m_s)=(0,0)\rangle &= \tfrac{1}{2}\Big\{\big(|u(1)\uparrow d(2)\downarrow\rangle - |d(1)\uparrow u(2)\downarrow\rangle\big)\\ &\quad +\big(|d(1)\downarrow u(2)\uparrow\rangle - |u(1)\downarrow d(2)\uparrow\rangle\big)\Big\}\end{aligned}$$

Note that the total spin of the two quarks is also zero as a result of the symmetry

[redacted]

negative. As a result the value of $\mu_{\Sigma^0\to\Lambda}$ may be used as a piece of information for our calculation.

Table 2-4 summarizes the contribution from each one of the three quarks to the magnetic dipole moments for the members of the baryon octet together with $\mu_{\Sigma^0\to\Lambda}$. The observed values are listed in the last column in units of nuclear magnetons, $\mu_N = e\hbar/(2M_pc)$ in cgs units or $e\hbar/(2M_p)$ in SI units. The values of μ_u, μ_d, and μ_s are deduced by fitting them to the eight measured dipole moments. Since the accuracies that can be achieved for the measured values of the various baryons differ by a large

[redacted]

few mega-electron-volts and that the value of the *s*-quark is larger than those of the *u*- and *d*-quarks by 100 to 200 MeV. Further support for *s*-quarks being more massive can be found in the mass differences between members of the baryon decuplet, between members of the pseudoscalar mesons, and between members of the vector mesons. As for the charm and beauty quarks, we have already seen evidence from the masses of J/ψ- and Υ-mesons in §2-6 that they are even more massive. From a comparison of the masses of hadrons made of different quarks, the masses of the various quarks can be deduced. The generally accepted values were given earlier in Table 2-2.

seen an example of this from the mass differences between the pseudoscalar mesons (sum of quark intrinsic spins $S = 0$) and the vector mesons ($S = 1$). For example, the quark contents of the π- and ρ-mesons are the same, but their masses are quite different, with $m_\pi c^2 \approx 140$ MeV and $m_\rho c^2 \approx 767$ MeV, respectively. The large difference must be attributed mainly to the dependence of the interaction on the total intrinsic spin of the quark-antiquark pair. This is quite different from the usual situation in quantum systems where the interesting physics often arises from small parts of the complete interaction. For example, in atomic physics the main contribution to

[redacted]

in terms of these operators, the expectation values of τ^2 for the isospin wave function of a proton and a neutron.

2-3. Antiprotons are created when a beam of high-energy protons strikes a hydrogen target. In the laboratory system what is the minimum proton kinetic energy required for the reaction to take place?

2-4. Construct the quark wave function of π^- by applying an isospin-lowering operator to the wave function of π^0 given in Eq. (2-34). Use the same technique to construct

[redacted]

Chapter 3

Nuclear Force and Two-Nucleon Systems

difference between M_d and the sum of those for a neutron, M_n, and a hydrogen atom, M_H:

$$\begin{array}{rrl} M_nc^2= & 939.5656 & \text{MeV} \\ + M_{\rm H}c^2= & 938.7833 & \text{MeV} \\ \hline = & 1878.3489 & \text{MeV} \\ - M_dc^2= & 1876.1244 & \text{MeV} \\ \hline E_B= & 2.2245 & \text{MeV} \end{array} \tag{3-1}$$

[redacted]

the intrinsic wave function of the neutron, and the orbital wave function for the relative motion between the proton and the neutron. Since a proton and a neutron are just two different states of a nucleon, their intrinsic wave functions have the same parity. As a result, the product of their intrinsic wave functions has positive parity, regardless of the parity of the nucleon. This leaves the parity of the deuteron to be determined solely by the relative motion between the two nucleons.

For states with a definite orbital angular momentum $\boldsymbol{L}$, the angular dependence in the wave function is given by spherical harmonics $Y_{LM}(\theta\phi)$. Under an inversion of the

[redacted]

the spherical harmonics. The transformation is, then, mathematically the same as that under a parity change. For $L = 0, 2$, the spatial wave function is symmetric under permutation as a result.

It is also easy to see that the intrinsic spin part of the deuteron wave function is even in the $S = 1$ state. Consider the state with $M_S = 1$ among the triplet of possible states of $M_S = 0, \pm1$ for $S = 1$. The intrinsic spin wave function may be written as the product of those for the two nucleons,

$$|S{=}1, M_S{=}1\rangle = |s{=}\tfrac{1}{2}, m_s{=}\tfrac{1}{2}\rangle\, |s{=}\tfrac{1}{2}, m_s{=}\tfrac{1}{2}\rangle \qquad (3\text{-}3)$$

[redacted]

to have a $T = 1$ bound state for two nucleons in general. The neutron-proton system can be either an isoscalar ($T = 0$) or an isovector ($T = 1$) state. Since there does not seem to be a bound state for the $T = 1$ system, the deuteron ground state must have isospin $T = 0$. We may also conclude from the same argument that there is an isospin dependence in the force between a pair of nucleons that is attractive only in the $T = 0$ state.

In summary, we have established using symmetry considerations that the deuteron ground state has $S = 1$ and $T = 0$. There remain, however, two possibilities, $L = 0$ and [redacted] electromagnetic units used. Similarly, contributions from the intrinsic spin of each nucleon may be expressed as

$$\mu_i^{(\mathrm{spin})} = g_s(i)\, \boldsymbol{s}_i \tag{3-7}$$

Since $s = \frac{1}{2}$, the gyromagnetic ratio for a free nucleon is

$$g_s(i) = \begin{cases} g_p = 2\mu_p = 5.585695\mu_N & \text{for a proton} \\ g_n = 2\mu_n = -3.826085\mu_N & \text{for a neutron} \end{cases} \tag{3-8}$$

[redacted]

(2) There are contributions from charged (virtual) mesons exchanged between the proton and the neutron, and these have not been included in Eq. (3-10).

(3) There is a small admixture of the $^3D_1$-state in the deuteron ground state.

Item 1 is extremely unlikely, as the deuteron is only a loosely bound system. The binding energy of 2.22 MeV can hardly be expected to affect the motion of quarks inside a nucleon that are bound by energies of the order of hundreds of mega-electron-volts. The effect of *mesonic current* suggested in item 2 is possible. In fact, it has been

[redacted]

On substituting the simplified form of $\boldsymbol{\mu}_d$ of Eq. (3-13) into (3-12), we obtain the result

$$\langle J, M|\mu_0|J, M\rangle = \frac{M}{J(J+1)}\langle J, M|\tfrac{1}{2}\{(g_p + g_n)(\boldsymbol{S}\cdot\boldsymbol{J}) + (\boldsymbol{L}\cdot\boldsymbol{J})\}|J, M\rangle$$

The scalar products on the right-hand side may be written in terms of $\boldsymbol{J}^2$, $\boldsymbol{L}^2$ and $\boldsymbol{S}^2$,

$$\boldsymbol{S}\cdot\boldsymbol{J} = \boldsymbol{S}\cdot(\boldsymbol{L}+\boldsymbol{S}) = \boldsymbol{S}^2 + \tfrac{1}{2}(\boldsymbol{J}^2 - \boldsymbol{L}^2 - \boldsymbol{S}^2) = \tfrac{1}{2}(\boldsymbol{J}^2 - \boldsymbol{L}^2 + \boldsymbol{S}^2)$$

[redacted]

3-3 Deuteron Electric Quadrupole Moment

In electrostatics, the potential due to an arbitrary charge distribution at points far away from the source may be characterized by the moments of a multipole expansion of the source. For a microscopic object like a nucleus, it is not possible to observe the distribution directly, and the measured multipole moments give us some information on the source. For the charge distribution in a nucleus, the lowest nonvanishing multipole moment is the quadrupole, as the expectation value of the electric dipole operator, as well as all the other odd multipoles, vanishes due to the fact that the operators change

[redacted]

the expectation value of $\boldsymbol{Q}_0$ vanishes in the $^3S_1$-state. The existence of a nonvanishing quadrupole moment is therefore a direct evidence of the presence of the $^3D_1$-component in the deuteron ground state.

Expectation value of the quadrupole operator. Let us work out the connection between the spatial part of the wave function and the quadrupole moment, assuming for the time being that the deuteron is in a state of definite orbital angular momentum L. Such a wave function $|\,LS;\,JM\,\rangle$ may be represented by the product of a spatial part

[redacted]

The radial integral here is the expectation value of r^2 and therefore must be a positive quantity. However, we cannot evaluate its value without making some assumptions on the radial wave function.

The angular integral over three spherical harmonics may be expressed in terms of $3j$-symbols,

$$\int_0^{2\pi}\int_0^{\pi} Y^*_{LM_L}(\theta\phi)Y_{20}(\theta\phi)\,Y_{LM_L}(\theta\phi)\sin\theta\,d\theta\,d\phi$$

[redacted]

3-4 Tensor Force and the Deuteron D-state

We have seen that both magnetic dipole and electric quadrupole moments support the idea that the deuteron ground state is a linear combination of $^3S_1$- and $^3D_1$-states. The orbital angular momentum is, therefore, not a good quantum number and the nucleon-nucleon interaction potential does not commute with the operator $\boldsymbol{L}^2$. In this way, presence of the $^3D_1$-component in the deuteron ground state provides us with one clear piece of information concerning the property of nuclear force.

[redacted]

That is, the nuclear potential is not diagonal in a basis span by states with definite orbital angular momentum and can, therefore, mix ${}^3S_1$- and ${}^3D_1$-states.

In order to have a nonvanishing off-diagonal matrix element. the potential V must have a spatial part that is a spherical tensor of rank 2 so as to be able to connect an S- to a D-state, as required by Eq. (3-29). Again, let us express the deuteron wave function as a product of spatial, intrinsic spin, and isospin parts. Similarly, the matrix element of V above may also be written as a product of three matrix elements: one in coordinate space, one in intrinsic spin space, and one in isospin space. For simplicity,

[redacted]

In terms of the spherical components given in Eq. (3-31), the same product may be written in the following way:

$$\boldsymbol{\sigma}(1)\cdot\boldsymbol{\sigma}(2) = \boldsymbol{\sigma}_0(1)\boldsymbol{\sigma}_0(2) - \boldsymbol{\sigma}_{+1}(1)\boldsymbol{\sigma}_{-1}(2) - \boldsymbol{\sigma}_{-1}(1)\boldsymbol{\sigma}_{+1}(2) \tag{3-33}$$

as done in Eq. (A-19). We can also make use of the explicit values of the following Clebsch-Gordan coefficients given in §A-3,

$$\langle 1{+}1\,1{-}1|00\rangle = \langle 1{-}1\,1{+}1|00\rangle = +\frac{1}{\ } \qquad \langle 1010|00\rangle = -\frac{1}{\ }$$

[redacted]

Table 3-2: Values of Clebsch-Gordan coefficients $\langle \mathbf{1}p\mathbf{1}q|2m\rangle$.

m	p	q	$\langle 1p1q\|2m\rangle$	m	p	q	$\langle 1p1q\|2m\rangle$
0	1	−1	$\sqrt{\frac{1}{6}}$	1	1	0	$\sqrt{\frac{1}{2}}$
0	−1	1	$\sqrt{\frac{1}{6}}$	1	0	1	$\sqrt{\frac{1}{2}}$
0	0	0	$\sqrt{\frac{2}{3}}$	−2	−1	−1	1
−1	−1	0	$\sqrt{\frac{1}{2}}$	2	1	1	1

[redacted]

the nucleus. As a result, there is a force acting on an electron even in cases where it is the only one present, such as the hydrogen atom. This is not true for nuclei, as there is no external source to provide a force on the individual nucleon. The only one-body operator in a nuclear Hamiltonian is the kinetic energy arising from the motion of each nucleon. We shall see later, for example in §7-3, that one may on occasion introduce an "effective" one-body term in the nuclear potential to approximate the average effect from all the other nucleons in the nucleus. The source of such an effective one-body potential is, however, the two-body interaction between nucleons.

[redacted]

independence of nuclear force implies the commutation relation,

$$[H, T_0] = 0 \tag{3-39}$$

where H is the nuclear Hamiltonian. This, in turn, means that the eigenvectors $|\psi\rangle$ of a nuclear Hamiltonian can also be the eigenvectors of T_0 at the same time,

$$T_0|\psi\rangle = \tfrac{1}{2}(Z - N)|\psi\rangle \tag{3-40}$$

[redacted]

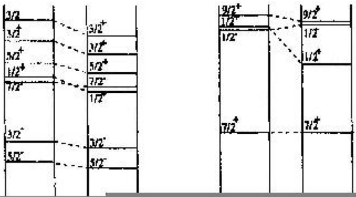
$3/2^-$
$3/2^+$
$5/2^+$
$1/2^+$
$7/2^-$
$3/2^-$
$5/2^-$
$3/2^+$
$3/2^+$
$5/2^+$
$7/2^-$
$1/2^+$
$3/2^-$
$5/2^-$
$9/2^+$
$1/2^-$
$1/2^-$
$7/2^+$
$9/2^+$
$1/2^-$
$1/2^+$
$7/2^+$

[redacted]

(2-16). As a result, the operator τ^2 may be replaced by the form 3 times the identity operator **1**.

For a system consisting of A nucleons, the isospin operator is the sum over those acting on individual nucleons,

$$\boldsymbol{T} = \frac{1}{2}\sum_{i=1}^{A} \boldsymbol{\tau}_i \tag{3-45}$$

For the two-nucleon system we are mainly interested in here, we can write

[redacted]

can enter as one of the arguments.

The nuclear potential V may depend on the momenta $\boldsymbol{p}_1$ and $\boldsymbol{p}_2$ of the two particles. On the other hand, since the sum $\boldsymbol{P} = \boldsymbol{p}_1 + \boldsymbol{p}_2$ corresponds to the center-of-mass momentum of the two-nucleon system as a whole, it cannot appear as an argument of the interaction between the two particles. The only possible momentum dependence V can have is on the relative value between two nucleons, defined by

$$\boldsymbol{p} = \tfrac{1}{2}(\boldsymbol{p}_1 - \boldsymbol{p}_2) \tag{3-50}$$

[redacted]

experimental data. When our understanding of QCD is fully developed in the future, it should also be possible to determine these functions from first principles.

The 12 terms in Eq. (3-51) may be divided into five groups. The first four,

$$V_{\text{central}} = V_0(r) + V_\sigma(r)\boldsymbol{\sigma}_1 \cdot \boldsymbol{\sigma}_2 + V_\tau(r)\boldsymbol{\tau}_1 \cdot \boldsymbol{\tau}_2 + V_{\sigma\tau}(r)(\boldsymbol{\sigma}_1 \cdot \boldsymbol{\sigma}_2)(\boldsymbol{\tau}_1 \cdot \boldsymbol{\tau}_2) \qquad (3\text{-}54)$$

are the *central force* terms, as the tensorial ranks of the spatial parts of all four operators are zero. Similar to isospin, there are only two two-body operators for intrinsic spin: unity and $\boldsymbol{\sigma}_1 \cdot \boldsymbol{\sigma}_2$. Analogous to Eq. (3-48), two-nucleon states with total intrinsic spin

[redacted]

parity of the orbital part of the wave function of a state with angular momentum L is $(-1)^L$. Under a space reflection, operators $\boldsymbol{L}$ and $\boldsymbol{S}$ do not change sign. The matrix element $\langle LS|\boldsymbol{L}\cdot\boldsymbol{S}|L'S'\rangle$, however, changes sign if $L' = L \pm 1$ and must therefore vanish. The net result is that the spin-orbit term is nonzero only between states of the same orbital angular momentum. However, the same constraint does not apply to the total intrinsic spin. As a result, $V_{\text{spin-orbit}}$ is not a central potential.

The next pair (seventh and eighth) of terms in Eq. (3-51) involve tensor force which we have already encountered in §3-4. The quadratic spin-orbit terms $V_Q(r)Q_{12}$ and [redacted]

The solution is the familiar Coulomb potential,

$$\phi(\mathbf{r}) = \left[\frac{1}{4\pi\epsilon_0}\right]\frac{q}{r} \tag{3-59}$$

When the electromagnetic field is quantized, photons emerge as the field quanta and the charge becomes the source of the field.

Nuclear force differs from its electromagnetic counterpart in several respects. The [redacted] has the well-known form of a Yukawa potential and reduces to Eq. (3-59) on letting $m = 0$ and $g = [(4\pi\epsilon_0)^{-1}]4\pi q$. On the other hand, if the field quantum has a finite mass, we find that the strength of the potential drops by $\sim 1/e$ at a distance $r_0 = \hbar/mc$. The quantity r_0 may be taken as a measure of the range of the force mediated by a boson with mass m. For pions ($m \sim 140$ MeV/c^2), the value of r_0 is around 1.4 fm. We shall see later that one-pion exchange gives a good representation of the long-range part of the nuclear potential.

[redacted]

(1) The subtraction procedure can be carried out with sufficient precision. This requires that the corresponding scattering data on a proton target are available with comparable or better accuracy and that the effect of deuteron binding energy can be corrected in a satisfactory manner. In general, both points are relatively easy to achieve.

(2) Three-body effects are negligible. When a nucleon interacts with a deuteron, the entire system now consists of three nucleons. If there are fundamental three-body forces, their contributions will be present in *pd*- and *nd*-scattering but not in the

[redacted]

In the nonrelativistic limit, the scattering of one particle off another is described by the Schrödinger equation. In the center of mass, the wave function is the solution of the equation

$$-\frac{\hbar^2}{2\mu}\nabla^2\psi + (V - E)\psi = 0 \tag{3-64}$$

where μ is the reduced mass in the two-nucleon system. We shall be mainly concerned with short-range nuclear forces here (see §B-5 for Coulomb scattering), and consequently we can assume that $V = 0$ except in a very small region where scattering takes

[redacted]

is independent of the azimuthal angle ϕ and the differential cross section is a function of the scattering angle θ alone. We shall return later to the more general case where the orientation of the intrinsic spin is also detected for one or more nucleons involved in the scattering.

Partial-wave analysis. For a central potential, the relative angular momentum ℓ between the two scattering nucleons is a conserved quantity. Under such conditions, it is useful to expand the wave function as a sum over the contributions from different

[redacted]

can contribute to the scattering at low energies, as shown in §B-2. For realistic nuclear potentials, the orbital angular momentum is not conserved. A partial-wave expansion remains to be useful as only a limited number of ℓ-values can be admixed by the noncentral forces. We shall see how to handle such cases later.

Nucleon-nucleon scattering phase shifts. Realistic nucleon-nucleon scattering differs in several important respects from the simple, central potential processes discussed above. First, we found out earlier in §3-5 that nuclear potential is a function of also

[redacted]

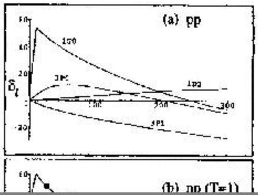

Figure 3-3: Real part of nucleon-nucleon scattering phase shifts in degrees for low-order partial waves [10]: (a) proton-proton scattering with con-

[redacted]

the tensor force can mix two triplet states of the same J but different in ℓ by two units ($\ell = J \pm 1$). For a given J-value, the scattering is now specified by two (energy-dependent) phase shifts, $\delta_{J>}$ for $\ell = J-1$ and $\delta_{J<}$ for $\ell = J+1$, as well as a parameter ϵ_J to indicate the amount of mixing between the two at a given energy.

There are several ways to define the parameter ϵ_J. The usual convention used in the literature today is that of Stapp, Ypsilantis, and Metropolis [132]. In this system of definitions, the scattering matrix (see §B-6) for a given J is written in the form

$$e^{2i\delta_{J>}}\cos 2\epsilon_J \qquad ie^{i(\delta_{J>}+\delta_{J<})}\sin 2\epsilon_J$$

[redacted]

unique for each type of nucleon pair, i.e., *np*- or *pp*-scattering. This can be seen by writing the five independent scattering amplitudes in the following manner:

$$\begin{aligned} f_1 &= f_{++,++} = f_{--,--} \qquad & f_2 &= f_{++,--} = f_{--,++} \\ f_3 &= f_{+-,+-} = f_{-+,-+} \qquad & f_4 &= f_{+-,-+} = f_{-+,+-} \end{aligned}$$
$$\begin{aligned} f_5 &= f_{++,+-} = f_{-+,--} = f_{--,+-} = f_{-+,++} \\ &= f_{--,-+} = f_{+-,++} = f_{++,-+} = f_{+-,--} \end{aligned} \qquad (3\text{-}73)$$

[redacted]

For additional information, the polarization of the scattered particle must be measured. The only efficient way to detect the polarization of a nucleon is to carry out a second scattering off a target of known analyzing power. The asymmetry in the differential cross section of the second scattering provides us with information on the polarization direction of the nucleon after the first scattering. Since the cross section is low in general for nuclear processes, a second scattering greatly complicates the experimental setup and reduces the rate of data collection. In spite of such difficulties, more and more high-precision data involving the polarization of the scattered particle are

[redacted]

wave by the expression

$$f(\theta) = \sum_{\ell=0}^{\infty} \sqrt{4\pi(2\ell+1)}\, f_\ell\, Y_{\ell 0}(\theta) \tag{3-77}$$

For purely elastic scattering,

$$f_\ell = \frac{1}{k} e^{i\delta_\ell} \sin\delta_\ell = \frac{1}{2ik}(e^{2i\delta_\ell} - 1) \tag{3-78}$$

[redacted]

scattering is essentially given by s-waves ($\ell = 0$) alone, as can be seen from Fig. 3-3 from the fact that only δ_0, the $\ell = 0$ phase shifts, are significantly different from zero.

When the kinetic energy $E \to 0$, the total cross section remains finite for nucleon-nucleon scattering. The limiting value is often characterized by a length parameter a defined by the relation

$$\lim_{E \to 0} \sigma = 4\pi a^2 \tag{3-82}$$

The quantity a is known as the *scattering length*, and it is often convenient to discuss extremely low energy scattering in terms of it instead of the s-wave phase shift. The molecule. The total intrinsic spin of the two protons in a para-hydrogen, in contrast, is $S_H = 0$ and there is only one possible state. At room temperature, the thermal energy is much higher than the difference between the para- and ortho-hydrogen, and we expect ortho-hydrogen to have three times the statistical weight of para-hydrogen in a sample at thermal equilibrium. On the other hand, at low temperatures, hydrogen molecules tend to go into the lowest possible energy state and, as a result, are almost completely in the lower energy para-hydrogen state. Thus the relative amount of para- and ortho-hydrogen in a sample may be controlled by varying the temperature of the

[redacted]

For unpolarized incident neutrons, the second term in the final form vanishes on averaging over all possible orientations of the intrinsic spin of an incident neutron. The third term may be simplified by applying the same argument in the following way. First, we expand the operator in terms of the Cartesian components of the intrinsic spins,

$$\begin{aligned}(\boldsymbol{s}_n \cdot \boldsymbol{S}_H)^2 &= s_{nx}^2 S_{Hx}^2 + s_{ny}^2 S_{Hy}^2 + s_{nz}^2 S_{Hz}^2 \\ &\quad + 2 s_{nx} s_{ny} S_{Hx} S_{Hy} + 2 s_{ny} s_{nz} S_{Hy} S_{Hz} + 2 s_{nz} s_{nx} S_{Hz} S_{Hx}\end{aligned}$$

The expectation values of the last three terms in the expression are again zero for an

[redacted]

signs in all three cases are negative. Using the definition for the sign given in §B-3, this means that there is no bound state for two nucleons in $T = 1$, a fact we encountered earlier in the discussion on deuterons.

The pp-scattering length a_{pp} is easily measured from low-energy proton scattering off a hydrogen target. However, since the cross section for Coulomb scattering, given later in Eq. (4-7), is inversely proportional to the square of the energy, the observed pp-scattering at low energies is dominated by electromagnetic effects. In principle, one can subtract the contributions of the Coulomb term from the measured values. However,

[redacted]

in chronological order, and the average of these values, shown as the dashed line in the figure, is listed in Table 3-3.

A comparison of the three values of $T = 1$ scattering length is of interest. First we find that the value $a_{np} = -23.715 \pm 0.015$ fm is noticeably larger than those for a_{pp} and a_{nn}. It is tempting to treat the difference as a possible indication of charge dependence in nuclear force. However, most of the difference may be explained by the following argument. At low scattering energies, the two nucleons are never very close to each other and, as a result, only the long-range part of the nuclear force is operating. The

[redacted]

The difference between $a_{pp} = -17.1 \pm 0.2$ fm and $a_{nn} = -16.6 \pm 0.6$ fm is not significant at this time because of the large uncertainty associated with the measured value of a_{nn}. Within experimental error, *pp*- and *nn*-scattering lengths are equal to each other and the results support charge independence of nuclear force. However, it is worth noting that the measurement of *nn*-scattering length by Gabioud et al. [70] gave a value $a_{nn} = -18.6 \pm 0.5$ fm from $\pi^- + d \rightarrow \gamma + n + n$ reactions. Using improved techniques, the experimental uncertainty in this measurement is reduced compared with previous results. Since the value obtained differs from a_{pp} by more than one standard

[redacted]

a nucleon must occupy one of the three lowest available states. When two nucleons are close together, a large fraction of their volumes overlap each other. As a result, the six quarks in a two-nucleon system can no longer be considered as two separate groups consisting of three quarks each. The Pauli exclusion principle between the quarks demands that three of the six quarks must go to states above the lowest ones already occupied by the other three. A large amount of energy is required to make this transition. From the point of view of nucleon-nucleon scattering, this additional energy shows up as a great resistance for the two nucleons to come very close to each other,

[redacted]

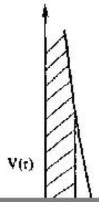

Figure 3-7: Schematic diagram showing the different parts of a nucleon-nucleon potential as a function of distance r between two nucleons. The hard core radius is around 0.4 fm and it takes energy >1 GeV to bring two nucleons

[redacted]

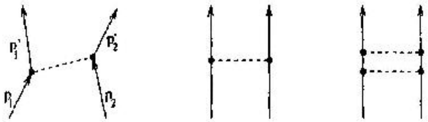

(a) (b) (c)

[redacted]

For example, a nucleon may be excited to become a Δ-particle in the intermediate state, as shown in Fig. 3-8(d). Since it is distinguishable from a nucleon, the Δ-particle is not affected by the Pauli exclusion principle with respect to nucleons in the nucleus. For applications involving nucleon energies above 300 MeV in the laboratory, the formation of a Δ-particle is expected to play a significant role and must be included as a part of the potential. On the other hand, it is not easy to incorporate such a strong inelastic channel in a potential except by putting in the resonance explicitly, an approach adopted by the Bonn group.

[redacted]

restricted by the relation

$$\frac{p_1^2}{2\mu_1}+\frac{p_2^2}{2\mu_2}=E \tag{3-91}$$

where μ_1 and μ_2 are the reduced masses of the two particles in their center of mass. In other words, the sum of the momenta of the two nucleons is confined to lie on a spherical "shell" in momentum space with the square of the radius, $p_x^2+p_y^2+p_z^2=2\mu E$, determined by the total available kinetic energy E in the center of mass. Under such circumstances, the two-body interaction t-matrix elements are said to be "on the energy shell" and

[redacted]

attractive and not too different from what is given by models involving the exchange of several pions and heavier mesons. With our present level of knowledge of low-energy strong interaction, it is not difficult to demonstrate such a relation must exist between quark-quark and nucleon-nucleon interactions; however, a proper derivation of nuclear force from QCD is still being developed.

Qualitatively we can see how nuclear force may arise from a quark-quark interaction by making an analogy with the force between chemical molecules. The fundamental force here is electromagnetic. Charge distributions in many molecules are spherically

[redacted]

van der Waals force is pleasing, the actual form it produces has a range much longer than what is observed. Currently, the color van der Waals force does not seem to be a correct model for nuclear interaction without modifications.

Problems

3-1. Find the possible range of values for the depth of a one-dimensional square well, 3 fm wide, that has only one bound state for a nucleon.

[redacted]

3-6. Show that the spherical tensor rank of the operator

$$S_{12} = \frac{3}{r^2}(\boldsymbol{\sigma}_1 \cdot \boldsymbol{r})(\boldsymbol{\sigma}_2 \cdot \boldsymbol{r}) - \boldsymbol{\sigma}_1 \cdot \boldsymbol{\sigma}_2$$

is 2 in intrinsic spin space. That is, it may be written as an operator of the form $\sum_{qq'}\langle j_1 q j_2 q' | \lambda M\rangle \sigma_{1q}\sigma_{2q'}$ with $\lambda = 2$ and $j_1 = j_2 = 1$. Here $\langle j_1 q j_2 q' | \lambda M\rangle$ is the Clebsch-Gordan coefficient.

[redacted]

3-9. Calculate the s-wave phase shift of a neutron scattered by an attractive square-well potential of depth V_0 and width W. Obtain the scattering length a and effective range r_0 in terms of V_0 and W.

3-10. Show that the angular distribution of an s-wave scattering is isotropic. If the only nonzero phase shifts in a hypothetical scattering of a particle off another are s- and p-waves, find the angular distribution of the scattering cross section assuming that the particle is a neutron, the s-wave phase shift is $\delta_0 = 45°$, the p-wave phase shift $\delta_1 = 30°$, and the scattering takes place with laboratory energy

[redacted]

Chapter 4

Bulk Properties of Nuclei

In general, observations made on atomic nuclei can be separated into four categories: energies, static moments, transition probabilities, and reaction rates. In this chapter, we shall be concerned primarily with the first two. In particular, we shall examine

[redacted]

Usually we are only interested in the radial dependence of the density. As a result, we can average over the angles and consider only $\rho_{\rm ch}(r)$. The angular part of the integration in Eq. (4-2) can be carried out explicitly in this case and the (radial) charge form factor reduces to the expression

$$F(q^2) = \frac{4\pi}{q}\int \rho_{\rm ch}(r)\sin(qr)r\,dr \qquad (4\text{-}3)$$

It is a function of q^2, the square of the momentum transfer to be defined later in Eq. (4-13), as q^2 (rather than q) is a proper Lorentz scalar. We shall also see in

[redacted]

where θ is the scattering angle. The additional contribution is characterized by the *transverse* form factor $F_T(q^2)$. In terms of operators, longitudinal and transverse form factors are related to electromagnetic moments given in §4-6, and transition probabilities between states are given in §5-3.

Scattering off point particles. A convenient starting point for discussing charged particle scattering is the Rutherford formula for differential cross sections at scattering angle θ,

[redacted]

where $\hbar\boldsymbol{k}_a$ is the incident electron momentum and $\hbar\boldsymbol{k}_b$ is the final electron momentum. If the electron energy is high, it is more appropriate to use, instead, the Mandelstam variable t. Let us represent the four-momenta of incident electron a and scattered electron b in the center of mass by

$$\varrho_a = \left(\frac{iE_a}{c}, k_{ax}, k_{ay}, k_{az}\right) \qquad \varrho_b = \left(\frac{iE_b}{c}, k_{bx}, k_{by}, k_{bz}\right) \tag{4-10}$$

where E_a and E_b are, respectively, the center-of-mass energies of a and b. The four-

[redacted]

where M is the mass of the target particle.

In the limit that the electron rest mass may be ignored, the cross section in the laboratory for elastic scattering of unpolarized electrons off spinless ($J = 0$), point-charge particles is given by

$$\left(\frac{d\sigma}{d\Omega}\right)_{\text{point}} = \left(\frac{Z\alpha\hbar c}{2E_a \sin^2(\theta/2)}\right)^2 \frac{E_b}{E_a} \cos^2\frac{\theta}{2} \tag{4-17}$$

For targets with a finite spin, there is an additional contribution coming from "mag-

[redacted]

where the overall factor Z comes from the normalization chosen for charge densities given in Eq. (4-1). Since the sine function involves only odd powers of q, the final result contains only even powers.

The radial integral in the second term of Eq. (4-19) is the expectation value of the radius squared. At low q^2, the behavior of the form factor is dominated by this term, and the slope of $F(q^2)$ in this region gives us the expectation value for the square of the radius. A plot of $\langle r^2\rangle^{1/2}$ deduced from electron scattering and other measurements is given as a function of nucleon number A in Fig. 4-2. To see the dependence of $\langle r^2\rangle^{1/2}$

[redacted]

This gives $R = \{(5/3)\langle r^2\rangle\}^{1/2} = 1.29\,\langle r^2\rangle^{1/2}$. For more realistic radial density distributions, such as the ones given below, the ratio $R^2/\langle r^2\rangle$ turns out to be slightly smaller than $\frac{5}{3}$. For the value of $\langle r^2\rangle^{1/2} \approx 0.97A^{1/3}$ obtained from Fig. 4-2, we come to the result $R = r_0A^{1/3}$ with $r_0 = 1.2$ fm, as given in Eq. (1-2).

Fourier-Bessel coefficients. Nuclear charge densities are often tabulated in terms of Fourier-Bessel coefficients. The density up to some cutoff radius R_c is expressed in terms of $j_0(\xi)$, with spherical Bessel function of order zero,

[redacted]

constant central region and a diffused edge may be represented by expressions involving fewer parameters than the number of Fourier-Bessel coefficients in Eq. (4-20). Several such forms are commonly used in both nuclear reaction and nuclear structure studies.

The radial dependence of a density distribution with a diffused edge may be written as

$$\rho_{2pF}(r) = \frac{\rho_0}{1 + \exp\{(r - c)/z\}} \tag{4-22}$$

The two parameters c and z are determined, for instance, by fitting to densities derived from measured form factors, and the factor ρ_0 is given by normalization. Equation

[redacted]

4-3 Nucleon Form Factor

At sufficiently high energies, giga-electron-volts and above, the de Broglie wavelength of an electron becomes much shorter than the size of a typical nucleus. In such cases, the scattering result is dominated by the charge distributions within individual nucleons. The primary interest shifts to the structure of nucleons rather than that for the nucleus as a whole. In the place of nuclear form factors, we are concerned with the analogous quantities for nucleons. We shall return at the end of §4-4 to the question of whether there is any difference in scattering off bound nucleons instead of free ones.

[redacted]

factors and the magnetic form factor of a neutron are identical to each other except for a *scaling factor*. The required factors can be deduced by examining Eq. (4-25),

$$G_E^p(q^2) = \frac{1}{\mu_p} G_M^p(q^2) = \frac{1}{|\mu_n|} G_M^n(q^2) = G(q^2) \tag{4-26}$$

The function $G(q^2)$ may be described by a *dipole form*,

$$G(q^2) = \frac{1}{\quad}$$

[redacted]

^{3}He. Based on the information available, the charge distributions obtained by applying Eq. (4-5) to the measured form factors are shown in Fig. 4-3. Since a neutron has no net charge, it is not surprising to find the $F_1(q^2)$ to be much smaller than the corresponding values for a proton. On the other hand, the values may be important in understanding some of the details in nuclear charge distribution to be discussed later in §4-5.

4-4 High-Energy Lepton Scattering

[redacted]

there is a spread of the order of 100 MeV in the energy transferred in quasi-elastic scattering, around 10% of the total.

Structure functions. At forward angles, the momentum transferred is small and the cross section is dominated by elastic scattering. Since form factors decrease in value very quickly with increasing momentum transfer, the elastic scattering cross section rapidly becomes very small as the momentum transfer is increased, and the presence of inelastic scattering processes becomes apparent. The reaction cross section now

[redacted]

Instead of Eq. (4-29), we may also write q^2 in terms of x and y,

$$q^2 = \frac{2ME_a}{\hbar^2}xy$$

Using Eqs. (4-31) and (4-32), the angular dependence on the right-hand side of Eq. (4-28) may be expressed in terms of x and y,

$$\frac{d^2\sigma}{\ } = \frac{4\pi Z^2\alpha^2}{\ }\frac{1}{\ }\Big\{F_2(q^2,x)(1-y) + F_1(q^2,x)xy^2\Big\}$$

[redacted]

Let us compare the structure functions per nucleon obtained from high-energy lepton scattering off free nucleons and off bound nucleons in nuclei.

From their differences in the charge distributions, we expect the structure functions for neutrons and protons to be different from each other and may, principle, be measured by separate experiments. However, for scattering off finite nuclei, the measured values will be an average between the contributions from neutrons and protons, without any easy way to distinguish between them. Let us assume for simplicity that we have $N = Z$, which is true for light nuclei. For such targets, the contributions from bound

[redacted]

the internal structure of a bound nucleon, as shown by $F_2(q^2, x)$, is somewhat different from that of a free nucleon. Most of the departure from $R(x) = 1$ can, however, be explained by the binding energy of nucleons in a nucleus. The only exception is in the very small x region, where measurements are difficult to make. As a result, it remains to be one of the unsolved problems in high-energy nuclear physics.

4-5 Matter Density and Charge Density

[redacted]

the case of ^{48}Ti, a nucleus with two more protons and six more neutrons than ^{40}Ca. Here, the size of the charge distribution is increased by 0.1 fm for ^{48}Ti, not far from the expectation of an $A^{1/3}$-dependence, instead of decreasing for ^{48}Ca.

There are two possible explanations for the decrease in the charge radius with increasing neutron number among even calcium isotopes. The first is that the addition of neutrons makes the protons more tightly bound and, hence, the charge radius is smaller. This is, however, not true for nuclei in general and has led to the speculation that there are some other nuclear structure reasons for ^{48}Ca to be a more tightly bound nucleus than its neighbors.

[redacted]

in this case may be considered to be concentrated at a point, as the electron is much further away than the extent of the nucleus. Since nothing special about the electron enters into the derivation, we can obtain the analogous results for a muonic atom by replacing m_e in Eq. (4-35) by m_μ, the mass of a muon,

$$r_n(\mu^-) = \frac{1}{\alpha\hbar c}\frac{n^2\hbar^2}{Zm_\mu} = a_0\frac{n^2 m_e}{Zm_\mu} \qquad (4\text{-}36)$$

Using similar arguments, we can arrive at the energy level of a muonic atom consisting

[redacted]

Pion-nucleus scattering. We have seen earlier in §2-6 that there is a strong pion-nucleon resonance in the spin-isospin $(T, S) = (\frac{3}{2}, \frac{3}{2})$ channel at pion laboratory energy of 195 MeV (see Fig. 2-3). The dominance of the P_{33}-resonance provides us with a unique opportunity to examine the difference between neutron and proton density distributions in a nucleus.

There are six different possible reactions in pion-nucleon scattering with charged pions as the projectile:

$$(a)\quad \pi^+ + p \rightarrow \pi^+ + p \qquad\qquad (b)\quad \pi^- + n \rightarrow \pi^- + n$$

[redacted]

the results of 180 MeV π^+-scattering off ^{40}Ca and ^{48}Ca are plotted on the same graph as shown in the left side of Fig. 4-5, very little difference can be detected. Since the energy is very close to the P_{33}-resonance and the cross sections are dominated by scattering off protons, the data give strong support to the similarity of proton distributions in ^{40}Ca and ^{48}Ca. On the other hand, a definite difference is found in the results of scattering of π^- off the same two nuclei at the same energy, as shown in the right side of Fig. 4-5. This is caused by the differences in the neutron distribution, a result expected from the eight additional neutrons in ^{48}Ca. When we examine the π^--scattering data off the same

[redacted]

and proton distributions. The isospin dependence of nuclear force is, however, not strong enough to clearly differentiate between neutrons and protons, as in pion-nucleon scattering at P_{33}-resonance. One way to proceed is to take it for granted that the proton density distribution in a nucleus is already known through electron scattering. Any difference observed in proton scattering may therefore be attributed to the presence of neutrons. Neutron density distributions obtained in this way depend a great deal on the model used to analyze the data, and the results are somewhat ambiguous compared with, for example, those obtained from charged pion scattering at the P_{33}-resonance.

is mainly in the lowest few multipoles, as the moments of these are the only ones that can be measured in practice.

Using the normalization for charge density given in Eq. (4-1), we can rewrite the right-hand side of Eq. (4-40) as an expectation value,

$$Q_{\lambda\mu} = \langle \Psi(\boldsymbol{r}) | e r^{\lambda} Y^{*}_{\lambda\mu}(\theta, \phi) | \Psi(\boldsymbol{r}) \rangle$$

This allows us to identify the operator for the (λ, μ) electric multipole as

[redacted]

either. For our purposes, we shall assume that both parity and time invariance are exact symmetries and only even-order electric multipole moments may be different from zero.

Angular momentum coupling imposes a restriction on the highest order multipole coefficients a state can have. The multipole operator $r^\lambda Y_{\lambda\mu}(\theta,\phi)$ is a spherical tensor of rank (λ,μ) and carries an angular momentum $\boldsymbol{\lambda}$. The expectation value of such an operator vanishes for a state with spin J unless $\boldsymbol{J}$, $\boldsymbol{\lambda}$, and $\boldsymbol{J}$ can be coupled together to form a closed triangle. This is the same as saying that only multipole coefficients of $\lambda \leq 2J$ can be nonzero. For this reason, a $J=0$ state has no multipole moment except

[redacted]

In contrast, nuclei in the middle of a major shell are often deformed and have large absolute values for their quadrupole moments. More detailed discussions of deformed nuclei are given later in §6-3 and §9-2.

The quadrupole moment is defined as the expectation value of the operator $r^2Y_{20}(\theta,\phi)$ in the substate of $M = J$,

$$Q = \sqrt{\frac{16\pi}{5}}\, e\, \langle J, M{=}J|r^2Y_{20}(\theta,\phi)|J, M{=}J\rangle$$

[redacted]

density may be written as a sum of the contributions from all the nucleons in the nucleus in the following way:

$$\mathcal{J}(\boldsymbol{r}) = \sum_{i=1}^{A}\left\{eg_\ell(i)\frac{\boldsymbol{p}(i)}{M_N} + \frac{c\hbar}{2M_N}g_s(i)\nabla\times\boldsymbol{s}(i)\right\}\delta(\boldsymbol{r}-\boldsymbol{r}(i)) \qquad (4\text{-}44)$$

where, in units of nuclear magneton μ_N,

$$g_\ell = \{\ 1 \quad \text{for a proton} \qquad\qquad g_s = \{\ 5.586 \quad \text{for a proton}$$

[redacted]

obtained, again, with the help of integration by parts. For a proton, orbital motion contributes $(e/M_p)\boldsymbol{p}$ to the magnetization current $\mathcal{J}(\ell)$, where $\boldsymbol{p}$ is the linear momentum of the proton. Using the fact that orbital angular momentum is the vector product of $\boldsymbol{r}$ and $\boldsymbol{p}$,

$$\boldsymbol{\ell}\hbar = \boldsymbol{r} \times \boldsymbol{p}$$

we obtain the contribution due to proton orbital motion as

$$O_{1\mu}(M1,\ell) = \frac{[c]}{} \left(\boldsymbol{r} \times \sum^{A} e g_\ell(i) \frac{\boldsymbol{p}_i}{} \right) = \frac{e\hbar[c]}{} \sum^{A} g_\ell(i) \boldsymbol{\ell}_\mu(i) \qquad (4\text{-}48)$$

[redacted]

total orbital angular momentum $\boldsymbol{L}$ and intrinsic spin $\boldsymbol{S}$ must be either the combination $(L, S) = (0, 0)$ or $(L, S) = (1, 1)$ to satisfy the Pauli principle. The $(L, S) = (1, 1)$ case has a higher energy and is of no interest in the ground state. To form an $S = 0$ state, the intrinsic spins of the two nucleons must be aligned antiparallel to each other. As a result, their contributions to the magnetic dipole moment cancel each other. Similarly, for a pair of protons coupled to $L = 0$, the net contribution from orbital motion must also vanish, as the two are moving in opposite directions.

In the limit that pairing completely dominates the nuclear ground state, all pairs of [redacted] given by the orbital angular momentum of the unpaired nucleon, $\pi = (-1)^\ell$. In this way, the spin and parity of the state, together with whether the unpaired nucleon is a proton or a neutron, provide all the information we need to calculate the magnetic dipole moment using Eq. (4-53). For each j-value, the results obtained fall into two groups depending on the two possible values of ℓ. These are known as the Schmidt values and they are compared with observations in Fig. 4-6.

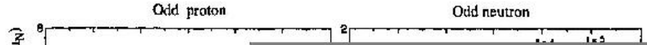

In calculating the expectation values, we have assumed that each nucleon in the nucleus has the same properties as a free one. For example, the intrinsic magnetic dipole moment of a proton is taken to be $\frac{1}{2}g_p$ and that of a neutron $\frac{1}{2}g_n$. Such an assumption is sometimes referred to as the *impulse approximation*, a term originated from scattering studies (see §8-4). There are two ways by which the impulse approximation may fail. The first is the effect of mesons in nuclei. If charged mesons are exchanged between nucleons, their flow constitutes an electric current which may also contribute to the observed magnetic moments. The influence of such a *mesonic current* may also be

[redacted]

where $t_i = \frac{1}{2}$ is the isospin of the ith nucleon. Even-mass nuclei can be divided further into two categories: Those with both neutron and proton numbers even (N = even, Z = even) are called even-even nuclei and those with both neutron and proton numbers odd (N = odd, Z = odd) are called odd-odd nuclei.

For even-even nuclei, the ground spin is observed to be zero without any exception. This remarkable phenomenon reflects a fundamental property of nuclear interaction known as pairing. Since ground state spins of odd-odd nuclei are observed to be nonzero in general, we conclude further that pairing interaction is important only between two

[redacted]

Here, $\eta = j_p - \ell_p + j_n - \ell_n$. In practice, many exceptions are found and the rule can only provide a general guide to the likely value for the ground state spin of an odd-odd nucleus.

Ground state isospin. The possible isospin of a nucleus may be deduced from the proton and neutron numbers. For a system of Z protons and N neutrons, the projection of isospin on the quantization axis is

[redacted]

level Coulomb force is much weaker than nuclear force, and may be ignored for most purposes, it is not true for the nucleus as a whole. As we have seen in §1-3, through short-range nuclear force a nucleon can only interact with a few of its neighbors. For this reason, its contribution in a many-body system increases, to a first-order approximation, only linearly with nucleon number. In contrast, the Coulomb term has a long range and its contribution to the binding energy, for example, increases quadratically with proton number. As a result, the effect of Coulomb interaction may be quite significant in heavy nuclei and isospin may no longer be a good quantum number.

[redacted]

From this expression, we see that the amount of mixing among the two basis states depends on the size of the off-diagonal matrix element as well as the difference in the values of the diagonal matrix elements.

In a real nucleus, the number of states that can be admixed by isospin-breaking forces is likely to be larger. However, the general features are well illustrated by our simple, two-dimensional example. Several interesting problems may be studied using this model. The first is that the admixture is important only between states whose "unperturbed" locations, given essentially by the values of the diagonal matrix elements

[redacted]

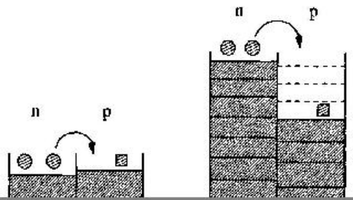

Figure 4-7: Occupancies of neutron and proton single-particle states. The location of the isobaric analogue state of an isobar with one more proton and one less neutron may be found by changing a valence neutron (circles) to a proton (squares). Because of neutron excess, such states are much

[redacted]

energies depend on the number of protons. The difference in the Coulomb energy between ^{16}O and ^{16}N may be estimated using the uniformly charged sphere model given by Eq. (1-7). The result, calculated with a radius of $R = 1.2A^{1/3} \approx 3.02$ fm, is 4.00 MeV. This means that, instead of 9.64 MeV, the IAS should be at excitation energy 13.64 MeV. A second correction comes from the difference in mass between a neutron and a proton [together with an atomic electron to keep the atom neutral as required in the definition of binding energy given in Eq. (1-1)]. Since ^{16}O has one more proton and one less neutron than ^{16}N, the calculated value of the excitation energy

[redacted]

around 12.9 MeV. However, the sequence of the four levels is different from what is observed in ^{16}N, showing that some small violation of the IAS idea is found in actual nuclei.

Besides $T = 1$ states, the IAS for $T = 2$ are also known in the $A = 16$ isobar. The ground state of $^{16}_{6}$C ($T_0 = -2$) is 0^+ and an excited 2^+ is found at 1.77 MeV. Similarly, the ground state of ^{16}Ne is $(J^\pi, T) = (0^+, 2)$ and a 2^+, $T = 2$ state is found at 1.69 MeV. The IAS of these two $T = 2$ states are found in ^{16}N at 9.93 MeV for the 0^+ state and at 11.90 MeV for the 2^+ state. Similarly, the same $T = 2$ pair is found in ^{16}O at

[redacted]

Taking $R = 1.2A^{1/3}$ fm, the result is

$$E_c = \left[\frac{1}{4\pi\epsilon_0}\right]\frac{3}{5}\frac{Z(Z-1)e^2}{R} = \frac{3\alpha\hbar c}{5r_0}\frac{Z(Z-1)}{A^{1/3}} = 0.72\frac{Z(Z-1)}{A^{1/3}}\ \text{MeV}$$

A real nucleus has a diffused surface region and its shape may not necessarily be spherical. For these reasons, we do not expect the uniformly charged sphere value to be completely correct. On the other hand, the expression captures the essence of the dependence on A and Z. We shall therefore adopt the form of the Coulomb correction

[redacted]

provides some idea of the magnitude of each of the terms. The value of the pairing parameter δ is, perhaps, the least well determined quantity among the five and is found to be much larger, for example, if we restrict the fit to heavy nuclei alone (see Problem 4-11).

The usefulness of such a mass formula lies, for example, in obtaining the energies involved when a heavy nucleus undergoes fission into lighter fragments. The calculated results give a correct overall picture of the dependence on A, Z, and N values. However, there are local increases in the binding energy for nuclei near closed shells, known as

[redacted]

in nature. We can test whether the premise is correct by calculating the differences between four such nuclei using known binding energies,

$$\Delta E_B = E_B(Z+1, N+1) + E_B(Z, N) - E_B(Z, N+1) - E_B(Z+1, N)$$

In practice, we find that the values of ΔE_B are rather large, reflecting the shortcomings in ignoring two-body terms.

There are, in general, three types of two-body contributions to be included: proton-proton, neutron-neutron, and neutron-proton interactions. For a nucleus of N neutrons

[redacted]

The sum of these two differences is the same as the difference between a pair with N neutrons and proton number differing by 2,

$$\begin{array}{rl} E_B(Z+1,N) = & b(Z+1) + dZ(Z+1) \qquad + eN(Z+1) + h(a,c,N) \\ -E_B(Z-1,N) = & b(Z-1) + d(Z-1)(Z-2) + eN(Z-1) + h(a,c,N) \\ \hline E_B(Z+1,N) - E_B(Z-1,N) = & 2b \qquad + 2d\,(2Z+1) \qquad + 2eN \end{array}$$

By eliminating b, d, and e from these three equations, we obtain the result given

[redacted]

the energy of α-particles emitted tends to be confined in a narrow range of 5 to 9 MeV whereas the half-lives vary by several orders of magnitude. As mentioned in Chapter 1, these observations led to the discovery of quantum-mechanical tunneling, a milestone in the development of modern physics.

Barrier for α-particle emission. It is perhaps easier to visualize the barrier an α-particle must tunnel through by considering first the inverse process of a low-energy α-particle approaching a heavy nucleus from large distances away. For simplicity, we

[redacted]

of the particle emitted is expected to be as least as large as the barrier height, as the α-particle carries with it all the energy it acquired to reach the top of the barrier. The observed values, however, are much smaller and, consequently, some other mechanism must be operating here. The quantum-mechanical explanation is that the α-particle does not have to go over the top of the potential barrier before being emitted. Instead, it tunnels through the barrier. The basic reason comes from the fact that the α-particle wave function does not vanish inside a small region of (finite) repulsive potential. In quantum mechanics, it is well known that the amplitude of a wave function, to a first-

[redacted]

following way:

$$\log_{10} W = C - \frac{D}{\sqrt{E_\alpha}} \tag{4-61}$$

where W is the decay probability. The parameters C and D are weakly dependent on Z but not on the neutron number, as can be seen from the plot in Fig. 4-10. This is known as the Geiger-Nuttall law. A simple, one-body theory of α-particle decay described below provides the foundation for this observed relation.

[redacted]

It is reasonable to expect that K is of the same order of magnitude as E_α, the kinetic energy of the α-particle emitted. For our simple model, we shall take $K = E_\alpha$. This leads to the result

$$\nu = \frac{\sqrt{2E_\alpha/M_\alpha}}{2R} = \frac{\sqrt{E_\alpha}}{A^{1/3}} \times 2.9 \times 10^{21}\ \mathrm{s}^{-1}$$

where E_α is measured in mega-electron-volts and, as usual, we have taken $R = r_0 A^{1/3}$ with $r_0 = 1.2$ fm. From this we obtain, for example, a value of $\nu = 10^{21}\ \mathrm{s}^{-1}$ for ^{238}U with $E_\alpha = 5.6$ MeV. It is about an order of magnitude larger than the best values deduced

[redacted]

Since we are interested here in the region outside the range of nuclear force, the potential $V(r)$ may be taken as purely Coulomb, having the form given by Eq. (4-60). All the angular dependence is contained in the $\ell(\ell+1)/r^2$ term and may be taken as a part of the potential barrier. For this purpose, we shall define an "effective" potential barrier,

$$V_b(r) = \left[\frac{1}{4\pi\epsilon_0}\right]\frac{zZe^2}{r} + \frac{\ell(\ell+1)\hbar^2}{2\mu r^2} = \frac{zZ\alpha\hbar c}{r} + \frac{\ell(\ell+1)\hbar^2}{2\mu r^2}$$

The radial equation reduces to the form

[redacted]

with η known as the Sommerfeld number.

Energy and mass dependence. Using p_α, ν, and $\mathcal{T}$ obtained above, we can write the transition probability as

$$\mathcal{W} = p_\alpha \nu \mathcal{T}$$

To put this expression into a form so that it can be compared with the Geiger-Nuttall law of Eq. (4-61), we take the logarithm in the base 10 for both sides and obtain the result

[redacted]

We have implicitly assumed in the above discussion that there is only a single kinetic energy E_α for all the α-particles emerging from a nucleus. In fact, it is common to find several different groups of α-particles emitted by the same parent nucleus. The example of ^{212}Bi shown in Fig. 4-12 has more than 14 different decays known and each one leaves the residual nucleus in a different state.

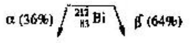

only thing preventing spontaneous fission from happening more often is the fission barrier through which the fragments must tunnel. We shall return to the source of this barrier later. Since the condition for large deformation required for fission is found only in extremely heavy nuclei, spontaneous fission does not become an important decay channel until $A > 240$. For example, the partial half-life for spontaneous fission of ^{232}U is around 10^{14} years, whereas the value for α-decay is only 2.85 years. On the other hand, by the time we get to $^{254}_{98}$Cf, the half-life reduces to 60 days with a branching ratio of 99% for spontaneous fission.

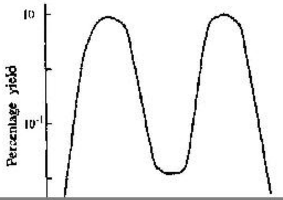

Figure 4-13: Schematic diagram showing the distribution of fission fragments as a function of nucleon number. The reason for a bimodal distribution comes from the larger ratio of neutron to proton numbers for the heavy parent than those

[redacted]

tions here. Similarly, changes in the pairing and symmetry energy terms are too small for us to be concerned with here. Only two terms, the surface energy $\alpha_2 A^{2/3}$ and the Coulomb energy $\alpha_3 Z(Z-1)/A^{1/3}$, remain and they form the main components of the fission barrier. Since both terms enter the binding energy equation with negative signs, a decrease in either term will increase the binding energy of the system as a whole.

When the hypothetical nucleus undergoes a transformation from $A = 300$ to two fragments of $A = 150$ each, the loss in binding energy due to changes in the surface energy is given by from the Coulomb term as a result of splitting the nucleus into two. The amount is obtained under the assumption that the two fragments are separated by an infinite distance without any Coulomb interaction between them. As the distance decreases, the Coulomb energy increases with a $1/r$ dependence if we ignore any possible shape changes in the fragments. At $d < 13$ fm, the value cannot be estimated easily. Again, we can take it to be something like that shown by the solid curve in Fig. 4-15(a).

The net change in binding energy as a result of fission in our simple model is the difference between the gain in the Coulomb energy and the loss in the surface energy

[redacted]

solving many-body problems. Furthermore, being an infinite system, we do not have complications caused by motion of the center of mass, as in the case of finite nuclei. Electromagnetic interactions are usually ignored in such studies, as the primary interest is nuclear.

There is obviously no observed data on such an idealized system. A neutron star is as close to an infinite system of nuclear matter as we can imagine; however, experimental measurements on neutron stars of direct interest to nuclear physics may not be forthcoming for a while. As a result, most information concerning infinite nuclear

[redacted]

In the absence of spin and isospin degrees of freedom, the allowed values for the wave numbers $\boldsymbol{k} = (k_x, k_y, k_z)$ are given by the condition that the wave function vanishes at the boundary of the box. As a result,

$$k_x = \frac{2\pi}{L}n_x \qquad k_y = \frac{2\pi}{L}n_y \qquad k_z = \frac{2\pi}{L}n_z$$

where n_x, n_y, and n_z are integers 0, ±1, ±2, … . The number of allowed plane wave states in a volume element d^3k is then

[redacted]

Compression modulus. The state of minimum energy is an equilibrium for infinite nuclear matter, stable against small variations of the density. Variations of the binding energy per particle due to changes in Fermi momentum must therefore vanish,

$$\frac{d}{dk_F}\left(\frac{E_B}{A}\right) = 0$$

The second-order derivative of E_B/A depends on the difficulty, or *stiffness*, of nuclear matter against changes in the density. This is measured by the compression modulus, nuclei: the binding energy per nucleon of Eq. (4-67), the saturation density in terms of the Fermi momentum of Eq. (4-70), and (not always carried out) the compression modulus of Eq. (4-74). The hope is that the simple geometry offered by the idealized system provides us with a direct and meaningful test for nucleon-nucleon interactions and techniques for many-body problem. The test is a nontrivial one. For example, most of the properties of finite nuclei are not very sensitive to the hard core in nucleon-nucleon interactions. In contrast, the value of this term is crucial in reproducing the saturation density in infinite nuclear matter. Without the short distance repulsion,

[redacted]

4-6. A muon (μ^-) can take the place of an electron in an atom and form a muonic atom. Since the muon is 207 times more massive than an electron, the radii of its orbits in an atom are much smaller. For a heavy atom, the low-lying muonic orbits may have a substantial overlap with the nuclear wave function as a result. Calculate the fraction of time a muon is inside a spherical nucleus of radius $R = 1.2A^{1/3}$ fm, when the muonic atom is in the lowest energy state. Take $A = 200$ and $Z = 70$.

4-7. Use a table of binding energies (e.g., from http://www.nndc.bnl.gov) to:

[redacted]

Using the value of binding energy obtained and a minimum amount of additional experimental data, find the locations of isobaric analogue states to the ground state of ^{12}O in ^{12}N and ^{12}C.

4-14. Calculate the average density of ^{238}U assuming it is a uniform sphere of radius $R = 1.2A^{1/3}$ femtometers. If, instead, R is the radius of ^{238}U measured from the center to a point on the surface where the density is half of that in the central region, and the nuclear density is given by the two-parameter Fermi form given in Eq. (4-22) with $z = 0.6$ fm, what is the central density of the nucleus? Compare

[redacted]

Chapter 5

Electromagnetic and Weak Interaction

The lifetime, or mean life, of an excited state is the average amount of time it takes for a radioactive nucleus to decay. It is connected to the transition probability and half-life by the relation

$$\overline{T} = \frac{\int_0^\infty t e^{-\mathcal{W}t}\,dt}{\int_0^\infty e^{-\mathcal{W}t}\,dt} = \frac{1}{\mathcal{W}} = \frac{T_{1/2}}{0.693}$$

Transition probability, half-life, and lifetime are three different ways to characterize the same physical observable.

[redacted]

To carry such a separation over to a decaying (excited) state, the energy E must be changed into a complex quantity,

$$E \longrightarrow \langle E\rangle - \tfrac{1}{2}i\hbar\mathcal{W}$$

The time-dependent wave function now takes on the form

$$\Psi(\boldsymbol{r},t) = \psi(\boldsymbol{r})e^{-i\langle E\rangle t/\hbar-\mathcal{W}t/2} \tag{5-4}$$

[redacted]

The relation between half-life $T_{1/2}$ and partial half-lives $T_{1/2}(i) = \ln 2/\mathcal{W}(i)$ is given by

$$\frac{1}{T_{1/2}} = \sum_i \frac{1}{T_{1/2}(i)}$$

as evident from Eq. (5-5).

The *branching ratio* gives the partial transition probability to a particular final state as a fraction of the total from a specific initial state. For example, the mean lifetime of a π^0-meson is 8.4×10^{-17} s and decays 98.8% of the time to two γ-rays, 1.17% of

[redacted]

square of the transition matrix element reduces to

$$
\begin{aligned}
|\mathcal{M}_{fi}|^2 &= \sum_{\mu M_f} \left| (-1)^{J_f - M_f} \begin{pmatrix} J_f & \lambda & J_i \\ -M_f & \mu & M_i \end{pmatrix} \langle J_f \xi \| O_\lambda \| J_i \zeta \rangle \right|^2 \\
&= |\langle J_f \xi \| O_\lambda \| J_i \zeta \rangle|^2 \sum_{\mu M_f} \left| \begin{pmatrix} J_f & \lambda & J_i \\ -M_f & \mu & M_i \end{pmatrix} \right|^2 \\
&= \frac{\Delta(J_f, \lambda, J_i)}{} |\langle J_f \xi \| O_\lambda \| J_i \zeta \rangle|^2 \qquad (5\text{-}7)
\end{aligned}
$$

[redacted]

Here, the expansion coefficients,

$$c_n = \int \phi_n^*(r) e^{iE_n t/\hbar} \psi(r, t)\, dV$$

are independent of time, since we have not yet included $H'(t)$.

For the complete Hamiltonian, the eigenfunctions $\Psi(r, t)$ may still be expressed in terms of $\phi_n(r)$ except that the expansion coefficients are now time dependent,

$$\Psi(r, t) = \sum_n c_n(t) \phi_n(r) e^{-iE_n t/\hbar} \tag{5-9}$$

[redacted]

for all time t of interest. As a result, we can approximate Eq. (5-10) by retaining only the $n = 0$ term in the sum on the right-hand side. This gives us the result

$$i\hbar \frac{dc_k(t)}{dt} = \langle \phi_k | H'(t) | \phi_0(t) \rangle \, e^{i\omega_{k0}t} \tag{5-12}$$

Furthermore, if the time variation of $H'(t)$ is slow compared with $\exp\{i\omega_{k0}t\}$, we may take H' to be a constant. In this approximation, Eq. (5-12) can be solved explicitly and the result may be expressed as

[redacted]

5-3 Electromagnetic Transition

In this section we shall deal mainly with nuclear decay through the emission of a γ-ray. The transition is caused by the interaction of the nucleus with an external electromagnetic field. For our purpose here, we may regard the nucleus as made of point nucleons, each carrying a magnetic dipole moment and, in the case of protons, a net charge as well. The charge distribution couples with the external field, causing "electric" transitions. At the same time, interaction with the intrinsic magnetism of each nucleon and the magnetism generated by current loops due to proton orbital

[redacted]

to more advanced textbooks, such as Blatt and Weisskopf [32] and Sakurai [121].

We can visualize the form of electromagnetic perturbation in a nucleus in the following way. Consider first the simple case of a point particle carrying a charge q and, for the time being, no magnetic moment. In the absence of any external electromagnetic field, the particle is free and the Hamiltonian consists of only the kinetic energy term,

$$H_0 = \frac{1}{2m}p^2 \tag{5-14}$$

[redacted]

In addition to the electric charge carried by protons in a nucleus, the intrinsic magnetic dipole moment of the nucleon can also interact with the external electromagnetic field. We have seen earlier, in Eq. (4-44), in the discussion of static magnetic moments, that the intrinsic magnetic dipole moment of a nucleon may also be expressed in the form of a current. Consequently, it is unnecessary to change the form of H' given in Eq. (5-18) to include the effect of nucleon magnetic moments, except that we need a new definition for the current density $\mathcal{J}$ than what is given in Eq. (5-17). The most general form of H' must also include the possibility for the charge distribution to interact with an

[redacted]

2. This is similar to expressing ordinary light waves as a linear combination of horizontal and vertical polarizations. At this stage, the factors $\boldsymbol{b}_{k\eta}$ and $\boldsymbol{b}^{\dagger}_{k\eta}$ remain as constants related to $\boldsymbol{B}_k$ and $\boldsymbol{C}_k$ and must be determined by boundary conditions.

Up to now the solution we have obtained for Maxwell's equation is purely classical in nature. Since the form of Eq. (5-21) is identical to the equation for a harmonic oscillator, we may think of the electromagnetic field as a collection of harmonic oscillators, one for each frequency (or wave number $\boldsymbol{k}$) and polarization direction η. The separation in energy between harmonic oscillator states is in units of $\hbar\omega = \hbar ck$. It is now quite

[redacted]

them are called *electric* multipole transitions, indicated hereafter as $E\lambda$, and *magnetic* multipole transitions, labeled $M\lambda$. In terms of spherical harmonics, they may be written in the following ways:

$$
\begin{aligned}
\boldsymbol{A}_{\lambda\mu}(E\lambda,\boldsymbol{r}) &= \frac{-i}{k}\nabla\times(\boldsymbol{r}\times\nabla)\Big(j_\lambda(kr)Y_{\lambda\mu}(\theta,\phi)\Big) \\
\boldsymbol{A}_{\lambda\mu}(M\lambda,\boldsymbol{r}) &= (\boldsymbol{r}\times\nabla)\Big(j_\lambda(kr)Y_{\lambda\mu}(\theta,\phi)\Big)
\end{aligned}
\qquad (5\text{-}24)
$$

where $j_\lambda(kr)$ is a spherical Bessel function of order λ. A general solution of $\boldsymbol{A}(\boldsymbol{r},t)$ is a

[redacted]

We are now in a position to calculate the contribution of each multipole order to the transition probability given in Eq. (5-13). On inserting the density of final states and using the multipole operator given in Eq. (5-25) for H', we can express the transition probability for multipole λ from an initial nuclear state $|J_iM_i\zeta\rangle$ to a final nuclear state $|J_fM_f\xi\rangle$ as

$$\mathcal{W}(\lambda; J_i\zeta \rightarrow J_f\xi) = \frac{8\pi(\lambda+1)}{\lambda[(2\lambda+1)!!]^2}\frac{k^{2\lambda+1}}{\hbar}B(\lambda; J_i\zeta \rightarrow J_f\xi) \tag{5-27}$$

[redacted]

magnetic multipole operators in the long-wavelength limit simplify to the following forms:

$$\begin{aligned}
\boldsymbol{O}_{\lambda\mu}(E\lambda) &= \sum_{i=1}^{A} e(i) r_i^{\lambda} Y_{\lambda\mu}(\theta_i, \phi_i) \qquad (5\text{-}29)\\
\boldsymbol{O}_{\lambda\mu}(M\lambda) &= \sum_{i=1}^{A} \Big\{ g_s(i)\boldsymbol{s}_i + g_\ell(i) \frac{2\boldsymbol{\ell}_i}{\lambda+1} \Big\} \cdot \nabla_i (r_i^{\lambda} Y_{\lambda\mu}(\theta_i, \phi_i))
\end{aligned}$$

[redacted]

of inverse length and $\hbar$ is in units of energy multiplied by time, the units of electric transition probability is

$$W(E\lambda): \quad \frac{[\mathrm{fm}^{-1}]^{2\lambda+1}}{[\mathrm{MeV\text{-}s}]} \times e^2[\mathrm{fm}]^{2\lambda}$$

Using the relation $e^2 = \alpha\hbar c$ and the fact that the fine structure constant α is a dimensionless quantity and $\hbar c$ is in units MeV-fm, we obtained the correct result,

[redacted]

The same condition is expressed also by the factor $\Delta(J_f, \lambda, J_i)$ in Eq. (5-7) and is implicit in the reduced matrix element of Eq. (5-28). Together with the energy dependence in $\mathcal{W}(\lambda)$, we have the multipolarity selection rule that, for allowed values of λ,

$$\mathcal{W}(E\lambda) \gg \mathcal{W}(E(\lambda+1)) \qquad\qquad \mathcal{W}(M\lambda) \gg \mathcal{W}(M(\lambda+1))$$

We shall not make a comparison of electric with magnetic transitions until later, as the nature of these two operators is quite different.

The operator for an $E\lambda$-transition is proportional to spherical harmonics $Y_{\lambda\mu}(\theta, \phi)$,

[redacted]

The reason for the dominance of electric over magnetic transitions may be inferred from the fact that the operators for magnetic transitions differ from the corresponding ones for electric transitions by a gradient operator ∇. Since it is a differential operator, it tends to reduce the size of the matrix element. Similar differences are also found in other electromagnetic processes.

Internal conversion and internal pair production. Besides γ-ray emission, electromagnetic decay can also take place through internal conversion and internal pair

[redacted]

to a higher state as a result of changes in the surrounding electromagnetic field. This can take place, for example, as the result of a charged particle passing nearby. We shall see in §8-1 that the nuclear transition matrix elements involved are identical to γ-ray transitions we have been discussing here.

5-4 Single-Particle Value

It is useful to have some feeling of the magnitude of reduced transition probability

[redacted]

We shall now make some further simplifying assumptions so that the averages of both quantities on the right-hand side may be evaluated without having to specify explicitly the single-particle states involved.

The radial dependence of Eq. (5-34) is contained in the integral

$$\langle r^{\lambda}\rangle = \int R^{*}_{n_f\ell_f}(r)\, r^{\lambda} R_{n_i\ell_i}(r)\, r^{2}\, dr$$

where $R_{n_f\ell_f}(r)$ and $R_{n_i\ell_i}(r)$ are, respectively, the normalized radial wave functions of

[redacted]

of the last form of operator $\boldsymbol{O}_{\lambda\mu}(M\lambda)$ given in Eq. (5-30) to reduce the nuclear matrix element to a single-particle matrix element. In parallel with Eq. (5-36), we have the expression

$$\begin{aligned}B_{\text{est.}}(M\lambda) &= \sum_{\mu M_f} |\langle J_f M_f \xi | \boldsymbol{O}_{\lambda\mu}(E\lambda) | J_i M_i \zeta\rangle|^2 \\ &= \lambda(2\lambda+1)\langle r^{(\lambda-1)}\rangle^2 \\ &\quad \times \sum \Big\{ \Big(g_s - \frac{2g_\ell}{\lambda+1} \Big)\end{aligned}$$

[redacted]

Table 5-2: Weisskopf single-particle estimates for $E\lambda$- and $M\lambda$-transition probabilities and widths.

Order	$E\lambda$			$M\lambda$		
λ	$\mathcal{W}$ (s^{-1})	Γ (MeV)		$\mathcal{W}$ (s^{-1})	Γ (MeV)	
1	1.02×10^{14}	6.75×10^{-8}	$A^{2/3}E_\gamma^3$	3.15×10^{13}	2.07×10^{-8}	E_γ^3
2	7.28×10^{7}	4.79×10^{-14}	$A^{4/3}E_\gamma^5$	2.24×10^{7}	1.47×10^{-14}	$A^{2/3}E_\gamma^5$
3	3.39×10	2.23×10^{-20}	$A^{2}E_\gamma^7$	1.04×10	6.85×10^{-21}	$A^{4/3}E_\gamma^7$

[redacted]

Reactions such as those given by Eqs. (5-39) to (5-42) are referred to as semi-leptonic processes, since both hadrons and leptons are involved. Some weak interaction processes do not involve any leptons at all and are called non-leptonic processes, such as those given by Eqs. (5-43) and (5-44). There are also purely leptonic processes, such as the decay of a muon,

$$\mu^- \rightarrow e^- + \overline{\nu}_e + \nu_\mu \tag{5-45}$$

Our main concern will be the semi-leptonic mode, as nuclear β-decay is a part of it.

[redacted]

are mediated by charged bosons, as illustrated by the examples given in Eq. (5-41) to (5-45). The neutral boson Z^0 is the source of *neutral weak current* and is responsible for reactions such as neutrino-electron scattering:

$$\nu + e^- \rightarrow \nu + e^-$$

In spite of its small cross section, such processes are important, for example, in trapping the energy inside the outer shell of a supernova, preventing large amounts being carried away by neutrinos immediately after the explosion (see §10-4).

[redacted]

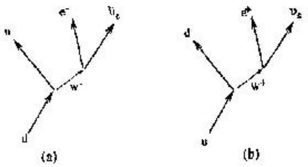
u
e⁻
ν̄e
W⁻
d
d
e⁺
νe
W⁺
u

(a) (b)

[redacted]

parity transformation is the operation that inverts the spatial coordinates,

$$(x, y, z) \xrightarrow[P]{} (-x, -y, -z)$$

It is often described in terms of taking a mirror image of the coordinate system, as can be seen from Fig. 5-3. Under a parity operation a scalar (S) is unchanged, but a vector (V) of the type we normally use changes sign. Where needed, we shall refer to such vectors as ***polar vectors***, to distinguish them from axial vectors, to be defined next. Examples of polar vectors are spatial location $\boldsymbol{r}$ and momentum $\boldsymbol{p}$.

[redacted]

weak decays was proposed as the resolution. The confirmation of this suggestion came from observing the β^--decay of ^{60}Co [154],

$$ {}^{60}\mathrm{Co} \rightarrow {}^{60}\mathrm{Ni} + e^- + \bar{\nu}_e $$

The ground state of odd-odd nucleus ${}^{60}_{27}$Co has spin-parity $J^\pi = 5^+$, as shown in Fig. 5-4. A nonzero spin is essential here so that the nucleus can be polarized (that is, have the nuclear spin aligned) along the direction of an external magnetic field. The ground state decays predominantly (99% of the time) to the $J^\pi = 4^+$ excited state of ${}^{60}_{28}$Ni at

[redacted]

we shall take here as twice the intrinsic spin $\boldsymbol{s}$ along its direction of motion

$$h = \frac{\boldsymbol{\sigma} \cdot \boldsymbol{p}}{|\boldsymbol{p}|} \tag{5-51}$$

For a massless particle, the eigenvalues of h can only be ± 1. An example of a particle with only two possible orientations is provided by the photon, which, as we have seen earlier, can have only two linearly independent polarization directions. For electrons and other particles with nonzero rest mass, the helicity takes on values $\pm v/c$. Particles

[redacted]

by a delta function. This leaves only the strengths, or coupling constants, of each of the two operators to be specified.

The two coupling constants for nuclear β-decay may be put in the form of a vector coupling constant G_V for the vector part of the operator and a Gamow-Teller coupling constant C_A for the axial-vector part. We have already seen that G_V is related to G_F, the coupling constant underlying all weak interaction processes. The second simplifying feature of nuclear β-decay processes is that G_A is related to G_V. This results from the belief that the difference between G_A and G_V is only because of modifications of the

[redacted]

5-6 Nuclear Beta Decay

Nuclear β-decay is the process by which a nucleus made of Z protons and N neutrons decays to a nucleus of the same nucleon number A but with $(Z \pm 1, N \mp 1)$. A β^--decay,

$$A(Z,N) \longrightarrow A(Z+1, N-1) + e^- + \overline{\nu}_e \qquad (5\text{-}55)$$

may be regarded as the transformation of one of the neutrons in the nucleus to a proton, and a β^+-decay,

[redacted]

The "additional" amount of $2m_ec^2$ is required to create the positron emitted and the atomic electron that must be ejected in going from a neutral atom of Z electrons to one with $Z - 1$ electrons.

In contrast, for electron capture, we have the relation

$$Q_{EC} = (M(Z, N) - M(Z - 1, N + 1))c^2 - B_e$$

where B_e is the ionization energy of the atomic electron captured. Since B_e is of the order of 10 eV, we may ignore it unless we are concerned with accuracies of such order

[redacted]

where $|J_f M_f \xi\rangle$ is the wave function of the daughter nuclear state. The two factors of $V^{-1/2}$ are required to normalize the two lepton wave functions. We may expand the product of the two plane waves in terms of spherical harmonics, as done in Eq. (B-11),

$$e^{i\boldsymbol{k}\cdot\boldsymbol{r}} = \sum_{\lambda=0}^{\infty} \sqrt{4\pi(2\lambda+1)}\, i^{\lambda} j_{\lambda}(kr)\, Y_{\lambda 0}(\theta, 0)$$

where $k = |\boldsymbol{k}| = |\boldsymbol{k}_e + \boldsymbol{k}_\nu|$ and θ is the angle between $\boldsymbol{k}$ and $\boldsymbol{r}$. The spherical harmonics $Y_{\lambda\mu}(\theta, \phi)$ are independent of the azimuthal angle ϕ for $\mu = 0$.

[redacted]

For the moment, we shall be mainly concerned with the two leading-order terms in the expression, generally known as the operators for "allowed transitions." The higher order terms involve spherical harmonics of orders greater than zero, and these induce the "forbidden decays."

For the allowed decays, the nuclear part of the $\beta^{\pm}$-decay operator has the form

$$O_{\lambda\mu}(\beta) = G_V \sum_{j=1}^{A} \tau_{\mp}(j) + G_A \sum_{j=1}^{A} \boldsymbol{\sigma}(j)\boldsymbol{\tau}_{\mp}(j) \tag{5-61}$$

[redacted]

The amount E_ν is a part of the energy released by the nucleus in going from the initial to the final state. The rest of the energy is taken up by the charged lepton and the daughter nucleus.

Instead of the Q-value, it is customary to express the energies involved in a β-decay in terms of the maximum kinetic energy of the charged lepton emitted. The reason for this is a practical one, as the electron (or positron) energy is a quantity that can be observed directly. The maximum value, E_0, is generally referred to as the *end-point* energy in the sense that it is the point, in a plot of the number of charged leptons

[redacted]

where all factors related to V, the (arbitrary) normalization volume, cancel each other, and the summation over M_f takes care of the requirement to include all the possible nuclear final states.

Let us ignore the possible small neutrino mass for the time being. The expression for $\mathcal{W}(p_e)$ simplifies to

$$\mathcal{W}(p_e) = \frac{1}{2\pi^3\hbar^7c^3}\sum_{\mu M_f}\left|\langle J_f M_f \xi|O_{\lambda\mu}(\beta)|J_i M_i \zeta\rangle\right|^2 F(Z,E_e)p_e^2(E_0-E_e)^2 \qquad (5\text{-}68)$$

[redacted]

The excited states of the daughter nucleus ^{3}He are very high in energy, and as a result, the ground state is the only possible final nuclear state for the decay. In addition, the radioactive tritium source is relatively easy to prepare. There are, however, several difficulties associated with the measurement that are hard to overcome. The first one arises mainly from the low counting rate near the end point, a common problem in all nuclear β-decays. The second one comes from the fact that the expected rest mass energy of the neutrino is comparable to the excitation energies in atoms. As a result, atomic effects, which are seldom a problem in nuclear measurements, become

[redacted]

where the dimensionless function

$$\begin{aligned} f(Z,E_0) &\equiv \int F(Z,E_e)\left(\frac{p_e}{m_e c}\right)^2\left(\frac{E_0-E_e}{m_e c^2}\right)^2\frac{dp_e}{m_e c} \\ &= \frac{1}{m_e^5 c^7}\int F(Z,E_e)\,p_e^2(E_0-E_e)^2\,dp_e \end{aligned} \qquad (5\text{-}69)$$

is known as the Fermi integral. Except in the trivial case of $Z = 1$ for the daughter nucleus, the integral must be evaluated numerically. Extensive tables of calculated

[redacted]

matrix element. The half-life, on the other hand, involves $f(Z, E_0)$, which depends in a complicated way on the proton number of the daughter nucleus and the end-point energy. We have already encountered a similar problem in the study of electromagnetic decays. There, half-lives are dominated by energy dependence and the quantities more directly related to nuclear physics are the reduced transition probabilities $B(\lambda)$ and transition rates measured in Weisskopf units. The ft-value in β-decay plays a similar role as $B(\lambda)$ in electromagnetic transitions.

The measured ft-values are found to vary over many orders of magnitude, especially

[redacted]

Allowed β-decay. Let us return to the operator for allowed decays, given earlier in Eq. (5-61). The Fermi term involves only the isospin-raising or isospin-lowering operator. As a result, it is possible to carry out the summation over all the nucleons explicitly,

$$\sum_{j=1}^{A} \boldsymbol{\tau}_{\mp}(j) = \boldsymbol{T}_{\mp}$$

where $\boldsymbol{T}_{\mp}$ lowers or raises the third component of the isospin for the nucleus as a whole. If isospin is an exact quantum number, the matrix element for the Fermi operator can

[redacted]

The last point, on the parity selection rule, comes from the fact that $\boldsymbol{\sigma}$ is an axial-vector operator and, consequently, cannot change the parity between initial and final states. The absolute values of Gamow-Teller matrix elements are generally smaller than those for Fermi transitions, as both spin and isospin are involved.

For allowed decays, the square of the nuclear transition matrix element may be written as

$$\sum_{\mu M_f} \left| \langle J_f M_f \xi | O_{\lambda\mu}(\beta) | J_i M_i \zeta \rangle \right|^2$$

[redacted]

daughter nuclei with one more proton than the parent. Most examples of superallowed β-decay are positron emitters for this reason. An example is the case of

$$^{14}\mathrm{O} \rightarrow {}^{14}\mathrm{N} + e^{+} + \nu_e$$

leading to the 0^{+} first excited state of ^{14}N at 2.311 MeV. The half-life of ^{14}O is 74 s and the Q-value of the reaction is 1.12 MeV. The ft-value is 3037.7 s, among the smallest known. If the initial and final nuclear states are truly isobaric analogue states of each other, the value of the Fermi matrix element may be obtained using Eq. (5-71) without

[redacted]

tensor ranks are $Y_{\ell m}(\theta, \phi)$ and $(Y_\ell(\theta, \phi) \times \sigma)_{\lambda\mu}$. The angular momentum and parity selection rules for the ℓth-order forbidden transition are then

$$\Delta J = \ell \text{ or } \ell \pm 1 \qquad \Delta\pi = (-1)^\ell$$

The isospin selection rule remains the same as for allowed decays,

$$\Delta T_0 = 1 \qquad \Delta T = 0,\ 1 \qquad \text{but } T_i = 0 \rightarrow T_f = 0 \text{ transitions forbidden}$$

[redacted]

particle, as well as the target nucleus, may be excited in the process. In addition, (π^+, π^0) and (π^-, π^0) reactions are also used to examine charge exchange processes, as we shall see later in §8-6.

With pions and heavy ions, it is also possible to initiate double-charge exchange reactions, such as (π^-, π^+) and (π^+, π^-). In such reactions, a pair of nucleons change their charge states at the same time. These reactions are sensitive to two-body correlations in nuclei, a question of importance in nuclear structure studies. The information is closely related to that obtained through two-nucleon transfer reactions discussed in

[redacted]

in an experiment using the reaction

$$\text{neutrino} + {}^{37}\text{Cl} \rightarrow e^- + {}^{37}\text{Ar}$$

The source of the neutrino for this classic experiment by Davis [48] in 1955 was a reactor which produces mainly $\bar{\nu}_e$. The observed cross section for this reaction was much smaller than one expected for Majorana neutrinos. The result therefore constitutes a proof that neutrinos are Dirac particles.

However, in a neutrinoless double β-decay, the neutrinos are virtual particles and

[redacted]

Problems

5-1. The first excited state of ^{20}Ne at 1.634 MeV has $J^{\pi} = 2^{+}$ and decays to the 0^{+} ground state with a half-life of 0.655 ps. Find the reduced transition probability $B(E2)$ in units of e^2fm^4 and the transition rate W in Weisskopf units.

5-2. The following list of corrected superallowed ft-values in seconds are taken from Sirlin [129]:

[redacted]

Chapter 6

Nuclear Collective Motion

The experimental observations outlined in the previous two chapters on energy level positions, static moments, transition rates, and reaction cross sections provide us with the basis for nuclear structure studies. Many of the observed properties of a nucleus

[redacted]

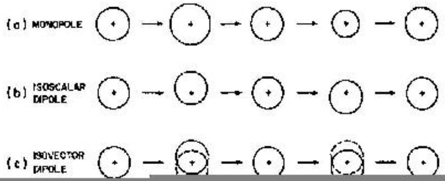
(a) MONOPOLE
(b) ISOSCALAR DIPOLE
(c) ISOVECTOR DIPOLE

[redacted]

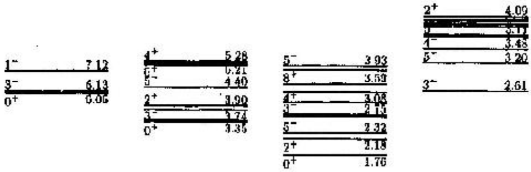
1⁻ 7.12
3⁻ 6.13
0⁺ 6.06
4⁺ 5.28
6⁺ 5.21
5⁻ 4.40
2⁺ 3.90
3⁻ 3.74
0⁺ 3.35
5⁻ 3.93
8⁺ 3.59
4⁺ 3.08
3⁻ 2.75
5⁻ 2.32
2⁺ 2.18
0⁺ 1.76
2⁺ 4.09
3.71
4⁻ 3.48
5⁻ 3.20
3⁻ 2.61

[redacted]

The energy associated with vibrational motion may be discussed in terms of the variations in the shape parameters $\alpha_{\lambda\mu}(t)$ as functions of time. When a nucleus changes its shape, nucleons are moved from one location to another. This constitutes the kinetic energy in the vibration. At the same time, when a nucleus moves away from its equilibrium shape, the potential energy is increased, the same as a spring is compressed or stretched. Unless constrained, it will return to its lowest potential energy state. The amount of energy involved in each case is related to the nuclear shape and, as a result, the shape parameters become the appropriate canonical variables to describe the motion

[redacted]

Comparing with the expression for an harmonic oscillator,

$$\frac{d^2x}{dt^2} + \omega^2 x = 0$$

we obtain the result that, for small oscillations, the amplitude $\alpha_{\lambda\mu}(t)$ undergoes harmonic oscillation with frequency

$$\omega_\lambda = \left(\frac{C_\lambda}{D_\lambda}\right)^{1/2}$$

[redacted]

admixture with states formed by other excitation modes becomes important. As a result, it is not always easy to identify a complete set of three-phonon excited states. One such example, shown in Fig. 6-3, is found in ^{118}Cd.

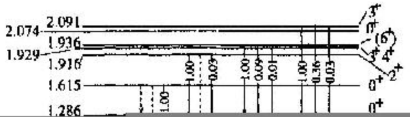
2.091
2.074
1.936
1.929
1.916
1.615
1.286
1.00
0.03
1.00
0.09
0.01
1.00
0.36
0.03
1.00
3^+
0^+
(6^+)
3^+
4^+
2^+
0^+
0^+

[redacted]

Since the reduced transition probability is proportional to the square of the transition matrix element, we find that its value between n- and $(n-1)$-phonon states is proportional to n, the number of phonons in the initial state of the decay,

$$B(E\lambda, n \rightarrow n-1) \propto n$$

Because of this relation, we expect the transition probability from a two-phonon state to a one-phonon state to be enhanced in comparison with single-particle estimates and roughly twice the value from a one-phonon state to a zero-phonon state in the same

[redacted]

there must be a superposition of many different vibrational modes. Furthermore, the various modes must be strongly coupled to each other so that energy can flow from one mode to another. The mathematical problem involved here is not simple, but the basic physical idea is a sound one. However, we shall not examine this topic here.

6-2 Giant Resonance

Giant resonance is a term used to describe the observed concentration of excitation

[redacted]

resonance in different nuclei is well described by the relation

$$E_1 \approx 78A^{-1/3} \tag{6-4}$$

Prominent dipole resonances, as well as other types of giant resonances, have been observed in almost all the nuclei studied, from ^{16}O to ^{208}Pb, as can be seen later in Figs. 6-5 and 6-6.

Giant resonances come from collective excitation of nucleons. As we shall see later in §7-2, the energy gap between two adjacent major shells, is roughly $41A^{-1/3}$ mega-

[redacted]

separate groups of particles and excitation comes from the motion of one group with respect to the other, with little or no excitations within each group. In the dipole mode, the neutrons are moving in one direction along some axis while the protons are going in the opposite direction, as shown schematically in Fig. 6-1(c). The opposite phase keeps the center of mass of the entire nucleus stationary. Since neutrons and protons are moving "out of phase" with respect to each other, it is an isovector mode of excitation. In contrast, if the neutrons and protons move in phase, it is an isoscalar dipole vibration, with all the nucleons moving in the same direction at any given time. The net result,

[redacted]

from the generally accepted value of $\eta \sim 0.5$, we see that the measured giant dipole cross sections exhaust most of the total possible strengths. Furthermore, the result is essentially independent of the particular nucleus from which the strength sum is taken. The large variety of nuclei included in Fig. 6-5 represents a wide spectrum of ground state wave functions. The fact that the value of S is essentially given by the TRK sum rule, without any specific reference to the ground state wave function of any of the nuclei involved, may be taken as another evidence of the collective nature of the excitation process itself.

[redacted]

in charge exchange reactions. For example, in the case of the ^{90}Zr$(p,n)^{90}$Nb reaction, part of the strength appears as a "giant resonance" in the neutron spectra, as shown in Fig. 6-7, at energies just below the isobaric analogue strength peak.

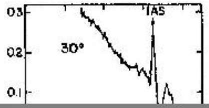

[redacted]

Components of the operators involved here have the following properties:

$$\boldsymbol{\sigma}_\mu^\dagger = (-1)^\mu \boldsymbol{\sigma}_{-\mu} \qquad\qquad \boldsymbol{\tau}_\mp^\dagger = \boldsymbol{\tau}_\pm$$

as can be seen for $\boldsymbol{\sigma}_\mu$ in Eq. (3-31) and for $\boldsymbol{\tau}_\pm$ in Eq. (2-20). On substituting the explicit form of the Gamow-Teller operator into Eq. (6-6), we obtain the strength sum for β^+-transitions,

[redacted]

may not depend on how high in energy the excitation strengths are measured and may therefore be tested against observations.

A departure from Eq. (6-10) may also indicate the presence of particles other than nucleons in the nucleus, such as Δ-particles, resulting from exciting the internal degrees of freedom in nucleons. Such a component in the intermediate state has been conjectured as a possibility in many other reactions. For this reason, there is a great amount of interest in measuring the difference in strength between (p,n) and (n,p) reactions. However, the experiments are difficult to carry out and, at this moment, the results are still too preliminary to draw any conclusion.

For stable nuclei, departure from spherical equilibrium shape is generally small in the ground state region. Relatively large deformations are found, for example, in medium-heavy nuclei with $150 \lesssim A \lesssim 180$ and heavy nuclei with $220 \lesssim A \lesssim 250$, as shown in Fig. 6-8. The largest deformations, or "superdeformations," as we shall see later in §9-2, are observed in the excited configurations of medium-weight nuclei, created when two heavy ions are fused together into a single entity.

There are five shape parameters, $\alpha_{2\mu}(t)$ for $\mu = -2$ to $\mu = +2$.

The orientation of a nucleus in space is specified by three parameters, for example, the Euler angles $(\omega_\alpha, \omega_\beta, \omega_\gamma)$. Since the orientation is immaterial, as far as the intrinsic nuclear shape is concerned, we can regard the Euler angles as three "conditions" to be imposed on the five parameters. This may be expressed formally by transforming the coordinate system to one fixed with the nucleus,

$$\alpha_{\lambda\mu} = \sum^{2} a_{\mu\nu} \mathcal{D}^{J}_{MM'}(\omega_\alpha, \omega_\beta, \omega_\gamma)$$

[redacted]

laboratory and the motion is more conveniently described by a coordinate system that is fixed in the laboratory. Each system is better suited for a different purpose, and we shall make use of both of them in our discussions. Following general convention, the intrinsic coordinate axes are labeled by subscripts 1, 2, and 3 to distinguish them from the laboratory coordinates, labeled by subscripts x, y, and z.

We can also see from Eq. (6-12) that there is a certain degree of redundancy in the values of β and γ. For example, with positive values of β, we have prolate shapes for $\gamma = 0°$, 120°, 240°. However, the symmetry axis is a different one in each case: 3 for

[redacted]

Rotational wave function. For the convenience of discussing rotational motion, we shall divide the wave function of a nuclear state into two parts, an intrinsic part describing the shape and other properties pertaining to the structure of the state and a rotational part describing the motion of the nucleus as a whole in the laboratory. Our main concern for the moment is in the rotational part, labeled by J, M, and K. Since it is a function of the Euler angles only, it must be given by $\mathcal{D}^J_{MK}(\alpha,\beta,\gamma)$ of Eq. (A-8), which relates the wave functions of an object in two coordinate systems rotated with respect to each other by Euler angles (α,β,γ). In terms of spherical harmonics, the function $\mathcal{D}^J_{MK}(\alpha,\beta,\gamma)$ may be defined by the relation

[redacted]

The parity of a rotational state is given by Eq. (6-15). Because of the phase factor, the wave function for a positive-parity $K = 0$ state vanishes if the J-value is odd. As a result, only states with even J-values are allowed for a $K = 0^+$ band. Similarly, there are no states with even J-values in a $K = 0^-$ band. The results may summarized as

$$J = \begin{cases} 0,\ 2,\ 4,\ldots & \text{for } K^\pi = 0^+ \\ 1,\ 3,\ 5,\ldots & \text{for } K^\pi = 0 \end{cases}$$

For $K > 0$, the only restriction on the allowed spin in a band is $J \geq K$, arising from

[redacted]

inertia and by the positions of their band heads. Both features, in turn, depend on the structure of the intrinsic state assumed by the deformed nucleus that is rotating in the laboratory frame of reference.

Quadrupole moment. Besides energy level positions, the static moments of members of a band and the transition rates between them are also given by the rotational model. The discussions below depend on the property that all members share the same intrinsic state and differ only in their rotational motion. Let us start with the quadrupole

[redacted]

To compare the values calculated using Eq. (6-19) with experimental data, we need a knowledge of the intrinsic quadrupole moment Q_0 as well as the value of K for the band. The latter may be found from the minimum J-value for the band. For Q_0, one way is to make use of the measured value of Q_{JK} for another member. If the values deduced in this way are available for several members of a band, they can be also used as a consistency check of the model. Unfortunately, it is difficult to measure the quadrupole moment for more than one member of a band. The alternative is make use of electric quadrupole transition rates, as we shall see next.

Magnetic dipole transitions may be studied in the same way. The $K = 0$ bands are not suitable for our purpose here, as the J-values of the members differ by at least two units and $M1$-transitions are forbidden by angular momentum selection rule. The magnetic transition operator defined in Eq. (5-30) is given in terms of single-nucleon gyromagnetic ratios g_ℓ for orbital angular momentum and g_s for intrinsic spin. Here, we are dealing with collective degrees of freedom. Instead of g_ℓ and g_s, it is more appropriate to use g_R and g_K, respectively, the gyromagnetic ratio for rotational motion and the intrinsic state of a deformed nucleus. In terms of these two quantities,

[redacted]

that the nucleus is not a rigid body and centrifugal force generated by the rotation can modify slightly the intrinsic shape when the angular velocities are high. Centrifugal stretching is observed at the higher J end of many rotational bands. In general, such small and gradual changes in the moment of inertia may be accounted for empirically by adding a $J^2(J+1)^2$-dependent term in the rotational Hamiltonian.

- Rotational bands have been observed with members having very high spin values, for example, $J \approx 40\hbar$ and beyond. Such high-spin states occur quite high in

[redacted]

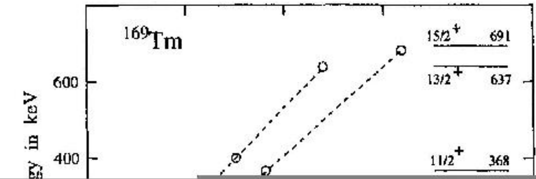

[redacted]

with spin one unit less, as seen in the ^{19}F example in Problem 6-3. The signature of a rotational band can still be recognized by the fact that one-half of the members, $J = \frac{1}{2}, \frac{5}{2}, \frac{9}{2}, \ldots$, possess a E_J versus $J(J+1)$ relation with one (almost constant) slope, and the other half with a different slope, as can be seen from Eq. (6-25).

The basic concept behind rotational models is the classical rotor. Quantum mechanics enters in two places, a trivial one in the discrete (rather than continuous) distribution of energy and angular momentum and a more important one in evaluating the moment of inertia. The latter is a complicated and interesting question, as

[redacted]

operators, we have the conjugate annihilation operators $\boldsymbol{s}$ and $\boldsymbol{d}_\mu$. To complete the definition of these operators, we need to specify the commutation relations between them:

$$\begin{aligned} &[\boldsymbol{s}^\dagger, \boldsymbol{s}] = 1 &\qquad& [\boldsymbol{s}^\dagger, \boldsymbol{s}^\dagger] = [\boldsymbol{s}, \boldsymbol{s}] = 0 \\ &[\boldsymbol{d}^\dagger_\mu, \boldsymbol{d}_\nu] = \delta_{\mu\nu} && [\boldsymbol{d}^\dagger, \boldsymbol{d}^\dagger] = [\boldsymbol{d}, \boldsymbol{d}] = 0 \\ &[\boldsymbol{s}^\dagger, \boldsymbol{d}_\mu] = [\boldsymbol{s}, \boldsymbol{d}^\dagger_\mu] = [\boldsymbol{s}, \boldsymbol{d}_\mu] = [\boldsymbol{s}^\dagger, \boldsymbol{d}^\dagger_\mu] = 0 \end{aligned} \tag{6-27}$$

All other operators necessary to calculate nuclear properties in the model are expressed

[redacted]

In addition to energy, operators corresponding to other observables in the space span by the s- and d-bosons can also be expressed in terms of tensor products of the boson creation and annihilation operators. For example, the possible electromagnetic transition operators in the space are

$$\boldsymbol{O}_0(E0) = \beta_0(\boldsymbol{d}^\dagger \times \overline{\boldsymbol{d}})_0 + \gamma_0(\boldsymbol{s}^\dagger \times \overline{\boldsymbol{s}})_0 \qquad \boldsymbol{O}_{1\mu}(M1) = \beta_1(\boldsymbol{d}^\dagger \times \overline{\boldsymbol{d}})_{1\mu}$$

$$\boldsymbol{O}_{2\mu}(E2) = \alpha_2\{(\boldsymbol{s}^\dagger \times \overline{\boldsymbol{d}})_{2\mu} + (\boldsymbol{d}^\dagger \times \overline{\boldsymbol{s}})_{2\mu}\} + \beta_2(\boldsymbol{d}^\dagger \times \overline{\boldsymbol{d}})_{2\mu}$$

[redacted]

written in terms of s-boson operators alone,

$$H_{\rm seniority} = \epsilon_s s^\dagger s + a_0 s^\dagger s^\dagger s s$$

This is the *seniority* scheme [49], known to be useful in classifying many-nucleon states in the jj-coupling scheme (see §7-1). Here, pairs of nucleons with their angular momentum coupled to zero are treated differently from those that are not coupled to $J = 0$. From this property, we see also that IBA-1 has a pairing structure built into the Hamiltonian and can therefore account for many of the observed nuclear properties in which

[redacted]

a binding energy to the valence nucleons. Active neutron pairs and proton pairs can be put into the space by boson creation operators acting on the vacuum. The IBA-2 therefore provides a basis to study a wide variety of nuclear structure phenomena, from single-particle to collective degrees of freedom (for more details, see Arima and Iachello [9]).

Interacting boson models belong to a more general type of approach to nuclear structure studies sometimes known as *algebraic* models. We have seen evidence that symmetries play an important role in nuclear structure. For each type of symmetry,

[redacted]

6-4. The ground state of ${}^{152}_{63}\mathrm{Eu}$ is known to be 3^- with an electric quadrupole moment of $+3.16 \times 10^2\ e\mathrm{fm}^2$. Find the intrinsic quadrupole moment of the nucleus for the ground state and deduce the value of δ defined in Eq. (6-18), the difference between R_3 and $R_\perp$. What is the shape of this nucleus?

6-5. The following $E2$-transition rates appear in a table of nuclei in terms of natural line width Γ for the $K = 0^+$ band in ${}^{20}\mathrm{Ne}$: 2^+ (1.63 MeV) → 0^+ (ground) 6.3×10^{-4} eV, 4^+ (4.25 MeV) → 2^+ (1.63 MeV) 7.1×10^{-3} eV, 6^+ (8.78 MeV) → 4^+ (4.25 MeV) 0.100 eV, and 8^+ (11.95 MeV) → 6^+ (8.78 MeV) 1.2×10^{-3} eV.

[redacted]

Chapter 7

Microscopic Models of Nuclear Structure

Matrix method to solve the eigenvalue problem. Our calculation is centered around the solution to the many-body eigenvalue problem

$$H\Psi_\alpha(r_1, r_2, \ldots, r_A) = E_\alpha \Psi_\alpha(r_1, r_2, \ldots, r_A) \tag{7-1}$$

where E_α is the energy of the state with wave function $\Psi_\alpha(r_1, r_2, \ldots, r_A)$. The Hamiltonian consists of a sum of the kinetic energy of each nucleon with reduced mass μ_i and the interaction between any two nucleons,

[redacted]

In terms of matrices, Eq. (7-4) may be written as

$$\begin{pmatrix} H_{11} & H_{12} & \cdots & H_{1D} \\ H_{21} & H_{22} & \cdots & H_{2D} \\ \vdots & \vdots & \ddots & \vdots \\ H_{D1} & H_{D2} & \cdots & H_{DD} \end{pmatrix} \begin{pmatrix} C_1^\alpha \\ C_2^\alpha \\ \vdots \\ C_D^\alpha \end{pmatrix} = E_\alpha \begin{pmatrix} C_1^\alpha \\ C_2^\alpha \\ \vdots \\ C_D^\alpha \end{pmatrix} \tag{7-5}$$

The eigenvalues E_α are the roots of the secular equation,

[redacted]

Hamiltonian in Eq. (7-1) may be expressed in the form

$$H = \sum_{i=1}^{A} h(\boldsymbol{r}_i) + \sum_{i \neq j = 1}^{A} \tilde{V}(\boldsymbol{r}_i, \boldsymbol{r}_j) \tag{7-7}$$

where $\tilde{V}(\boldsymbol{r}_i, \boldsymbol{r}_j)$ is the *residual* two-body interaction, the original nucleon-nucleon interaction V_{ij} in Eq. (7-2) minus contributions already included in $h(\boldsymbol{r}_i)$. We shall not be concerned here with the technical question of transforming the Hamiltonian from the

[redacted]

- Single-neutron and single-proton removal energies,

$$\begin{aligned} S_n(Z,N) &= E_B(Z,N) - E_B(Z,N-1) && (7\text{-}8) \\ S_p(Z,N) &= E_B(Z,N) - E_B(Z-1,N) && (7\text{-}9) \end{aligned}$$

  are much larger than those in the neighboring even-even nuclei, as shown in Fig. 7-2.

- The intrinsic shape of the ground states is spherical, as can be seen from observations

[redacted]

the many-body Hamiltonian in the independent particle model may be rewritten in terms of the single-particle energies

$$H = \sum_k \epsilon_k n_k$$

Here the summation on k is over all single-particle states and n_k is the number operator measuring the occupancy of single-particle state k.

In this picture, the magic numbers arise because of the fact that the nuclear single-

[redacted]

Table 7-1: Harmonic oscillator radial wave functions.

$R_{1s}(r) = 2\left(\frac{\nu^3}{\pi}\right)^{1/4} e^{-\nu r^2/2}$	$R_{1p}(r) = \sqrt{\frac{2^3}{3}}\left(\frac{\nu^5}{\pi}\right)^{1/4} r e^{-\nu r^2/2}$
$R_{1d}(r) = \sqrt{\frac{2^4}{15}}\left(\frac{\nu^7}{\pi}\right)^{1/4} r^2 e^{-\nu r^2/2}$	$R_{2s}(r) = \sqrt{\frac{2^3}{3}}\left(\frac{\nu^3}{\pi}\right)^{1/4} (\frac{3}{2} - \nu r^2) e^{-\nu r^2/2}$
$R_{1f}(r) = \sqrt{\frac{2^5}{105}}\left(\frac{\nu^9}{\pi}\right)^{1/4} r^3 e^{-\nu r^2/2}$	$R_{2p}(r) = \sqrt{\frac{2^4}{15}}\left(\frac{\nu^5}{\pi}\right)^{1/4} (\frac{5}{2} - \nu r^2) r e^{-\nu r^2/2}$

[redacted]

where the factor $\frac{1}{2}$ on the right-hand side comes from the fact that, for a particle in a three-dimensional harmonic oscillator well, the average of potential energy is half of the total energy. Using this relation, we obtain the expectation value of r^2 in a state with N harmonic oscillator quanta to be

$$\langle r^2\rangle_N = \frac{\hbar}{\mu\omega_0}\left(N + \tfrac{3}{2}\right) \tag{7-14}$$

The mean-square radius of a nucleus made of A nucleons is given by the average over

[redacted]

Combining the results of Eqs. (7-16) and (7-17), we obtain

$$\begin{aligned}\hbar\omega_0 &= \frac{1}{A}\frac{\hbar^2}{\mu\langle r^2\rangle}\frac{1}{2}\left(\frac{3}{2}A\right)^{4/3}\\ &= \frac{\hbar^2}{\mu\frac{3}{5}(r_0A^{1/3})^2}\frac{3}{4}\left(\frac{3}{2}A\right)^{1/3}\\ &= \frac{5}{4}\left(\frac{3}{2}\right)^{1/3}\frac{\hbar^2}{\mu r_0^2}A^{-1/3}\approx 41A^{-1/3}\ \text{MeV}\end{aligned} \tag{7-18}$$

[redacted]

For $a < 0$, a single-particle state with $j = j_> = \ell + \frac{1}{2}$ is lowered in energy. Since the amount of depression increases with increasing ℓ-value, a $j_>$-state for large ℓ may be pushed down in energy by an amount comparable to $\hbar\omega_0$, the energy gap between two adjacent harmonic oscillator major shells. As a result, the $j_>$-states of the largest ℓ in a shell with N oscillator quanta may be moved closer to the group of states belonging to the $N - 1$ shell below. [In practice, as we shall later in Eq. (7-29), one needs also an ℓ^2-dependent term in the single-particle Hamiltonian to lower the centroid energy of states with large ℓ-values so that the $j_<$-states are prevented from moving up to join the states

[redacted]

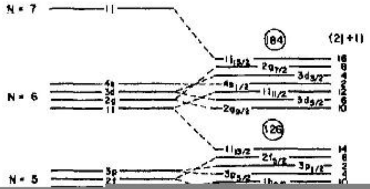
N = 7
1j
184
(2j+1)
1j15/2
2g7/2
3d3/2
4s1/2
1i11/2
3d5/2
2g9/2
16
8
4
2
12
6
10
N = 6
4s
3d
2g
1i
126
1i13/2
2f5/2
3p1/2
3p3/2
14
6
2
4
10
N = 5
3p
2f

[redacted]

the single-particle orbits. The alternate convention is basically the same except that instead of starting with 1 for the first occurrence of a particular ℓ-value, it starts with 0. Both conventions are equally well used and some confusion may arise on occasion. Furthermore, both conventions are different from that used in atomic physics and in certain quantum mechanics textbooks.

7-3 Hartree-Fock Single-Particle Hamiltonian

[redacted]

wave function. Either we can modify the single-particle wave functions themselves such that Eq. (7-22) is satisfied or, alternatively, we can keep the single-particle basis fixed and alter Φ_0 by adding to it small amounts of Slater determinants made of products of different A single-particle states. As long as there is a complete set of states and all possible variations are applied, these two methods are equivalent to each other.

We shall take the latter approach for our derivation here. With a fixed single-particle basis, each many-particle basis state may be labeled by the single-particle states occupied. For example, the trial ground state wave function Φ_0 in Eq. (7-20)

[redacted]

each term in the sum vanishes. From this requirement, we obtain the condition

$$\langle \Phi_{kt} | H | \Phi_0 \rangle = \langle \Phi_{kt} | \sum_{i=1}^{A} h(\boldsymbol{r}_i) + \sum_{i \neq j=1}^{A} V(\boldsymbol{r}_i, \boldsymbol{r}_j) | \Phi_0 \rangle = 0 \tag{7-23}$$

For the one-body part of the Hamiltonian, the only possible nonvanishing contribution comes from cases where the left- and right-hand sides of the matrix element differ by no more than the single-particle state of one nucleon. Similarly, for the two-body part of the Hamiltonian, only matrix elements with occupied single-particle states on the two

[redacted]

only on the single-particle state k to its right (or the single-particle state i to its left). However, $V(\boldsymbol{r}_1, \boldsymbol{r}_2)$ is a two-body operator, and we shall see how to "reduce" it to one-body.

Let us distinguish between two sets of single-particle states here by using Greek letters α, β, ... to indicate the original, or trial, single-particle states and the Roman alphabet, r, s, ... , for the Hartree-Fock single-particle states that satisfy Eq. (7-24). A two-body interaction potential may be expressed in the original basis as an operator in the following way:

[redacted]

approximately using the trial functions for $|r\rangle$ and $|t\rangle$. The solutions obtained are only a first approximation, as we have not used the proper wave functions to evaluate the matrix elements to start with. On the other hand, the results represent a better approximation of the "true" Hartree-Fock wave functions than the trial wave functions used as the input. Now we can make improvements by using the first approximation results as the input and carrying out the calculation again. The process is repeated until self-consistency in the solution is achieved; that is, the solutions obtained are essentially identical to the wave functions used to evaluate the matrix elements.

[redacted]

Deformed single-particle Hamiltonian. Let us again assume axial symmetry for simplicity. Instead of Eq. (7-19), we can adopt a semi-empirical single-particle Hamiltonian of the following form:

$$h(\boldsymbol{r}) = h_0 + h_\delta + a\,\boldsymbol{\ell}\cdot\boldsymbol{s} + b\,\boldsymbol{\ell}^2 \qquad (7\text{-}29)$$

Here h_0 is the spherical part, generally taken to be the Hamiltonian of an isotropic three-dimensional harmonic oscillator similar to that given in Eq. (7-10),

[redacted]

ℓ^2 terms and treat $h_0 + h_\delta$ in a cylindrical coordinate system. The Hamiltonian of Eq. (7-29) can now be written as

$$h = -\frac{\hbar^2}{2\mu}\nabla^2 + \tfrac{1}{2}\mu\{\omega_3^2 x_3^2 + \omega_\perp^2(x_1^2 + x_2^2)\} \tag{7-31}$$

where the oscillator frequency along the symmetric axis has the value,

$$\omega_3 = \omega_0\sqrt{1 - \tfrac{4}{3}\delta_{\rm osc}} = \overline{\omega}(1 - \tfrac{2}{3}\delta_{\rm osc})$$

[redacted]

The label n_3 (or $n_\perp$) is a good quantum number in this limit and may be used as a label for Nilsson states even in cases where the deformation is not large.

When the term $a\boldsymbol{\ell}\cdot\boldsymbol{s}$ is included, states with different projections of orbital angular momentum on the symmetry axis are no longer degenerate. As a result, in the limit of large deformation, the projection of the orbital angular momentum along the symmetry axis,

$$\lambda = \pm n_\perp, \pm(n_\perp - 2), \ldots, \pm 1, 0$$

may be used as the fourth label. The set of four labels $[Nn_3\lambda\Omega]$ completely specifies

[redacted]

the nuclear shape. Furthermore, the Hamiltonian given by Eq. (7-29) is a very simple and intuitive one. The fact that it works so well in describing a wide range of nuclear properties has led to a number of interesting developments in nuclear structure. Some of these will be discussed in §9-2.

For an independent particle approximation in the deformed basis, we can ignore the residual interaction. The nuclear Hamiltonian is then a sum of the single-particle Hamiltonian given in Eq. (7-29) for all the active nucleons. The single-particle states may be divided into three groups: the core states, the valence states, and the empty

[redacted]

$1d_{5/2}$-orbit with nucleons. The even-even nuclei are not of interest here, as the ground states must have $J^\pi = 0^+$ because of pairing interaction. For an odd-mass nucleus, the ground state spin in an independent particle model is given by that of the single-particle state occupied by the unpaired nucleon. Consequently, nuclei ^{19}F, ^{19}Ne, ^{21}Ne, and ^{23}Na are expected to have $J^\pi = \frac{5}{2}^+$ for their ground state spins if they are spherical. Experimentally, they turn out to be different and have, instead, values $\frac{1}{2}^+$, $\frac{1}{2}^+$, $\frac{3}{2}^+$, and $\frac{3}{2}^+$, respectively.

In the deformed basis, the observed values are understood in the following way. The

[redacted]

particle model. We shall discuss this topic in the next section for the spherical case. In a deformed basis, the mathematics involved is far more complicated, as we no longer have the simplicity of rotational symmetry, and hence spherical tensors and angular momentum algebra, to help us.

7-5 Spherical Shell Model

We have seen in the previous three sections that independent particle models, using ei-

[redacted]

Alternatively, in the jj-coupling scheme, the orbital angular momentum and the intrinsic spin of each nucleon is coupled together first to form the nucleon spin $\boldsymbol{j}_i$,

$$\boldsymbol{j}_i = \boldsymbol{\ell}_i + \boldsymbol{s}_i$$

then the nuclear spin

$$\boldsymbol{J} = \sum_{i=1}^{A} \boldsymbol{j}_i$$

[redacted]

single-particle states is therefore essentially always empty for our purposes and, as a result, may also be ignored.

The only remaining single-particle states are the few near the Fermi energy and they form the *active*, or *valence*, space from which reasonable approximate wave functions of the nuclear states of interest can be constructed. The aim of the nuclear shell model is to solve the eigenvalue problem in the space constructed out of single-particle states in the active space alone.

[redacted]

observed energy level positions of single-particle states in the region of interest. The empirical values of ϵ_i may be found, for example, in nuclei one nucleon away from closed shells where some of the low-lying states are made predominantly by the coupling of one nucleon or one hole to the ground states of the closed shell nuclei. Such states are, in principle, exactly the ones described by Hartree-Fock eigenvectors. If a realistic Hamiltonian is used in the Hartree-Fock calculation, one may expect to obtain essentially the same eigenvalues as the experimental energies. For nuclei away from closed shells, correlations other than $1p1h$ also play an important role, and the

[redacted]

Equations (7-39) and (7-40) may be regarded as two coupled equations for $P\Psi$ and $Q\Psi$.

We can now proceed to solve these equations by expressing $Q\Psi$ in terms of $P\Psi$. Equation (7-40) may be put into the form

$$EQ\Psi - QHQ\Psi = QHP\Psi$$

This can be rewritten as

$$(E - QH)Q\Psi = QHP\Psi$$

[redacted]

From the comparison we identify that

$$V_{\text{eff}} = V + V\frac{1}{E - QH}QV \tag{7-44}$$

This is still a formal solution and its usefulness lies mainly in the possibility of making an infinite series expansion for $(E - QH)^{-1}$. This is an advantage, as it permits an order-by-order calculation of the effective potential.

An equivalent way of writing the second term on the right-hand side of Eq. (7-44)

[redacted]

The procedure outlined above to find the effective interaction in a shell-model space is also known as a *renormalization* procedure, as it "renormalizes" an interaction for the complete Hilbert space to one suitable for the truncated space. We have now a complete set of procedures that can generate a effective interaction in a truncated shell-model space starting from one between free nucleons. The steps involved are the following. Using free nucleon-nucleon interactions, we construct an interaction for bound nucleons. This allows us to carry out a Hartree-Fock type of calculation to obtain a physical single-particle basis and a residual interaction in the space. Finally,

[redacted]

Since the overlap of $|1' \cdots k'-1, k'+1 \cdots t'-1, t'+1 \cdots A'>$ and $|1 \cdots k-1, k+1 \cdots t-1, t+1 \cdots A>$ vanishes unless all $A-2$ single-particles states are the same on both sides, we find the result that the A-body matrix element is zero if more than two single-particle states are different from each other, a result we used earlier in going from Eq. (7-23) to Eq. (7-24). If, on the other hand, no more than two single-particle states are different from each other, the A-body matrix element can be expressed in terms of two-body matrix elements $< k', t'|\hat{O}(2)|k, t>$. Thus, if all the matrix elements in two-particle space are given, we can calculate any Hamiltonian matrix elements in

[redacted]

the two single-particle states as given by Eq. (A-11), and a similar factor $(-1)^{j_r+j_s-J}$ for recoupling the spins. Because of these relations, we have the following symmetries among two-body matrix elements:

$$W^{JT}_{rstu} = (-1)^{j_r+j_s-J-T} W^{JT}_{srtu} = (-1)^{j_t+j_u-J-T} W^{JT}_{rsut} = (-1)^{j_r+j_s-j_t-j_u} W^{JT}_{srut} \tag{7-47}$$

Because of Eqs. (7-46) and (7-47), the number of independent two-body matrix elements required to define an effective interaction in a finite shell-model space may be sufficiently

[redacted]

two-body matrix elements,

$$\epsilon = -8.36 \text{ MeV} \qquad W^0 = -3.12 \text{ MeV} \qquad W^2 = -1.59 \text{ MeV}$$
$$W^4 = -0.366 \text{ MeV} \qquad W^6 = 0.0714 \text{ MeV}$$

With these five pieces of input obtained from ^{41}Ca and ^{42}Ca, we are now in a position to calculate all the energy levels in the $1f_{7/2}$ shell-model space from ^{43}Ca to ^{48}Ca.

The calculated results for ^{43}Ca to ^{46}Ca are listed in Table 7-3. The binding energies with respect to the ^{40}Ca core are given in the first row and the excitation energies in

[redacted]

the single-particle energy instead.) Such overall shifts in the defining matrix elements, in general, do not affect the excitation energies.

The calculated energy level positions of the excited states in ^{43}Ca to ^{46}Ca are also compared with experimental values in Table 7-3. There are obviously more excited states in these nuclei than the ones listed. Since our model space is restricted to the $1f_{7/2}$-orbit alone, only observed levels belonging to this model space may be used in the comparison. In principle, one can identify a $1f_{7/2}$-level by measuring the angular distribution of one-nucleon transfer strengths (see §8-2). In practice, the identification

[redacted]

This was done by Cohen and Kurath [45]. The calculation serves two useful purposes. The first is to demonstrate that the idea behind a semi-empirical effective Hamiltonian is a sound one. Once the 17 parameters are determined from fitting a given number of pieces of data, the effective Hamiltonian obtained may be used to calculate the shell-model values corresponding to the data used. Since a fitting procedure was used, the calculated results are not necessarily identical to the observed ones used as input. The quality of the agreement serves as a measure for the validity of such an approach. Normally the success of a least-squares fit to some functional form is given

[redacted]

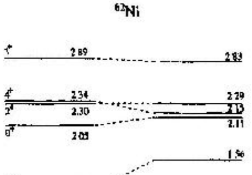
^{62}Ni
4+
2.89
2.83
4+
2.34
2.29
2+
2.30
2.15
0+
2.05
2.11
1.56
1.17

Figure 7-6: Comparison of the observed energy levels of ^{62}Ni with the results of a shell-model calculation in the $1f_{5/2}$-, $2p_{3/2}$-, and $2p_{1/2}$-space using a renormalized effective interaction. The observed quadrupole

[redacted]

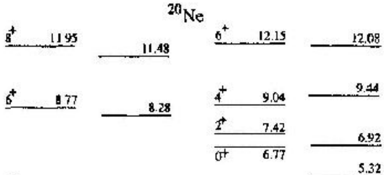
^{20}Ne
8^+ 11.95
11.48
6^+ 12.15
12.08
6^+ 8.77
8.28
4^+ 9.04
9.44
2^+ 7.42
6.92
0^+ 6.77
5.32

[redacted]

is exactly what is expected from the Fourier transform of the density of a nucleon in the 1*p*-shell (see Problem 7-7). On the other hand, two minima are observed in ^{16}O. A simple shell model puts the active nucleons for the ground state of ^{16}O also in the 1*p*-shell. The appearance of the second minimum implies that there is a substantial admixture of configurations having nucleons excited into the *ds*-shell. If we insist on carrying out the form factor calculation for ^{16}O using only active nucleons in the 1*p*-shell space, a correction factor, for example, in the form

$$f(r) = 1 - e^{-\alpha r^2}$$

[redacted]

Because of its direct connection with the individual nucleon degrees of freedom in a finite nucleus, the shell model can also be used to "simulate" data for testing other models. This is similar to numerical simulations used in many other fields to supplement data and to help us to probe aspects of nature that are difficult to examine experimentally. Such numerical "experiments" do not substitute actual observations involving real nuclei. However, they provide a convenient avenue to test our models and our understanding of the physical situation and are useful as a tool to further our knowledge of nuclei.

the effect of nucleon-nucleon interaction into the mean field experienced by individual nucleons. There is a large variety of mean-field theories. One of the attractive features here is that the approach can also be extended easily to a relativistic one (see, e.g., Celenza and Shakin [43]). Although we have limited ourselves to nonrelativistic quantum mechanics here, many aspects of nuclear structure and nuclear scattering, especially those involving intermediate- and high-energy probes, require a relativistic treatment. For this reason, mean-field theories are becoming an increasingly more important tool in nuclear studies.

[redacted]

Problems

7-1. If ${}^{25}_{12}\mathrm{Mg}$ is a spherical nucleus, what are the most likely spin, parity, and isospin of its ground state? If, instead, it is a deformed nucleus with prolate deformation, what are the most likely spin and parity?

7-2. The nuclei ${}^{5}_{2}\mathrm{He}$, ${}^{5}_{3}\mathrm{Li}$, ${}^{17}_{8}\mathrm{O}$, ${}^{17}_{9}\mathrm{F}$, ${}^{41}_{20}\mathrm{Ca}$, ${}^{41}_{21}\mathrm{Sc}$, ${}^{209}_{82}\mathrm{Pb}$, and ${}^{209}_{83}\mathrm{Bi}$ may be considered to be made of a neutron or a proton outside a closed shell core. Use an independent particle model to deduce their ground state spin and parity. From this information

[redacted]

7-7. The explicit forms of the radial wave function for a spherical harmonic oscillator potential well are given in Table 7-1. Use these to show that the form factor, the Fourier transform of the radial density $\rho_{n\ell}(r) = |R_{n\ell}(r)|^2$, is positive for the 1$s$-orbit in the region $q = 0$ to infinity [i.e., no node in $F^2(q)$] and changes sign once at $q^2 = 6\nu$ for the 1p-orbit [one node in $F^2(q)$]. For the 1d-orbit, the sign changes twice, i.e., there are two nodes in $F^2(q)$.

[redacted]

Chapter 8

Nuclear Reactions

A large fraction of our knowledge on the properties of nuclei is derived from nuclear reactions. When an incoming particle is scattered off a target nucleus, the outcome depends on a combination of three factors: the reaction mechanism, interaction between

[redacted]

From this expression, we see that the Sommerfeld number may be viewed as the ratio between $\frac{1}{2}R_s$ and the reduced de Broglie wavelength,

$$\frac{\lambda}{2\pi}=\frac{1}{2\pi}\frac{h}{p}=\frac{\hbar}{\mu v}$$

A small η means that the Coulomb field is weak compared with the available kinetic energy in the scattering. Under such conditions, the wave function of the incident particle is not greatly modified by the Coulomb field and Born approximation applies.

[redacted]

spirit, the Coulomb excitation cross section, from an initial state i to a final state f, may be expressed as

$$\left(\frac{d\sigma}{d\Omega}\right)_{fi} = \frac{1}{2J_i+1}\sum_{M_fM_i}|P_{M_fM_i}|^2\left(\frac{d\sigma}{d\Omega}\right)_{\text{point}} \tag{8-3}$$

where J_i is the initial spin of the target nucleus and M_i and M_f are, respectively, the projections of the initial and final spins on the quantization axis. The square root of the constant of proportionality is given by the expression

[redacted]

The spherical harmonics in Eq. (8-4), with $\theta = \frac{1}{2}\pi$ and $\phi = 0$, may be written explicitly in terms of λ and μ,

$$Y_{\lambda\mu}(\tfrac{1}{2}\pi, 0) = \begin{cases} (-1)^{(\lambda+\mu)/2}\sqrt{\dfrac{2\lambda+1}{4\pi}}\dfrac{\sqrt{(\lambda-\mu)!(\lambda+\mu)!}}{(\lambda-\mu)!!(\lambda+\mu)!!} & \text{for } \lambda+\mu = \text{even} \\ 0 & \text{otherwise} \end{cases}$$

The differential scattering cross section for Coulomb excitation in Eq. (8-3) now reduces to

[redacted]

Eq. (8-6), except that $B(E\lambda)$ is replaced by the corresponding $B(M\lambda)$, the reduced transition probability for magnetic multipole λ. Differences in the angular distribution between $M\lambda$- and $E\lambda$-transitions are contained in the differences between $df(M\lambda)/d\Omega$ and $df(E\lambda)/d\Omega$. These are also given in Alder et al. [6, 7], and the values for low-order magnetic multipoles are plotted in Fig. 8-1.

Multiple scattering. Coulomb excitation is useful in creating excited states in the target or projectile nucleus. Because of the intense electromagnetic fields accompany-

[redacted]

substate M of a $J^\pi = 2^+$ level. Instead of proceeding to a higher state, the second "scattering" takes the nucleus to a state having a different M-value for the same 2^+ level. This is known as *reorientation* effect. Such a process is sensitive to the expectation value of $O(E2)$ of the level involved, the 2^+-state in the example here. The matrix element, in this case, is related to the quadrupole moment of the excited state. As a result, the quadrupole moment of an excited state may be deduced from the cross section of Coulomb excitation. The value obtained depends somewhat on the nuclear model used; however, this is not a serious problem in general, as reliability of the

[redacted]

For a reaction involving two particles, we need three sets of quantum numbers to label the channel in an unambiguous way. For instance, in the exit channel we need a set of labels to specify the wave function of the emerging particle, a second set to identify the wave function of the residual nucleus, and a third set to describe the relative motion between these two particles, as illustrated in §B-4. Returning again to the ^{48}Ca$(p,n)^{48}$Sc example above, the reaction can also leave the ^{48}Sc nucleus in an excited state. Since the wave function for an excited state of ^{48}Sc is different from that for the ground state, we have a different exit channel, distinguishable from the

[redacted]

and Γ_β/Γ is the probability for $\mathcal{N}$ decaying through channel β. The reaction cross section from an entrance channel α to an exit channel β is given by the product of the probability to form the compound nucleus $\mathcal{N}$ and that for $\mathcal{N}$ to decay through β,

$$\sigma_{\beta\alpha} = \sigma_\alpha \frac{\Gamma_\beta}{\Gamma} \tag{8-8}$$

To make further progress, we shall make use of some of the results given in §B-4.

Let us assume that in each reaction channel there is a radius R_c, the *channel radius*, outside which there is no interaction between the scattered particle and the residual

[redacted]

From Eq. (B-40), we arrive at the expression for the reaction cross section

$$\sigma^{\mathrm{re}} = \frac{\pi}{k^2}(1 - |\eta_0|^2) = \frac{\pi}{k^2}\frac{-4kR_c\Im\rho_0}{(\Re\rho_0)^2 + (\Im\rho_0 - kR_c)^2} \tag{8-11}$$

If ρ_0 is real, corresponding to the case of scattering from a real potential, σ^{re} vanishes, as expected. Furthermore, since the reaction cross section cannot be negative, the absolute value of η_0 must be less than or equal to unity. This, in turn, implies that the imaginary part of ρ_0 must be negative.

[redacted]

The cross sections are expressed here in terms of the relevant widths instead of parameters a and b as we have done above.

The elastic channel has two parts, a nonresonating part with amplitude proportional to $1-\exp\{2ikR_c\}$ and a resonating part containing an energy-dependent factor $(E-E_r)$ in the denominator. The contribution of the nonresonating part corresponds to a smooth background in the cross section and is usually called *shape-elastic* or *potential* scattering. At $E \approx E_c$, the elastic cross section is dominated by the resonating part,

[redacted]

$W \gg \Gamma^i$. Our discussion is still limited to s-wave scattering for simplicity. We shall not attempt a more general discussion here, as it will also involve angular momentum coupling factors.

Using the fact that the number of levels in the interval is given by W/D, where D is the average level spacing, we can define a mean width,

$$\bar{\Gamma}_\alpha = \frac{D}{W}\sum_i \Gamma_\alpha^i$$

[redacted]

8-3 Direct Reaction

Stripping and pickup reactions. A good example of a direct reaction is a (d,p) process in which a deuteron, with more than a few mega-electron-volts of kinetic energy, incidents on a target nucleus. In the exit channel, a proton is observed. Since the deuteron is a loosely bound system of a proton and a neutron, we can envisage that the neutron is captured into one of the single-particle orbits of the target nucleus without

[redacted]

We shall take the Green's function here to have the explicit form

$$G(\boldsymbol{r},\boldsymbol{r}') = -\frac{1}{4\pi}\frac{e^{ik|\boldsymbol{r}-\boldsymbol{r}'|}}{|\boldsymbol{r}-\boldsymbol{r}'|} \tag{8-19}$$

It satisfies the equation

$$(\nabla^2 + k^2)G(\boldsymbol{r},\boldsymbol{r}') = \delta(\boldsymbol{r}-\boldsymbol{r}')$$

More generally, we can include in the defining equation for $G(\boldsymbol{r},\boldsymbol{r}')$ a part of $V(\boldsymbol{r})$, for example, the part representing the average effect of the target nucleons on the incident particle. This is similar in spirit to the mean-field approach used in nuclear structure

[redacted]

function $\psi(\boldsymbol{r}')$ in Eq. (8-21) is replaced by its first term in Eq. (8-18), and we obtain an approximate form of the scattering amplitude,

$$f(\theta) \approx -\frac{\mu}{2\pi\hbar^2}\int e^{-i\boldsymbol{k}_f\cdot\boldsymbol{r}'}V(\boldsymbol{r}')\,e^{i\boldsymbol{k}_i\cdot\boldsymbol{r}'}\,d^3r' \tag{8-22}$$

This result may be used to find the differential scattering cross section for stripping and pickup reactions.

The expression in Eq. (8-22) can be simplified further by expressing the results in terms of the momentum transfer vector

[redacted]

The multiplication symbols here imply that the wave functions are coupled together to some definite values in angular momentum and isospin.

In the spirit of direct reaction, the deuteron wave function may be taken as the (weakly) coupled state of a proton and a neutron,

$$\phi(d) = \{\phi(p) \times \phi(n)\}$$

To simplify the argument and avoid complications due to angular momentum recoupling, we shall treat the proton purely as a spectator in the entire scattering process. If the neutron is captured into a single-particle state of the target nucleus with orbital

[redacted]

shall see in the next paragraph. Since we have used a plane wave here to approximate the solution to the scattering equation, it is known as the plane wave Born approximation (PWBA). A more rigorous derivation can be found in standard references on direct reactions such as Tobocman [137] and Satchler [123].

From Eqs. (8-26) and (B-7), we find that the differential cross section for direct reaction is given by

$$\frac{d\sigma}{d\Omega} \sim |j_{\ell_t}(qR)|^2$$

[redacted]

Figure 8-4: Angular distribution of neutrons observed in the reaction $^{20}\mathrm{Ne}(d,n)^{21}\mathrm{Ne}$ leading to (a) the 0.338-MeV, $J^\pi = 5/2^+$ level in $^{21}\mathrm{Ne}$ showing a typical $\ell = 2$ one-nucleon transfer and (b) the 2.41-MeV, $J^\pi = 1/2^+$ level, an $\ell = 0$

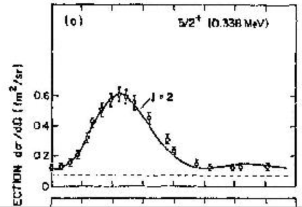

[redacted]

nuclear structure studies.

To simplify the discussion, we shall for the most part consider only elastic scattering. There are two main sources of contribution to the cross section. The first is potential scattering, described earlier in Eq. (8-12). The second comes from multiple scattering with intermediate states involving the excited states of nuclei participating in the scattering. Not all such scattering returns the system back to the incident channel and, as a result, some of the incident flux is lost. Rather than trying to calculate the cross section for each one of the inelastic channels exactly, we shall attempt to represent

[redacted]

Schrödinger equation:

$$H_A(\boldsymbol{r}_1, \boldsymbol{r}_2, \ldots, \boldsymbol{r}_A)\Phi_i(\boldsymbol{r}_1, \boldsymbol{r}_2, \ldots, \boldsymbol{r}_A) = \epsilon_i \Phi_i(\boldsymbol{r}_1, \boldsymbol{r}_2, \ldots, \boldsymbol{r}_A) \tag{8-30}$$

Furthermore, we shall take that Φ_i is normalized to unity and is a part of an orthogonal set of eigenfunctions. The general solution for the complete system, including both the projectile particle and the target nucleus, may be expressed as a linear combination of the products of $\chi_i(\boldsymbol{r}_0)$ and $\Phi_j(\boldsymbol{r}_1, \boldsymbol{r}_2, \ldots, \boldsymbol{r}_A)$,

$$\Psi(\boldsymbol{r}_0; \boldsymbol{r}_1, \boldsymbol{r}_2, \ldots, \boldsymbol{r}_A) = \sum \chi_i(\boldsymbol{r}_0)\Phi_j(\boldsymbol{r}_1, \boldsymbol{r}_2, \ldots, \boldsymbol{r}_A) \tag{8-31}$$

[redacted]

This result may be used to express $Q\Psi$ formally in terms of $P\Psi$,

$$Q\Psi = \frac{1}{E - QHQ} QHP\,P\Psi$$

When this "solution" for $Q\Psi$ is substituted into the right-hand side of Eq. (8-35), we obtain an expression for $P\Psi$,

$$\left\{E - PHP - PHQ\frac{1}{E - QHQ}QHP\right\} P\Psi = 0$$

[redacted]

where the equivalent potential is given by

$$\mathcal{V}(\mathbf{r}_0) = \langle\Phi_0|V|\Phi_0\rangle + \langle\Phi_0|VQ\frac{1}{E - QHQ}QV|\Phi_0\rangle \tag{8-39}$$

Since we have not yet made any approximation in arriving at Eq. (8-38), we do not have any better chance of solving it than the original equation given by Eq. (8-28). The aim of an optical model is to replace the equivalent potential $\mathcal{V}(r_0)$ by an optical model potential U_{opt}, such that the equation

[redacted]

The potential given by Eq. (8-41) is only the *volume term*, in the sense that it depends on the distribution of matter in the whole nucleus. In addition, optical model potentials are known to have a spin dependence. When a nucleon is scattered from a nucleus, the result is sensitive to the relative orientation of the nucleon spin before and after the scattering. One way to measure such a dependence is through the ***analyzing power*** parameter A_y.

Let us define the transverse polarization of the incident and scattered nucleons as positive (or up) if they are oriented in the same direction as the unit vector

[redacted]

To relate to an electrostatic potential $V(\boldsymbol{r})$, we have made use of the relation

$$\boldsymbol{E}(\boldsymbol{r}) = -\frac{dV}{dr}\frac{\boldsymbol{r}}{r}$$

The spin-orbit interaction energy for an atomic electron is then given by

$$W(\boldsymbol{r}) = -\boldsymbol{\mu}_e \cdot \boldsymbol{B}(\boldsymbol{r}) = \frac{e\hbar^2}{m_e^2c^2r}\frac{dV}{dr}\,\boldsymbol{\sigma}\cdot\boldsymbol{\ell}$$

[redacted]

Table 8-1: Proton-nucleus scattering optical model potential parameters for $40 \leq A \leq 208$ and proton laboratory energy $80 \leq T_p \leq 180$ MeV [126].

$$V_0 = 105.5(1 - 0.1625 \ln T_p) + 16.5(N - Z)/A$$

$$r_v = \begin{cases} 1.125 + 0.0010 T_p & \text{for } T_p \leq 130 \text{ MeV} \\ & \text{(except } T_p \leq 180 \text{ MeV for Ca)} \\ 1.255 & \text{for } T_p > 130 \text{ MeV (except Ca)} \end{cases}$$

[redacted]

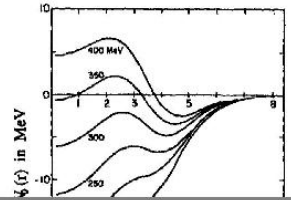

Figure 8-5: Radial shapes of the volume term of a proton-nucleus opti-

[redacted]

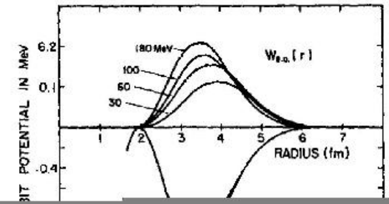
BIT POTENTIAL IN MeV
6.2
0.1
-0.4
180 MeV
100
60
30
$W_{s.o.}(r)$
1
2
3
4
5
6
7
RADIUS (fm)

[redacted]

Figure 8-7: Real part of the volume term of a proton-nucleus optical model potential at different bombarding energies. The upper curves are the direct part of a microscopic potential given by Eq. (8-48) and the lower curves are

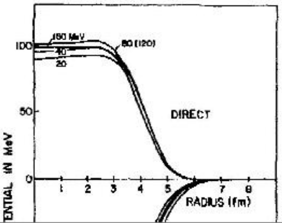

[redacted]

energy dependence of the direct and exchange parts of the folding potential. As illustrated in Fig. 8-7, the direct part is repulsive and the exchange part is attractive. Since the exchange part has a slightly sharper energy dependence than the direct part, the cancellation between repulsive and attractive parts, when we sum the two terms to produce $U_{\rm opt}$, produces an energy dependence that cannot be represented by a simple Woods-Saxon form. In Fig. 8-8 the results for the elastic scattering of 362-MeV protons off a ^{40}Ca target are given as an illustrative example to show that a microscopic optical model potential is quite capable of describing intermediate-energy proton-nucleus scattering to very large momentum transfers.

model potential and favors only specific final states. This is the essence of DWBA for direct reaction. The scattering is separated into two parts, a "background" given by the optical model potential and a direct reaction contribution because of special features in the final state involved. The calculated results obtained this way, as we shall see in the next section, have been found to give a fairly good description of the observed cross sections.

8-5 Intermediate-Energy Nucleon Scattering

[redacted]

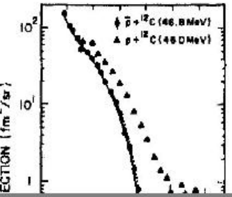

Figure 8-9: Differential cross section for proton (triangles) and antiproton (circles) scattering off ^{12}C

[redacted]

may be thought of as one in which the incident proton excites the target nucleus by promoting one of the nucleons to a higher single-particle state. For a (p, n) reaction, the incident proton is captured and one of the neutrons in the target is ejected in the process. In either case, we find that states strongly excited by the these reactions are those made predominantly of one-particle one-hole $(1p1h)$ excitations built upon the ground state of the target nucleus.

The relation between initial and final nuclear wave functions may be expressed in terms of a "transition density." In the form of an operator, the $1p1h$-transition density of interest here may be written as

[redacted]

(p, p') reaction against, for example, electromagnetic transitions and inelastic electron scattering. For (p, n) and (n, p) reactions, the transition densities are related to β-decay rates and cross sections of charge exchange reactions induced by other probes such as pions and light ions.

So far we have considered the scattered nucleon in a (p, p') reaction to be one and the same as the incident nucleon and distinguishable from those in the target. As we have already seen in the previous section, this is only the direct part of the scattering amplitude which, with the help of Eq. (8-51), may be expressed as

[redacted]

is the one developed by Franey and Love [65]. Alternatively one can take a nuclear matter approach and develop a density-dependent potential, as described earlier for optical model potential studies. In both cases, good descriptions of the observed results up to very large momentum transfers have been obtained for both differential scattering cross sections and spin observables.

Let us recapture what is happening when an intermediate-energy nucleon is scattered off a nucleus. Before the incident nucleon is within the range to interact with one of the nucleons in the nucleus, it is in the field of the nuclear optical model potential.

[redacted]

incident and scattered nucleons, a relativistic treatment is needed (see, e.g., Celenza and Shakin [43] and Danos, Gillet, and Cauvin [47] and references therein).

One possible interest in charge exchange reactions is to relate strong and weak interaction processes, as mentioned earlier in §5-6. Intermediate-energy (p, n) and (n, p) reactions are ideal here, as the reaction mechanism is sufficiently simple and the nuclear matrix elements involved are the same as those in nuclear β-decay. Apart from kinematic factors, the only distinction between nuclear β-decay and charge exchange reactions induced by intermediate-energy nucleons is expected to be the difference in

[redacted]

expect to learn something new about scattering that cannot be achieved with baryons and leptons. It is an integral part of hadron-nucleus scattering studies and forms an essential element of our understanding of hadrons.

Experimentally, intense sources of pions are available from "meson" factories, such as LAMPF (Los Alamos Meson Physics Facility), SIN (Swiss Institute for Nuclear Research), and TRIUMF (Tri-University Meson Facility) (see, e.g., Ref. [109]). There are two features that are special to pion scattering. The first is the strong P_{33}-resonance that produces a Δ-particle from a pion and a nucleon. As we have seen in §2-6, the

[redacted]

reaction

$$\pi^+ + d \rightarrow p + p$$

we can conclude that the two-nucleon process is important in the absorption of fast pions by nuclei. This idea is also corroborated by the relatively large cross sections observed for (π^+, pp) reactions on nuclei in general. Since it involves two nucleons, fast-pion absorption is sensitive to two-particle correlations in nuclei and, as a result, is one of the ways to make such studies. A concise review of the subject can be found, e.g., in Ashery and Schiffer [11].

[redacted]

the form of Eq. (8-54) may be expressed as the operator

$$U_{\rm opt}(r) = -\frac{2\pi}{\mu}\Big\{(b(r)+B(r)) - \nabla\cdot\big\{L(r)(c(r)+C(r))\big\}\nabla + \frac{p_1-1}{2}\nabla^2 c(r) + \frac{p_2-1}{2}\nabla^2 C(r)\Big\} \qquad (8\text{-}55)$$

where μ is the reduced mass of a pion. The kinematic factors

$$p_1 = 1 + \frac{\hbar\omega}{\quad} \qquad\qquad p_2 = 1 + \frac{\hbar\omega}{\quad}$$

[redacted]

and A. These factors express various first-order correlations between nucleons in a nucleus. Second-order correlations in s-waves are included in Eq. (8-55) through the factor

$$\bar{b}_0 = b_0 - \frac{3k_F}{2\pi}(b_0^2 + 2b_1^2)$$

where k_F, the Fermi momentum of a nucleon in a nucleus, is taken to be 1.4 fm^{-1}. A typical set of parameters for 50-MeV incident pions has the values

λ=1.4

[redacted]

particles produced through electromagnetic fields. Both the limited initial flux and the short lifetimes of pions put stringent limitations on what can be achieved. The same difficulties are also present in the detection equipment, as the pion energies we have here are still relatively low for some of the more efficient detection techniques to work well. As a result, measurements of pion-nucleus scattering are usually carried out on light nuclei where the low-lying nuclear levels are well separated in energy. Both elastic and inelastic data are available, and they have been useful in complementing the information obtained with other probes.

[redacted]

that can be carried out.

There are two different double-charge exchange reactions that can be studied with pions, (π^+, π^-) and (π^-, π^+). They are interesting for two reasons. First, these processes must involve at least two nucleons and are therefore useful for investigating nucleon correlations inside a nucleus. Second, the nuclear matrix element that enters into the scattering cross section is related to double β-decay, a process important for understanding the nature of weak interaction itself, as described in §5-6. For all practical purposes, DCX reactions are unique to pions. A nucleon, being an isospin-$\frac{1}{2}$ particle,

[redacted]

Kaons and other mesons. In addition to pions, kaons have been available for scattering off nuclei. Kaons are "strange" mesons involving either an s-quark (K^- and $\overline{K^0}$, strangeness $\mathcal{S} = -1$) or an $\bar{s}$-quark (K^+ and K^0, $\mathcal{S} = +1$). Conservation of strangeness requires that, when a K^--meson is absorbed by a nucleus, one of the nucleons changes into a "strange" baryon such as a Λ-particle ($m_\Lambda c^2 = 1115.6$ MeV) or a Σ-particle ($m_{\Sigma^0}c^2 = 1192$ MeV). The nucleus A becomes a *hypernucleus* ${}_YA^*$ in the process. Because of the large kaon mass ($\sim$500 MeV/c^2), the nucleus is left in a highly excited state, much more so than the case of pion absorption. On the other hand, since there

[redacted]

and the nucleus consisting of A nucleons. Take $c = 5.0$, $z = 0.5$ fm, $Z = 50$, and $A = 120$.

8-7. Find the angular distribution of neutrons emerging from a (n, n) reaction on ^{208}Pb. If the incident energy is sufficiently low, multiple scattering may take place. Assume that each neutron suffers two elastic collisions with the nucleons in the target nucleus before leaving and that the angular distribution of each scattering is given by $|j_0(qR)|^2$, where R is the radius of the target nucleus. Take the incident neutron energy to be 10 MeV in the center of mass and ignore any

[redacted]

Chapter 9

Nuclei under Extreme Conditions

For the most part, we have been looking at stable nuclei and their low-lying excited states. This is, to a large extent, dictated by the availability of data. Until quite

[redacted]

state is another indication that we have a neutron-deficient nucleus at the edge of the valley of stability. The possibility of making such proton-rich species gives us a new window to study nuclear physics. Furthermore, a number of different projectile-target combinations can be used to reach the same final nucleus, providing us with a chance here to examine such nuclei from different angles and to see if their properties can be understood from what we have learned from stable nuclei.

In practice, direct fusion of two heavy ions is not the normal way to create neutron-deficient nuclei. The reason comes from the "extra" energy required to penetrate the

[redacted]

aware of so far. Since it is unlikely that any such nuclei are stable (otherwise they would have been discovered), the only way we can detect their presence is through their decay scheme to lighter ones. As a result, it is necessary to make first the lighter nuclei below the superheavy ones before we can make the identification. Furthermore, from a practical point of view, the only way to build up to the superheavy "island" of relative stability is go one step at time. A recent addition to such a list is the element $(A, Z) = (277, 112)$, created at GSI (Gesellschaft für Schwerionenforschung, Darmstadt, Germany) using a beam of $^{70}_{30}$Zn on a $^{208}_{82}$Pb target [84]. The identification

[redacted]

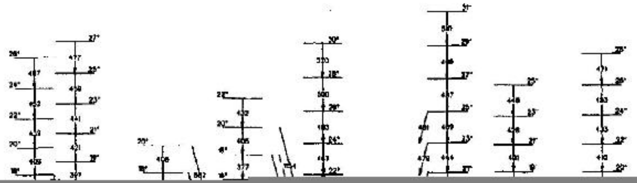
27+
477
25+
459
23+
441
21+
421
26+
487
24+
462
22+
20+
405
18+
408
22+
432
20+
405
377
30+
28+
500
26+
24+
22+
31+
29+
27+
457
25+
23+
21+
448
21+
23+
24+
22+
20+

[redacted]

For a uniform charged sphere of radius reasonable for nuclei, a result of $Z_{\rm cr} < 200$ is obtained. This higher value can also be exceeded in heavy-ion collisions.

The physical meaning of a supercritical field may be seen from the following arguments. As the charge number of a nucleus is increased, the eigenvalues of atomic levels decrease from those given roughly by Eq. (9-1) until the critical value is reached. When this happens, the 1*s*-level becomes degenerate with the negative-energy continuum filled with equal numbers of electrons and positrons. The charge-neutral vacuum is no longer the state of minimum energy. To lower the energy, positrons are released and the remaining vacuum becomes a charged one. This phenomenon is referred to

[redacted]

single-particle states.

The time available for two heavy ions to overlap each other and coalesce in a heavy-ion scattering under such conditions is very short. To gain some perspective, we can make an order-of-magnitude estimate of the amount it takes for the two nuclei to go around each other once. For simplicity, let us assume that the relative speed between the two ions is 1/15 of the speed of light, corresponding to about 5 MeV/nucleon in energy. If the centers of two ions are 10 fm apart, the time to go around each other once at speed $c/15$ is on the order of 10^{-21} to 10^{-20} s. Compared with the interaction

[redacted]

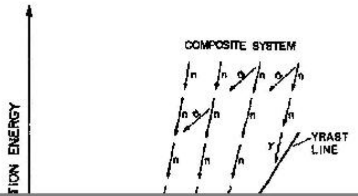
COMPOSITE SYSTEM
n
α
γ
YRAST LINE
TION ENERGY

Figure 9-5: Schematic diagram showing the formation of yrast levels. The composite system created in a heavy-ion collision contains large quantities of excess energy and angular momentum. The amounts carried away by neutron,

[redacted]

also be of interest to the study of the transition from quantum-mechanical to classical description of physical phenomena in general.

Deep inelastic scattering. If the collision energy is slightly above the Coulomb barrier between a pair of heavy ions, many reaction channels are open and compete with each other. In such cases, it is usually impossible to investigate each type of final state individually and the inclusive cross sections are studied instead. The reaction is often referred to as *deep-inelastic* collision, similar to the situation of high-energy

[redacted]

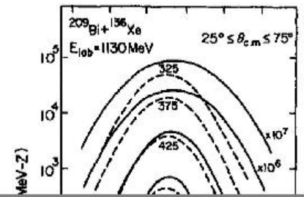

Figure 9-6: Double-differential cross section for the reaction ^{136}Xe on ^{209}Bi at $E_{\rm lab}$=1130 MeV. Each curve is the

[redacted]

particle physics. Let us examine the reasons for putting the enormous investment into this particular effort by looking into the energy densities involved.

In a nucleus of radius $R = 1.2A^{1/3}$, the energy density is given by

$$\rho_A \approx \frac{M_A c^2}{(4\pi/3)R^3} \approx 130 \text{ MeV/fm}^3$$

For three quarks confined in a nucleon of radius $r \approx 1$ fm, the value is even higher, roughly 250 MeV/fm^3. If heavy ions are made to collide with each other at center-of-

[redacted]

contrast to nearly spherical shapes found by putting particles pairwise in $+m$ and $-m$ magnetic substates.

We saw earlier in §6-3 that collective states, under appropriate conditions, form rotational bands. In fact, it is usually through such band structures that rotational features are identified. In general, the spin of a state cannot be measured directly. Instead, it is deduced from such observations as the multipolarities of transitions to states of known spin. A simple example is one that decays by electromagnetic radiation to a state with $J^\pi = 0^+$. If the transition is known to be $E2$ from, for example, the angular distribution of the γ-rays emitted, we can identify the spin-parity of the state

[redacted]

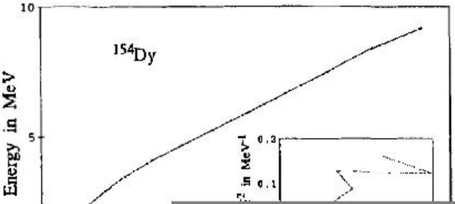

[redacted]

From the point of view of rotational alignment, it may be more instructive to view the same explanation from the following perspective. Consider again a low-lying rotational band in an even-even nucleus for simplicity. The intrinsic state is formed mostly by zero-coupled pairs of particles filling up the lowest available (deformed) single-particle states. As we move up in angular momentum, the rotational energy increases. At some point, it may be more advantageous instead to increase the spin value by breaking a zero-coupled pair and aligning the angular momenta of the two (identical) particles to the maximum possible value of $(2j-1)$ (as the value $2j$ is forbidden by the

[redacted]

γ-rays emitted in transitions from one member to another stand out as sharp lines over and above the background from a large variety of sources.

Heavy-ion reaction has been the method of choice to excite superdeformed bands and high-spin states. The bombarding energy is usually kept as low as possible so that only a minimum amount of excess energy is put into the system. At the same time, the incident energy must be high enough for the ions to penetrate the Coulomb barrier with sufficient probability for the results to be observed. Except for small amounts carried away by nucleons and γ-rays emitted in the reaction, the bulk of the angular

[redacted]

quantities are related to the deformation parameter β of Eq. (6-11) by the relations

$$\begin{aligned} \mathcal{I} &\approx \tfrac{2}{5}AM_NR_0^2(1+0.31\beta)+O(\beta^2) \\ Q_0 &\approx \frac{3}{\sqrt{5\pi}}ZR_0^2\beta(1+0.36\beta)+O(\beta^3) \end{aligned}$$

(See Problem 9-5.) If the spins of the states are known, the (transition) quadrupole moment may be deduced by measuring the lifetimes of the members. For example, Eqs. (6-21) and (6-22) can be used for the case of a $K=0$ band to find the reduced

[redacted]

independent of the actual value of the spins involved.

A related quantity, the kinematical moment of inertia,

$$\mathcal{I}^{(1)} = \frac{\hbar^2}{2}\left(\frac{dE}{d(J_x^2)}\right)^{-1} = \hbar\frac{J_x}{\omega} \tag{9-6}$$

is also used on occasion to characterize rotational bands. At high spin values, we have $J_x \approx J$, and $\mathcal{I}^{(1)}$ reduces to be the same as the classical expression for the moment of inertia (the *static* moment of inertia) given in Eq. (6-13). By differentiating Eq. (9-6)

[redacted]

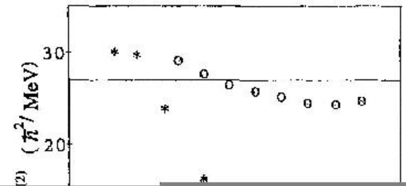

[redacted]

single-particle spectra.

For this purpose, we shall consider only axially symmetric nuclei and, to further simplify the calculation, make use of the harmonic oscillator single-particle Hamiltonian in Cartesian coordinates we saw earlier in Eq. (7-31),

$$h = -\frac{\hbar^2}{2\mu}\nabla^2 + \tfrac{1}{2}\mu\{\omega_3^2x_3^2 + \omega_\perp^2(x_1^2 + x_2^2)\}$$

The eigenvalues are given by Eq. (7-33). For our purpose here, it is more instructive

[redacted]

we have not included terms depending on ℓ^2 and $\ell \cdot s$, the orbits are degenerate with respect to Ω as well as orbital angular momentum. We see that, at large deformations, beyond those shown in the Nilsson diagram of Fig. 7-5, there are new shell structures in the form of large energy gaps in the single-particle spectrum. This happens for both prolate and oblate deformation. The degeneracies, corresponding to magic numbers in the case of the spherical shell model, are marked for the special cases of $\delta_{\rm osc} = +0.6$, corresponding to $\omega_\perp : \omega_3 = 2 : 1$, and $\delta_{\rm osc} = -0.75$, for $\omega_\perp : \omega_3 = 1 : 2$. The fact that shell structure in this simple case happens to match with those for superdeformation [redacted]

By taking out the smoothed value $\langle E_{\text{micro}}\rangle$ in the microscopic result, we avoid any double counting.

Macroscopic calculation. In §4-9, we saw that a crude liquid drop model in the form of a Weizacker semi-empirical calculation can achieve an overall accuracy of a few percent using a set of parameters obtained from fitting known binding energies. For the special case of the variation in energy as a function of deformation we are interested in here, the model can be further simplified in the following ways. Since nuclear matter

[redacted]

with average radius $R_0 = r_0 A^{1/3}$. Similarly, the Coulomb energy may be written as

$$E_{\text{Coulomb}}(N, Z, \text{def.}) = \frac{1}{2}\left(\frac{3Ze}{4\pi R_0^3}\right)^2 \left\{\int d^3r \int d^3r' \frac{1}{|\mathbf{r}-\mathbf{r}'|} - \int d^3r \int d^3r' \left(1 + \frac{|\mathbf{r}-\mathbf{r}'|}{2a_{\text{den}}}\right) \frac{e^{-|\mathbf{r}-\mathbf{r}'|/a_{\text{den}}}}{|\mathbf{r}-\mathbf{r}'|}\right\}$$

where a_{den} has the value $0.99/\sqrt{2}$.

The form of the Coulomb term is taken as

$$V_{\text{Coul}}(\boldsymbol{r}, \text{def.}) = Ze \int_{\Sigma} \frac{d^3r'}{|\boldsymbol{r} - \boldsymbol{r}'|}$$

where the subscript Σ reminds us that the integral is over the (deformed) nuclear volume (for protons).

Shell corrections. The single-particle energy ϵ_i found by solving the eigenvalue equa-

[redacted]

The smoothed Fermi energy is given by

$$N = \int_{-\infty}^{\bar{\lambda}(\nu)} \bar{g}(e, \nu)\, de \qquad\qquad Z = \int_{-\infty}^{\bar{\lambda}(\pi)} \bar{g}(e, \pi)\, de$$

The values of parameters p and γ are adjusted until the final results are essentially independent of small changes in them. In Ref. [145], they are taken to be $p = 6$ and $\gamma = 1.2\hbar\omega_0$, with $\hbar\omega_0$ given by Eq. (7-18).

[redacted]

Instead, we can solve Eq. (9-10) using a suitable value for ω. In this case, nucleons appear as independent particles moving in an average field that is rotating with the frame of reference. The approach belongs to the general one of a cranking model and, for this reason, h^ω is also called a *cranked Hamiltonian.*

The contribution of rotation to the macroscopic term $E_{\rm macro}(N, Z, {\rm def.})$ is quite simple, as the calculation is purely classical. This gives us the result

$$E^{\omega}_{\rm macro}(N, Z, {\rm def.}) = E^{\omega=0}_{\rm macro}(N, Z, {\rm def.}) + \tfrac{1}{2}\mathcal{I}(N, Z, {\rm def.})\,\omega^2$$

[redacted]

data available so far can only give us some rough guidance on what we can expect from RHIC and LHC. We shall briefly review what we have learned from these observations and extrapolate from them what are the initial set of experiments to be carried out at RHIC and LHC once they are in operation. We shall also describe some of the results from lattice gauge calculations to see what are the predications we can make based on our theoretical understanding of the physics of strong interaction.

Transformation of nucleons to quark-gluon plasma. A complete understanding

[redacted]

For massless quarks, the energy carried by each one is pc. From this, we obtain the total energy

$$\begin{aligned} E_q &= g_q \frac{V}{(2\pi)^3\hbar^3} 4\pi \int_0^{\epsilon_F/c} p^3 c \, dp \\ &= g_q \frac{V}{8\pi^2(\hbar c)^3} \epsilon_F^4 \end{aligned}$$

The pressure in a relativistic noninteracting gas is given by

[redacted]

over the contributions from each state k. On replacing the summations by integrations, we obtain the results

$$\begin{aligned} N &= g\frac{V}{(2\pi\hbar)^3}\int_0^\infty \frac{4\pi p^2\,dp}{e^{pc/kT}\pm 1} = g\frac{V}{2\pi^2}\left(\frac{kT}{\hbar c}\right)^3\int_0^\infty \frac{z^2\,dz}{e^z\pm 1} \\ E &= g\frac{V}{(2\pi\hbar)^3}\int_0^\infty \frac{4\pi p^3 c\,dp}{e^{pc/kT}\pm 1} = g\frac{V}{2\pi^2}\left(\frac{kT}{\hbar c}\right)^3 kT\int_0^\infty \frac{z^3\,dz}{e^z\pm 1} \end{aligned}$$

[redacted]

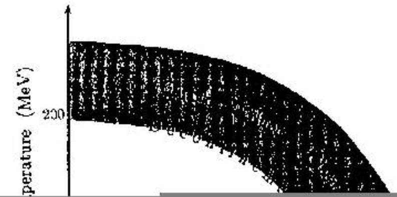

[redacted]

by the relation

$$< \mathbf{r}_f | e^{-iH(t_f - t_i)/\hbar} | \mathbf{r}_i > = \frac{1}{Z} \sum_{\text{all paths}} e^{iS}$$

where the factor $1/Z$ represents all the necessary constants and normalization factors. The physical meaning of the equation is that time evolution is equivalent to averaging over all possible paths, each one weighted by the action. This is very similar to ensemble averaging in statistical mechanics, and for this reason, the whole approach is sometimes referred to as *statistical field theory*.

[redacted]

relation between hadronic matter and QGP. For example, calculations carried out without dynamical quarks show a first-order phase transition at critical temperature around $kT = 260$ MeV. The results with dynamic quarks are less clear, in part, because of the uncertainties due to finite lattice size. Depending on the fermion masses adopted in the calculation, the phase transition can be either first- or second-order. There is also the possibility of hadronic matter crossing over smoothly to QGP without undergoing a phase change.

The interest in lattice gauge calculations is not limited to transition from hadronic

[redacted]

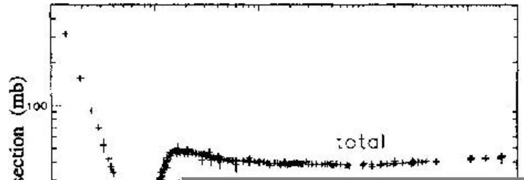

[redacted]

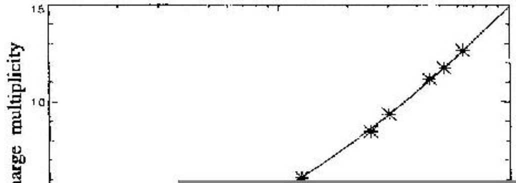

[redacted]

the lack of interference when one nucleus passes through another during a collision. One way to have some idea of the stopping power is to consider E_{zd}, the energy in a small cone around the beam axis. The angle is chosen such that particles within the cone are essentially those from the initial projectile without having undergone any energy loss. In the case of complete stopping, the reaction cross section should peak at $E_{zd} = 0$. Observations at SPS energies show that the maxima occur at small values of E_{zd}, consistent with stopping power of around 90% [131].

A large nuclear stopping power implies a baryon-rich environment, as there is not

[redacted]

of $s\bar{s}$, the production in sulfur+uranium is found to be a factor of 2 to 3 higher relative to that in proton+tungsten (and proton-proton) collisions [3].

If strange quarks are in thermal equilibrium with their lighter counterparts, as expected in a quark-gluon plasma, the ratio of strange to nonstrange mesons is given essentially by that of their respective Boltzmann factors $\exp\{-m_q c^2/kT\}$. Here m_q is the mass of the quark involved. Since the temperature of the plasma is comparable to the mass difference between strange and nonstrange quarks, an enhancement of strange meson production is expected compared with nonequilibrium situations, such

[redacted]

of a QGP scenario [18].

Two-particle interferometry When two identical particles are located close to each other, there is an interference between them, similar to that for optical waves in a double-slit experiment. This phenomenon may be used to deduce the extent of a source of particles. The principle was first applied in 1956 by Hanbury-Brown and Twiss to measure the angular diameter of a star using the correlation between two photons originating from the source. For this reason, it is known as the Hanbury-Brown-Twiss effect. The correlation exists only for a chaotic source and is absent for a coherent one [150].

[redacted]

weakly with quarks, gluons, and hadrons through electromagnetic interaction. As a result, there is a high probability for photons to emerge from the interaction zone without suffering any collisions. In contrast, hadrons have much shorter mean free path and undergo many interactions before leaving the region. For this reason, they reflect mainly the condition near freeze-out. Photons measured in heavy-ion collisions are therefore expected to be related more directly to the thermodynamic state of the QGP created than hadrons.

Photons are also produced in high-energy collisions from a variety of reasons other

[redacted]

of nucleons involved and forms a dominant part of the lepton pairs produced. There are also other sources of lepton pairs, such as $\pi^+\pi^-$ annihilation and decay of neutral mesons. Our concern is with the lepton pairs produced in a QGP. The cross section depends on the temperature of the plasma and, hence, the initial condition that creates it. Theoretical investigations have shown that the production rate increases with temperature. At temperatures below 300 MeV, the cross section is too small to be seen above those coming from the dominant part by the Drell-Yan process. Once the temperature is above 300 MeV, there is a chance that one can isolate the leptons from

[redacted]

to first order in β. Here M is the mass of the nucleus and R_0 is the radius of a sphere having the same volume, and ρ_0 may be found from normalization.

9-6. Use Eqs. (6-18) and (6-12) to show that

$$\delta = 0.95\beta + 0.15\beta^2 + O(\beta^3)$$

where δ is the deformation parameter defined by Eq. (6-18).

[redacted]

Chapter 10

Nuclear Astrophysics

On a bright sunny day, one cannot help but be amazed at the enormous amount of energy outpouring from the sun. At a distance of 1.5×10^{11} m, the amount of electromagnetic radiation received by the earth is 1.4 kW/m^2, corresponding to a total output

[redacted]

Big-bang nucleosynthesis. The variety of nuclei we observe today in the interstellar space comes from a combination of two different sources. The first is the primordial proton and helium together with minute amounts of other light nuclei. The second is made up of material blown off stars that have ended their lives. We shall start with the first one, as it supplies the bulk of the raw material to form stars.

For proton and helium, the relative abundance is observed to be roughly 3 to 1 in mass. This is essentially determined by the neutron-proton mass difference of 1.29 MeV and the deuteron binding energy of 2.23 MeV. When the universe was at temperatures

[redacted]

for each nucleon. For this reason, photodisintegration constitutes an important sink for any deuterons created when the temperature is still sufficiently high.

On further cooling, some deuterons can exist long enough to capture a proton to form ^{3}He. In turn, ^{3}He can capture a neutron and transform it into ^{4}He. We see that once the temperature is sufficiently low for deuterons to last long enough to undergo proton and neutron captures, free neutrons are transformed into bound ones and the total number of neutrons in the universe stays more or less constant until the start of stellar nucleosynthesis at much later stages in the evolution of our universe.

[redacted]

temperature T is given by a Maxwell-Boltzmann distribution

$$\frac{dN}{N} = \frac{2}{\sqrt{\pi}\,kT}\sqrt{\frac{E}{kT}}\,e^{-E/kT}\,dE$$

The long exponential tail ensures that there is a small fraction of the particles with kinetic energies much higher than kT. The second reason is that, since the collision is a quantum-mechanical process, the probability of tunneling is important for any exothermic process, such as proton burning.

mass. For our sun, the present status has been going on already for roughly 5 billion years and is expected to remain in more or less the same state for another 5 billion years or so. In more massive stars, the temperature is higher. This leads to much faster rates of nuclear reaction, and the life span of the hydrogen burning stage can be as short as millions of years.

When the hydrogen fuel is used up in a star, production of nuclear energy from fusing protons into ^{4}He stops and the temperature drops. Without adequate thermal pressure to offset gravity, contraction starts again. However, since the outer layer of the

[redacted]

structure, with each successive inner layer undergoing a later stage of evolution, as shown later in Fig. 10-6.

Nucleosynthesis by α-particle capture produces mainly $4n$ nuclei. Through collisions, decays, and the presence of small amounts of protons, neutrons, deuterons, and ^{3}He, other nuclear reactions participate also in the process and these produce nuclei outside the $4n$ sequence. Partly for this reason, the relative abundances are lower for species other than the $4n$ nuclei.

The release of fusion energy stops at $A \approx 56$ where the binding energy per nucleon

[redacted]

10-2 Rate for Nonresonant Reactions

In a region where there are no resonances, the cross section for nuclear reactions is expected to vary smoothly with energy. This is the most likely situation in nucleosynthesis where the kinetic energy involved is very low compared with those encountered in nuclear excitations. Except for the few cases where there happen to be states near the threshold with the same quantum numbers as the reaction channel of interest, the reaction is nonresonant. In this case, the cross section $\sigma(E)$ as a function of energy E may be written as a product of three factors,

[redacted]

where the reduced mass μ may be approximated as

$$\mu = \frac{A_1 A_2}{A_1 + A_2}$$

with A_1 and A_2 as the nucleon numbers of the two nuclei involved. For $p(v)$, we have made use of the Maxwell-Boltzmann distribution

$$p(v)\,dv = \left(\frac{\mu}{2\pi kT}\right)^{3/2} e^{-\mu v^2/(2kT)} 4\pi v^2\,dv$$

[redacted]

10-3 Conversion of Proton into Helium

The sun is classified as a young star with an age somewhere around the middle of its hydrogen burning phase. The radiant energy comes from fusing four protons into a helium nucleus. The actual process, however, takes place in several distinct steps, as direct conversion of four protons into ^{4}He, being a four-body reaction, is extremely unlikely.

The first step is to make a deuteron through the reaction,

[redacted]

Being unstable, ^{8}B decays by β^+-emission into a ^{8}Be with a half-life of 770 ms,

$$^8\mathrm{B} \rightarrow {}^8\mathrm{Be} + e^+ + \nu_e$$

Since ^{8}Be is unstable with respect to α-decay,

$$^8\mathrm{Be} \rightarrow {}^4\mathrm{He} + {}^4\mathrm{He}$$

we end up again with two ^{4}He nuclei. This is the PPIII-chain, and it converts four [redacted]

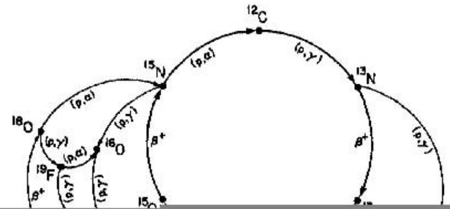

^{12}C
(p,γ)
^{13}N
β+
(p,γ)
^{15}N
(p,α)
^{18}O
(p,α)
(p,γ)
(p,γ)
^{16}O
^{19}F
(p,α)
(p,γ)
(p,γ)
β+
β+
^{15}O

[redacted]

The ^{17}O in the intermediate step above may return some ^{15}N to the main cycle and produce a ^{4}He nucleus through the chain of reaction

$$\begin{aligned} p + {}^{17}\mathrm{O} &\rightarrow {}^{18}\mathrm{F} + \gamma \\ {}^{18}\mathrm{F} &\rightarrow {}^{18}\mathrm{O} + \beta^{+} + \nu_{e} \\ p + {}^{18}\mathrm{O} &\rightarrow {}^{15}\mathrm{N} + \alpha \end{aligned}$$

The ^{18}O produced in the intermediate stage here may also undergo further proton capture and produce ^{19}F through the process

[redacted]

let us summarize first the different types of neutrinos produced in the sun from proton burning. In the previous section, we have seen that neutrinos are produced in the following three reactions in PP-chains:

$$p + p \rightarrow d + e^+ + \nu_e \tag{10-7}$$

$$^8\mathrm{B} \rightarrow {}^8\mathrm{Be}^* + e^+ + \nu_e \tag{10-8}$$

$$e^- + {}^7\mathrm{Be} \rightarrow {}^7\mathrm{Li} + \nu_e \tag{10-9}$$

The neutrino from the $p(p,\gamma)d$ reaction in Eq. (10-7) is the most important one to

[redacted]

$$\begin{aligned} {}^{15}\mathrm{O} &\rightarrow {}^{15}\mathrm{N} + \beta^+ + \nu_e \\ {}^{17}\mathrm{F} &\rightarrow {}^{17}\mathrm{O} + \beta^+ + \nu_e \end{aligned}$$

The end-point energies are given in Table 10-3 together with those for the other reactions.

Table 10-3: Maximum energy in MeV of neutrino produced in proton burning.

[redacted]

of ^{8}B decay, the energy dependence of $P(E_\nu)$ is symmetric around the peak value at $E_\nu = E_0/2$, as shown in (a) of Fig. 10-4. On the other hand, if E_0 is comparable to m_ec^2, as, for example, in converting two protons to a deuteron, the function $P(E_\nu)$ is forward peaked, as shown in (b) of Fig. 10-4. In a log-log plot, the forward peaking appears even more pronounced, as we shall see later in Fig. 10-5.

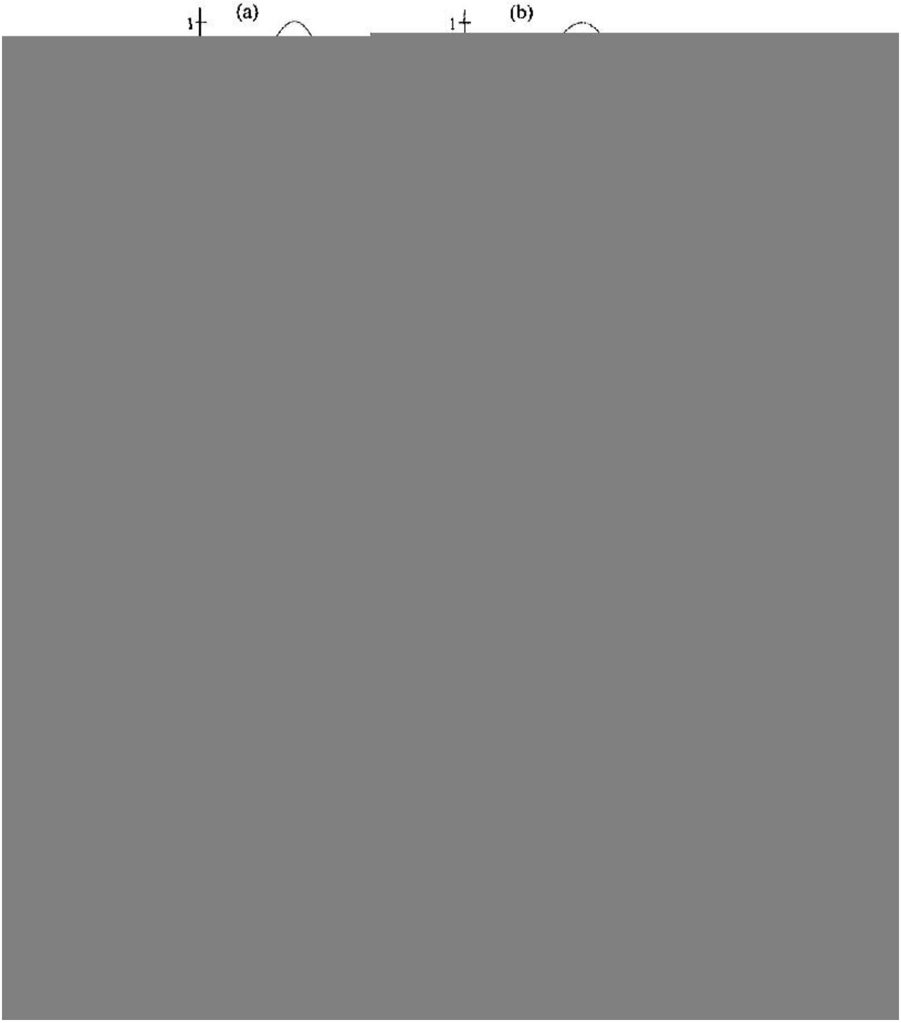

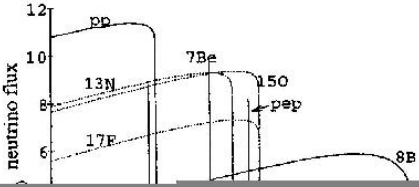

[redacted]

the inverse of that given by Eq. (10-5), is sensitive only to electron neutrinos. The reason that the type of neutrino is of interest here comes from the possibility of neutrino oscillation. We saw earlier in §5-5 that, under weak interaction, the decay products of quarks do not have definite flavor. If this happens also to neutrinos, the neutral lepton emitted in a nuclear β-decay will not be in an eigenstate either, and the observed neutrino flavor may change under suitable conditions, such as those encountered in passing through the outer layers of a star. If this does happen, some of the ν_e emitted from nuclear reactions in the interior of the sun may be transformed into ν_μ or ν_τ and

[redacted]

Two other experiments, Gallium Neutrino Observatory (GNO, more commonly known as GALLEX) and Russian-American Gallium Experiment (SAGE), make use of the reaction

$$\nu_e + {}^{71}\mathrm{Ga} \rightarrow {}^{71}\mathrm{Ge} + e^-$$

The threshold energy here is only 0.232 MeV, below the end-point energy of the *pp*-reaction common to all three PP-chains. Since each ^{4}He produced in the PP-chains involves one *pp*-reaction, the *pp*-neutrinos bear almost a direct connection with the energy produced. Such a simple relation has the advantage of making the comparison

[redacted]

independent of neutrinos, to make observations on the conditions existing in the interior of the sun, where the nuclear reactions take place. As a result, models must be constructed on the neutrino spectra we can expect using the best known physical principles and available values for the input parameters. The expected value for the ^{37}Cl measurement, obtained from the "standard solar model," is 7.9 ± 2.4 SNU [19]. The uncertainty represents very conservative estimates of the input parameters that went into the model. The discrepancy of the calculated values from the measured ones is, therefore, statistically significant and may well imply new physics. Partly for this reason, it

[redacted]

first exhausting the available fuel and then contracting to even smaller size and higher temperature (and density) until the next group of nuclear fusion reactions can take place. Since the reactions are going on at higher rates in the central part of the star, the evolution takes place on shorter time scales than the outer layers. The net result is that an onion-like structure develops, with successive inner layers of the star undergoing later and later stages of evolution. This is schematically shown in Fig. 10-6.

Triple-α process. Let us return first to the end of hydrogen burning. Gravitational contraction starts again, and both stellar temperature and density begin to rise. Conversion of ^{4}He to heavier nuclei becomes possible when the interior of a star reaches temperature $kT \sim 10$ to 20 keV and density $\rho \sim 10^5$ to 10^8 kg/m^3. This is the hydrostatic helium burning stage of a star.

From a nuclear physics perspective, there are several interesting points that merit special attention. The first is the absence of stable $A = 5$ nuclei, as we saw earlier in §10-1. Neither ^{5}He ($\tau_{1/2} = 0.7 \times 10^{-22}$ s) nor ^{5}Li ($\tau_{1/2} = 3.0 \times 10^{-22}$ s) nuclei live long

[redacted]

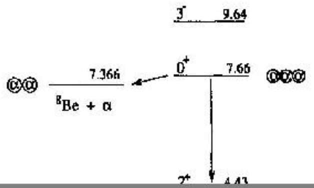
3⁻ 9.64
0⁺ 7.66
7.366
⁸Be + α
2⁺ 4.43

Figure 10-7: Low-lying energy level structure of ^{12}C and the triple-α process. (Plotted using data from Ref. [95].)

[redacted]

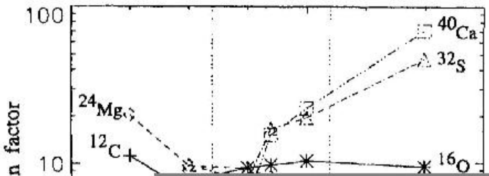

[redacted]

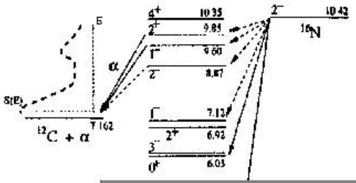
4+ 10.35
2+ 9.85
1− 9.60
2− 8.87
1− 7.12
2+ 6.92
3−
0+ 6.03
2− 10.42
16N
α
E
S(E)
7.162
12C + α

[redacted]

Recently, the uncertainty in the $\ell = 1$ part, i.e., contributions from 1^- states, has been reduced greatly using the α-decay rates from low-lying excited states of ^{16}O [15],

$$^{16}\mathrm{O}^* \rightarrow {}^4\mathrm{He} + {}^{12}\mathrm{C}$$

This is the inverse of the $^{12}\mathrm{C}(\alpha,\gamma)^{16}\mathrm{O}$ reaction. The excited states of ^{16}O are obtained from the β^--decay of ^{16}N, a radioactive nucleus ($\tau_{1/2} = 7.13$ s) that can be produced in large quantities from a radioactive beam setup. The equivalent $^{12}\mathrm{C}(\alpha,\gamma)^{16}\mathrm{O}$ cross section is obtained in this way down to ~800 keV in energy, far below the values that

[redacted]

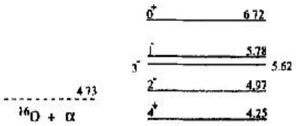
0^+
6.72
1^-
5.78
3^-
5.62
2^-
4.97
4.73
$^{16}O + \alpha$
4^+
4.25

Figure 10-10: Low-lying energy level spectrum of ^{20}Ne and $^{16}O(\alpha,\gamma)^{20}$Ne reaction. (Plotted using data from Ref. [95].)

[redacted]

10-6 Supernova and Synthesis of Heavy Nuclei

Supernovas hold a special place in nucleosynthesis because of the heavy elements they produce. Since binding energy per nucleon decreases beyond $A \sim 56$, it takes energy to create elements that are heavier. The processes we saw in previous sections are ineffective for the present purpose. Through random chance, some heavy elements are produced in the various hydrostatic processes; however, the total amounts are inconsequential. In a supernova explosion, on the other hand, a shock wave is generated

[redacted]

are a large number of electrons around, the same number as protons. The positrons that result from conversion of protons into neutrons are quickly annihilated by the surrounding electrons through the reactions

$$e^+ + e^- \rightarrow \gamma + \gamma \qquad\qquad e^+ + e^- \rightarrow \nu + \bar{\nu}$$

The former is electromagnetic and, therefore, much more likely to occur than the latter weak interaction process by a factor as high as 10^{19}. However, except at the outer layer, the γ-ray pairs produced must penetrate through a thick blank of matter before they for photodisintegration to generate substantial numbers of α-particles and nucleons. The particles produced are important, as we shall see soon, in making some of the nuclei beyond $A \sim 56$ during the rebound after the core collapse. At the same time, the energy consumed in the reactions depletes the thermal energy further.

Without counteraction by thermal pressure, the core contracts further. Since the density is already quite high at the end of silicon burning, in excess of 10^{10} kg/m^3, any further collapse results in electron capture to convert the protons, bound as well as free ones, to neutrons. The neutrinos released in the neutronization process carry energy

[redacted]

main circle in Fig. 10-3. Since the time scale is much shorter, it is possible for the ^{13}N created to capture another proton to form ^{14}O before β^+-decay to ^{14}N. Here, it rejoins the main CNO cycle again through one further proton capture to form ^{15}O. The product then β^+-decays to ^{15}N. The cycle is completed through a $^{15}\mathrm{N}(p,\alpha)^{12}\mathrm{C}$ reaction to go back to ^{12}C. Although the nuclei involved are very similar to the corresponding CNO cycle in hydrostatic hydrogen burning, the reaction rates are quite different because of the higher temperature. As a result, the production rates and, hence, the resulting relative abundances of isotopes produced are also different. For example, the observed

[redacted]

Since neutrons do not carry a net charge, we have the advantage over charged particle reactions in that we do not have the large hindrance factor at low energies due to Coulomb barrier penetration, $\exp\{-b/\sqrt{E}\}$ in Eq. (10-2). The distribution of neutron reaction rates is controlled essentially by the Maxwellian distribution for neutron thermal energy, rather than that shown in Fig. 10-2 for protons and α-particles. At the same time, the density of excited states for heavy nuclei is high, more than 10^5 MeV^{-1}. As a result, we can expect that a neutron can always be captured under the most favorable condition, such as $\ell = 0$, unlike the situation we saw earlier for ^{4}He

[redacted]

burning shell is 10^{10} kg m^{-3}. This is equivalent to a baryon density on the order of $10^{10}/(1.67 \times 10^{-27}) \sim 10^{37}$ m^{-3}. If we have one free neutron for every 10^9 bound nucleons, equivalent to about 1 for every 10^7 nuclei, we reach the required density for the r-process to take place.

There are several sources for free neutrons. One of these is photodisintegration at the silicon burning stage. The bulk, however, comes (indirectly) from α-capture by carbon, nitrogen and oxygen in the CNO cycle, as shown in Fig. 10-3. For example, α-capture by ^{14}N followed by β^+-decay through the reactions

[redacted]

Problems

10-1. What is the gravitational energy released when noninteracting particles with a total mass 1.99×10^{30} kg collapse from an infinite distance of separation to a spherical ball of radius 6.96×10^{8} m? Assuming an ideal gas equation of state, what is the temperature of this sphere? Compare the result with the value of 15×10^{6} K for the interior of our sun.

10-2. Show that the maximum amount of energy released in the form of electromagnetic

[redacted]

(b) A neutron star is one of the possible remanents of a supernova explosion such as SN 1987a, the one which took place in the Large Magellanic Cloud 160,000 light years away and was first observed on earth on February 24, 1987. When the core of a large star exhausts its nuclear fuel, there is no longer the thermal pressure to counterbalance the gravitational force, and the core of the star collapses. For simplicity, we can consider that all the material in the core of the collapsing star is in the form of ^{56}Ni made of 28 neutrons and 28 protons. Because of the tremendous gravitational force, the

[redacted]

Chapter 11

Nuclear Physics: Present and Future

Radioactive beam. Many laboratories around the world are starting to have facilities for producing beams of radioactive nuclei. We have seen that a large part of our knowledge on nuclear physics, and subatomic physics in general, comes from collisions between two particles. With radioactive beams, our horizon is extended to include projectiles made of nuclei that are unstable. Many of these reactions are important by their own right. For example, interactions with unstable nuclei form an integral part of the events going on in stars, such as that we saw in the case of the triple-α process in §10-5. Better knowledge of their reaction rates are essential to improve our

[redacted]

physics under such extreme conditions.

The construction of detectors and data acquisition systems for the complicated events expected from these experiments present new challenges to our ingenuity. To leave room for discovering the unexpected, one must record as much information of the collision as possible so that one can analyze the results for phenomena not necessarily expected in the original design. For this reason, detectors are also built to make comprehensive studies of all the particles produced in each collision. Once these facilities are in operation, we can expect a new burst of information that will keep both

[redacted]

ties for heavier nuclei. We have seen earlier in §4-7 that the question of mesonic current is essential to understand how the electromagnetic operators are modified when nucleons are embedded in nuclei. More generally, the question of "medium" effect—how certain operators are modified when nucleons are bound—is important in understanding nuclear properties. Many aspects of such studies are ideally suited for the high precision that can be reached using electron scattering.

Improvement in the precision of experiments involving particles other than electrons, such as protons and neutrons, are also expected to come with technological

[redacted]

particle known in the early part of the 1930s with a mass of $\sim 200 m_e$ was the muon. As we know now, the muon cannot be the candidate, as it is not a hadron. Furthermore, it is a fermion and therefore cannot be absorbed and emitted freely as bosons can.

Even though the energies we have achieved in the laboratory are quite impressive, they do not compare with those associated with some of the highest energy particles observed from extra-terrestrial sources. Cosmic rays and γ-bursts have been recorded to reach energies many orders of magnitude higher than what we can hope to achieve in the laboratory in the foreseeable future. Both the production mechanism of these

[redacted]

has two components, one with spin pointing up and the other with spin down. In the more general Dirac picture, the corresponding wave function has four components, two for the particle and two for the antiparticle. The four-component Dirac equation may be expressed as a set of two coupled equations, each one having only two components. At nonrelativistic energies, the coupling between the "upper" two components and the "lower" two components may be replaced by a spin-orbit term and the two equations decouple from each other in this approximation.

Traditionally, nuclear structure problems are solved by following the time-honored

[redacted]

Fundamental problems in physics. There are several fundamental questions in physics that involve atomic nuclei. The solar neutrino problem described in §10-4 is a good example. It cuts across several disciplines, particle physics, cosmology, hydrodynamics, just to name a few. In addition to the intrinsic interest in the problem itself, it has the potential of pointing the way to new physics, such as neutrino oscillation. Nuclear physics enters in understanding the processes that produce the particles and in interpreting the measured results. The importance of the problem cannot be understated. This is especially true in view of the great expectation we have in neutrino

[redacted]

Appendix A

Parity and Angular Momentum

[redacted]

In terms of spherical polar coordinates, the radial distance r is not affected by a parity transformation. The only changes are in the angular variables,

$$(r,\theta,\phi) \xrightarrow[P]{} (r,\pi-\theta,\pi+\phi) \tag{A-2}$$

This relation can be shown to be identical as that in Eq. (A-1), for example, by transforming both sides to Cartesian coordinate systems. Because of Eq. (A-2), radial wave functions are not changed by a parity transformation. As a result, the parity of a wave function of a state is given by the angular part alone. For a state $\Psi(\boldsymbol{r})$ with definite

[redacted]

Before the reaction, the total angular momentum J of the π-mesic atom is 1, as the intrinsic spin of the pion is 0 (see also §2-7), the spin of the deuteron is 1 (see §3-1), and the orbital angular momentum of the πd-system is 0 (the π^- is in the atomic s-state). Total angular momentum is conserved in the reaction of Eq. (A-4) and, as a result, the final state produced by the reaction must also have $J = 1$.

The two neutrons in the final state, being identical fermions, must be in an antisymmetric state to satisfy the Pauli principle. The symmetry of the wave function of the two-neutron system is determined by L, the relative orbital angular momentum,

[redacted]

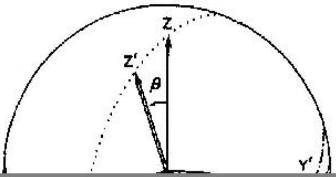

Figure A-1: Rotation of the coordinate axes from (X, Y, Z) to (X', Y', Z') by Euler angles (α, β, γ) in three steps. First, a rotation around the Z-axis through angle α brings (X, Y, Z) to (X_1, Y_1, Z).

[redacted]

between components M and M' of a spherical tensor of rank J. The orthogonality relation among the $\mathcal{D}$-functions is given by

$$\sum_{M'}(\mathcal{D}^J_{M'N}(\alpha,\beta,\gamma))^*\mathcal{D}^J_{M'M}(\alpha,\beta,\gamma)=\sum_{M'}\mathcal{D}^J_{MM'}(\alpha,\beta,\gamma)(\mathcal{D}^J_{NM'}(\alpha,\beta,\gamma))^*=\delta_{MN}$$

and

$$\int_0^{2\pi}\int_0^{2\pi}\int_0^{\pi}(\mathcal{D}^{J'}_{M'M}(\alpha,\beta,\gamma))^*\mathcal{D}^J_{N'N}(\alpha,\beta,\gamma)\sin\beta\,d\beta\,d\alpha\,d\gamma=\frac{8\pi^2}{2J+1}\delta_{M'N'}\delta_{MN}\delta_{J'J}$$

[redacted]

that transforms under a rotation of the coordinate axes in the same way as given by Eq. (A-6) and is, therefore, a proper tensor. It should be pointed out that the phase factor $(-1)^q$ in Eq. (A-9) is unique but the factor $(-1)^k$ is somewhat arbitrary. There are also other conventions found in the literature. The one adopted here has the advantage that it is convenient for tensors of half-integer rank, for example, like those used in Eqs. (2-26) and (2-27).

In problems where spherical symmetry is important, such as those commonly encountered in subatomic physics, spherical tensors are useful for a variety of reasons. Some technical advantages of using spherical tensors are related to the algebra of an-

[redacted]

It is often more convenient to express the coupling coefficients between two spherical tensors in terms of Wigner $3j$-symbols, related to the Clebsch-Gordan coefficients by a simple factor,

$$\begin{pmatrix} j_1 & j_2 & j_3 \\ m_1 & m_2 & m_3 \end{pmatrix} = \frac{(-1)^{j_1-j_2-m_3}}{\sqrt{2j_3+1}} (j_1 m_1 j_2 m_2 | j_3 -m_3)$$

In terms of $3j$-symbols, the symmetry in the arguments of the coupling coefficient may be expressed as

$$\begin{pmatrix} j_1 & j_2 & j_3 \\ m_1 & m_2 & m_3 \end{pmatrix} = \begin{pmatrix} j_2 & j_3 & j_1 \\ m_2 & m_3 & m_1 \end{pmatrix} = \begin{pmatrix} j_3 & j_1 & j_2 \\ m_3 & m_1 & m_2 \end{pmatrix}$$

[redacted]

Table A-1: Some useful Clebsch-Gordan coefficients.

$(\frac{1}{2}m_s,\ell m_\ell|jm)$

j	$m_s=+\frac{1}{2}$	$m_s=-\frac{1}{2}$

[redacted]

A-4 Racah Coefficient and 9j-Symbol

When three spherical tensors R_{j_1}, S_{j_2}, and T_{j_3} are coupled together, the final rank J alone is not adequate to specify the product uniquely. In order to distinguish between the different possibilities, an intermediate rank specifying the coupling between two of the three tensors is used. There are two equivalent ways to construct this intermediate coupling. One is to couple the first two tensors R_{j_1} and S_{j_2} together to rank J_{12} and then couple the product to T_{j_3} to obtain the final rank J. The angular momentum structure

[redacted]

couplings are related to each other through 9j-symbols,

$$
\begin{aligned}
&((R_{j_1} \times S_{j_2})_{J_{12}} \times (T_{j_3} \times U_{j_4})_{J_{34}})_J \\
&\quad = \sum_{J_{13} J_{24}} \sqrt{(2J_{12}+1)(2J_{34}+1)(2J_{13}+1)(2J_{24}+1)} \\
&\qquad \times \left\{ \begin{matrix} j_1 & j_2 & J_{12} \\ j_3 & j_4 & J_{34} \end{matrix} \right\} ((R_{j_1} \times T_{j_3})_{J_{13}} \times (S_{j_2} \times U_{j_4})_{J_{24}})_J
\end{aligned}
$$

[redacted]

matrix element is independent of the projections and, as a result, is only a function of the nature of the operator and the states involved. That is,

$$\langle JM|T_{kq}|J'M'\rangle = (-1)^{J-M}\begin{pmatrix} J & k & J' \\ -M & q & M' \end{pmatrix}\langle J\|T_k\|J'\rangle \tag{A-15}$$

where the double-bar matrix element $\langle J\|T_k\|J'\rangle$ represents the invariant part and is generally known as the *reduced matrix element.* The angular momentum dependence of the matrix element is contained in the $3j$-coefficients and is independent of the

[redacted]

We can check that this is the same as scalar products defined in terms of Cartesian components of the vectors by noting that

$$\begin{aligned} \boldsymbol{J}_{\pm 1} &= \mp \frac{1}{\sqrt{2}}(\boldsymbol{J}_x \pm i\boldsymbol{J}_y) \qquad\qquad \boldsymbol{J}_0 = \boldsymbol{J}_z \\ \boldsymbol{V}_{\pm 1} &= \mp \frac{1}{\sqrt{2}}(\boldsymbol{V}_x \pm i\boldsymbol{V}_y) \qquad\qquad \boldsymbol{V}_0 = \boldsymbol{V}_z \end{aligned}$$

This is slightly different from the definition of angular momentum raising and lowering

[redacted]

Appendix B
Scattering by a Central Potential

B-1 Scattering Amplitude and Cross Section

[redacted]

The relation between wave function and intensity of the incident beam is given by the quantum-mechanical probability current density

$$S(\boldsymbol{r},t) = \frac{\hbar}{2i\mu}\left\{\psi^*\nabla\psi - \psi\nabla\psi^*\right\} = \Re\Big\{\psi^*\frac{\hbar}{i\mu}\nabla\psi\Big\}$$

where $\Re$ stands for the real part. For an incident plane wave traveling along the positive z-direction, the number of particles passing through a unit area perpendicular to the z-axis is then

[redacted]

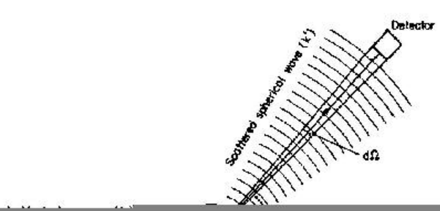
Detector
Scattered spherical wave (k')
dΩ

[redacted]

The differential scattering cross section, $d\sigma/d\Omega$, sometimes represented also as $\sigma(\theta)$, is defined as the number of particles scattered into a solid angle $d\Omega$ at angle θ divided by the incident flux,

$$\frac{d\sigma}{d\Omega} = \frac{S_r r^2}{S_i} = |f(\theta)|^2 \tag{B-7}$$

As we have seen in §1-3, it has the dimension of an area and gives a measure of the probability of scattering into a particular direction.

The scattering cross section is the integral of the differential cross section over all

[redacted]

For short-range potentials, $V(r)$ goes to zero as $r \to \infty$. The same is also true for the $\ell(\ell+1)/r^2$ term. In the asymptotic regions, we are left with a simple second-order differential equation of the form

$$\frac{d^2u_\ell(r)}{dr^2} + k^2u_\ell(r) = 0$$

The solution for this equation is the familiar linear combination of $\sin(kr)$ and $\cos(kr)$. That is, at large r, the function $u_\ell(r)$ must take on the form we have implicitly assumed here, only elastic scattering can take place. Furthermore, if the potential is also a central one, orbital angular momentum ℓ is a good quantum number and the probability current density in each ℓ-partial wave *channel* is conserved. The only thing in the wave function that can change as a result of scattering is the phase angle, and this is represented by the phase shift δ_ℓ. We shall return at the end of this section with an example using a square-well potential as illustration.

In general, elastic as well as inelastic scattering can take place. Such a situation is represented by a complex scattering potential, with the imaginary part representing loss of probability from the incident channel due to such inelastic events as excitation

$$= \frac{\sqrt{4\pi}}{k}\sum_{\ell=0}^{\infty}\sqrt{2\ell+1}\,e^{i\delta_\ell}\sin\delta_\ell Y_{\ell 0}(\theta) \tag{B-16}$$

In terms of the phase shifts, the differential scattering cross section may be written as

$$\frac{d\sigma}{d\Omega} = \frac{4\pi}{k^2}\left|\sum_{\ell=0}^{\infty}\sqrt{2\ell+1}\,e^{i\delta_\ell}\sin\delta_\ell Y_{\ell 0}(\theta)\right|^2 \tag{B-17}$$

by substituting the results of Eq. (B-16) into (B-7).

[redacted]

When $r \to \infty$, the spherical Bessel function $j_\ell(\rho) \to \rho^{-1}\sin(\rho - \frac{1}{2}\ell\pi)$, as we have seen earlier, and we obtain the results

$$f_\ell(\rho) \to \sin(\rho - \tfrac{1}{2}\ell\pi) \qquad \frac{df_\ell}{d\rho} \to \cos(\rho - \tfrac{1}{2}\ell\pi)$$

and

$$u_\ell(\rho) \to \sin(\rho - \tfrac{1}{2}\ell\pi + \delta_\ell) \qquad \frac{du_\ell}{d\rho} \to \cos(\rho - \tfrac{1}{2}\ell\pi + \delta_\ell)$$

The quantity within the curly brackets in Eq. (B-22) becomes

[redacted]

Consequently,

$$\delta_\ell \xrightarrow[\ell\to\infty]{} 0$$

We shall now establish a criterion by which ℓ may be considered as large enough such that phase shifts may be ignored for partial waves of order greater than this value.

Let the range of the potential $V(r)$ be represented by r_0. At low energies, the classical turning radius r_1 is large and we have $r_0 < r_1$. We may therefore ignore the contribution of $V(r_t)$ in the definition of the turning radius. Equation (B-25) can now be approximated by the expression

[redacted]

where

$$\kappa = \frac{1}{\hbar}\sqrt{2\mu(E+V_0)}$$

The amplitude $\mathcal{A}$ will be determined later. For a repulsive well, V_0 is a negative quantity. In this case κ becomes purely imaginary for $E < |V_0|$, and instead of a sine function, the radial wave function inside the well is a hyperbolic sine function.

Outside the well, $V(r) = 0$, and the radial wave function is sinusoidal for both attractive and repulsive wells,

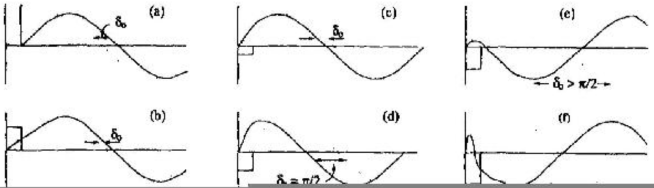
(a)
δ_0
(c)
δ_0
(e)
$\delta_0 > \pi/2$
(b)
δ_0
(d)
(f)

[redacted]

interaction, and $a < 0$ if there is no bound state, as for example in the case of isovector ($T = 1$) nucleon-nucleon interaction.

Effective range. The energy dependence of scattering at low energies is given by the *effective range* r_e. The origin of this parameter comes from the following rationale. For $\ell = 0$, Eq. (B-9) may be written as

$$\frac{d^2u_0(k,r)}{dr^2} - \left\{\frac{2\mu}{\hbar^2}V(r) - k^2\right\}u_0(k,r) = 0 \tag{B-29}$$

[redacted]

If the potential has a short range, Eqs. (B-29) and (B-32) are identical to each other in the asymptotic region. As a result, we may require that their solutions have the same form at $r = \infty$,

$$v_0(k,r) \underset{r\to\infty}{=} u_0(k,r) \underset{r\to\infty}{=} \mathcal{A}\sin(kr+\delta_0) \tag{B-34}$$

where the amplitude $\mathcal{A}$ will be determined later. Since the radial wave function $R_0(r)$ itself must be finite at the origin,

$$u_0(k,r) \xrightarrow[r\to 0]{} 0$$

[redacted]

The energy dependence of the s-wave phase shift can now be expressed in the form

$$k\cot\delta_0(k) = (k\cot\delta_0)_{k=0} + \tfrac{1}{2}r_e k^2 + \cdots \tag{B-37}$$

Using the definition of scattering length a in Eq. (B-28), the first term on the right-hand side of Eq. (B-37) can be shown to be equal to $-1/a$. Up to order k^2, we find

$$k\cot\delta_0(k) = -\frac{1}{a} + \frac{1}{2}r_e k^2$$

One way to see the difference between scattering by a real and a complex potential is to examine the intensities of the incoming and outgoing waves for partial wave ℓ. Using the last form of Eq. (B-10), we obtain the difference as

$$1 - |\eta_\ell|^2 = 1 - |e^{2i\delta_\ell}|^2$$

If the phase shift δ_ℓ is real, the difference vanishes and only elastic scattering can take place. For a complex phase shift, the difference does not vanish in general, as some of the incident flux is transferred to channels other than the incident one. This part of the scattering is represented by the "reaction" cross section

[redacted]

shall use a single letter, c, the channel quantum number, to represent the complete set of labels,

$$c \equiv \{j_p\alpha_p, j_t\alpha_t; \gamma\mu : \ell m\}$$

where ℓ is the relative angular momentum and m is its projection on the quantization axis. The wave function of the projectile (or scattered particle) is represented by $\phi_{j_p\alpha_p}$, where j_p is the spin and α_p represents all the other quantum numbers required to specify the state for the projectile (or the scattered particle). The wave function of the target (or the residual) nucleus is given by $\psi_{j_t\alpha_t}$, where j_t is the spin and α_t represents all the

[redacted]

be obtained using the appropriate boundary condition for the outgoing wave and that in channel c for the incoming wave. We shall return to the topic of the s-matrix in the final section of this Appendix.

The general solution of the Schrödinger equation (B-3) outside the range of scattering potential V is a linear combination of those given in Eq. (B-44),

$$\Psi(r) = \sum_c C_c\Big\{\mathcal{I}_c(r) - \sum_{c'} S_{c'c}\mathcal{O}_{c'}(r)\Big\} \tag{B-45}$$

[redacted]

except that elements of the *s*-matrix between incident and final scattering states are used to replace the phase shifts. The summation over ℓ', the orbital angular momentum in the outgoing channel, is required since in a scattering experiment only the states of the scattered particle and the residual nucleus are observed and their relative angular momentum ℓ' is not usually identified. On integrating over the angles, we obtain the scattering cross section as

$$\sigma_{\gamma\mu\alpha;\gamma'\mu'\beta} = \frac{\pi}{k^2}\sum_{\ell}(2\ell+1)\left|S_{c'(\ell\gamma'\mu'\beta)\,c(\ell,m=0,\gamma\mu\alpha)}\right|^2 \tag{B-47}$$

[redacted]

where the factor inside the square brackets converts the expression from cgs to SI units. Since the range of this potential is infinite, the techniques employed in §B-2 to find the scattering solution no longer apply. This is not a problem, as exact solutions are available (see, e.g., Messiah [104], Morse and Feshbach [106], and Blatt and Weisskopf [32]). A short summary of the results is given here.

For scattering involving only Coulomb potential, the Schrödinger equation can be written as

$$\left\{\nabla^2 + k^2 - \frac{2\gamma k}{r}\right\}\psi_c(r) = 0 \qquad \text{(B-49)}$$

[redacted]

we obtain the result

$$|\psi_c(0)|^2 = \frac{2\pi\gamma}{e^{2\pi\gamma} - 1} \tag{B-50}$$

This gives the Fermi function $F(Z, E_e)$ of Eq. (5-67) for nuclear β-decay in the limit that the charge distribution in the daughter nucleus can be considered to be concentrated at a point located at the origin.

For scattering, we are more concerned with the asymptotic behavior of the wave function. As in Eq. (B-5), we need the values at large distances away from the origin and expressed as a sum of incident wave $\psi_i(\boldsymbol{r})$ and scattered wave $\psi_s(\boldsymbol{r})$,

[redacted]

However, for scattering problems, it is more convenient to use

$$u_\ell^c(r) = e^{i\delta_\ell^c} F_\ell(\gamma, \rho) \tag{B-51}$$

where

$$\delta_\ell^c = \arg \Gamma(\ell + 1 + i\gamma)$$

is the Coulomb phase shift for partial wave ℓ.

Asymptotically, the Coulomb wave function has the properties

[redacted]

The eigenfunction of the scattering equation is the solution of the equation

$$(H_0 - E)\psi_{\boldsymbol{k}}^{\pm}(\boldsymbol{r}) = -V\psi_{\boldsymbol{k}}^{\pm}(\boldsymbol{r}) \tag{B-54}$$

where the superscript + on $\psi_{\boldsymbol{k}}(\boldsymbol{r})$ indicates that the solution satisfies *outgoing* boundary conditions and the superscript − refers to *incoming* boundary conditions. Our concern will be mainly with the former. The subscript $\boldsymbol{k}$, with magnitude $k = \sqrt{2\mu E}/\hbar$, displays the explicit dependence of the solution on energy.

The solution of the homogeneous equation

[redacted]

inside the integral without changing the final result. Furthermore, since $\boldsymbol{r}$ appears only in $G(\boldsymbol{r},\boldsymbol{r}')$, we obtain, using Eq. (B-57), the result

$$(H_0 - E)\psi_{\boldsymbol{k}}^{+}(\boldsymbol{r}) = -\int \delta(\boldsymbol{r}-\boldsymbol{r}')V(\boldsymbol{r}')\psi_{\boldsymbol{k}}^{+}(\boldsymbol{r}')\,d\boldsymbol{r}' = -V(\boldsymbol{r})\psi_{\boldsymbol{k}}^{+}(\boldsymbol{r})$$

the same equality given in Eq. (B-54).

Scattering amplitude. It is easy to see how the scattering amplitude may be obtained

[redacted]

In terms of H_0 and E, the Green's function operator G^+ may be expressed as

$$G^+ = \lim_{\epsilon \to 0} \frac{1}{E - H_0 + i\epsilon} \tag{B-62}$$

where the factor $+i\epsilon$, with ϵ as some small positive quantity, is required to ensure that the operator corresponds to the outgoing boundary condition. The derivation of Eq. (B-62) may be found in quantum mechanics texts such as Merzbacher [103], Messiah [104], and Schiff [125].

Using the series expansion of ψ_k^+ given in Eq. (B-63), we can write the elements of the t-matrix as

$$\langle\phi_{k'}|t|\phi_k\rangle = \langle\phi_{k'}|V(1+\sum_{n=1}^{\infty}(G^+V)^n)|\phi_k\rangle$$

Since the equality holds for arbitrary ϕ_k and $\phi_{k'}$, we obtain a relation between the operators involved,

$$t = V(1+\sum_{n=1}^{\infty}(G^+V)^n)$$

[redacted]

As a result, the time development of a state in the interaction representation is given by the equation

$$i\hbar\frac{\partial}{\partial t}\Psi(t) = H_I(t)\Psi(t)$$

as can be seen by substituting the inverse of Eq. (B-66) into (B-65). For many purposes, such an approach can be simpler than working in the Schrödinger representation, especially if H_I is only a small part of the complete Hamiltonian.

We can now define the time development operator $U(t_0, t)$ that takes a state from

[redacted]

Bibliography

[1] S. Åberg, H. Flocard, and W. Nazarewicz. Nuclear shapes in mean field theory. *Ann. Rev. Nucl. Part. Sci.*, 40:439, 1990.

[2] M. Abramowitz and I.A. Stegun, editors. *Handbook of Mathematical Functions.* Dover, New York, 1965.

[3] M.C. Abreu et al. Production of $\rho+\omega$ and ϕ in $p-$W and S$-$U collisions at 200 [redacted]

[15] R. Azuma et al. Constraints on the low-energy $E1$ cross section of $^{12}\mathrm{C}(\alpha,\gamma)^{16}\mathrm{O}$ from the β-delayed α spectrum of $^{16}\mathrm{N}$. *Phys. Rev. C*, 50:1194, 1994.

[16] H.W. Baer et al. Isobaric-analogue-state transitions in pion charge-exchange reactions above the $\Delta(1232)$ resonance. In R.J. Peterson and D.D. Strottman, editors, *Pion-Nucleus Physics*, volume 163 of *AIP Conf. Proc.*, page 67. American Institute of Physics, New York, 1987.

[17] C. Baglin et al. J/ψ and muon-pair cross-sections in proton-nucleus and nucleus-

[redacted]

[32] J.M. Blatt and V.F. Weisskopf. *Theoretical Nuclear Physics.* Wiley, New York, 1952.

[33] R.J. Blin-Stoyle. *Fundamental Interactions and the Nucleus.* North-Holland, Amsterdam, 1973.

[34] A. Bohr and B.R. Mottelson. *Nuclear Structure*, volume I. Benjamin, New York, 1969.

[redacted]

[49] A. de Shalit and H. Feshbach. *Theoretical Nuclear Physics.* Wiley, New York, 1974.

[50] A. de Shalit and I. Talmi. *Nuclear Shell Theory.* Academic Press, New York, 1963.

[51] H. de Vries, C.W. de Jager, and C. de Vries. Nuclear charge-density-distribution parameters from elastic electron scattering. *Atom. Data Nucl. Data Tables*, 36:495, 1987.

[redacted]

[66] D. Frekers et al. Elastic and inelastic scattering of 362 MeV polarized protons from ^{40}Ca. *Phys. Rev. C*, 35:2236, 1987.

[67] B. Frois et al. High momentum-transfer electron scattering from ^{208}Pb. *Phys. Rev. Lett.*, 38:152, 1977.

[68] R.F. Frosch et al. Electron scattering studies of calcium and titanium isotopes. *Phys. Rev.*, 174:1380, 1968.

[redacted]

[82] W. Hauser and H. Feshbach. The inelastic scattering of neutrons. *Phys. Rev.*, 87:366, 1952.

[83] K. Hikasa et al. Review of particle properties. *Phys. Rev. D*, 45:S1, 1992.

[84] S. Hofmann et al. The new element 112. *Z. Phys. A*, 354:229, 1996.

[85] R. Hofstadter and R. Herman. Electric and magnetic structure of the proton and neutron. *Phys. Rev. Lett.*, 6:293, 1961.

[redacted]

[99] V.A. Lubimov et al. An estimate of the ν_e mass from the β-spectrum of tritium in the valine molecule. *Phys. Lett. B*, 94:266, 1980.

[100] R Machleidt. The meson theory of nuclear forces and nuclear matter. In M.B. Johnson and A. Picklesimer, editors, *Relativistic Dynamics and Quark-Nuclear Physics*. Wiley, New York, 1986.

[101] R. Machleidt, K. Holinde, and Ch. Elster. The Bonn meson-exchange model for the nucleon-nucleon interaction. *Phys. Rep.*, 149:1, 1987.

[redacted]

[117] W. Reuter, F.K. Merle, and H. Miska. Nuclear charge distribution and rms radius of ^{12}C from absolute elastic electron scattering measurements. *Phys. Rev. C*, 26:806, 1982.

[118] M. Rho and G.E. Brown. The role of chiral invariance in nuclei. *Comments Nucl. Part. Phys.*, 10:201, 1981.

[119] P. Ring and P. Schuck. *The Nuclear Many-Body Problem.* Springer-Verlag, New York, 1980.

[redacted]

[134] V.M. Strutinsky. Influence of nucleon shells on the energy of a nucleus. *Soviet J. Nucl. Phys.*, 3:449, 1966.

[135] W. Thomè et al. Charged particle multiplicity distributions in pp collisions at ISR energies. *Nucl. Phys. B*, 129:365, 1977.

[136] D.R. Tilley, H.R. Weller, and C.M. Cheves. Energy levels of light nuclei $A = 16 - 17$. *Nucl. Phys. A*, 564:1, 1993.

[redacted]

[149] D. Wilkinson. Fundamental symmetries. *J. Phys. Soc. Jpn.*, 55 (Suppl.):347, 1986.

[150] C.Y. Wong. *Introduction to High-Energy Heavy-Ion Collisions*. World Scientific, Singapore, 1994.

[151] S.S.M. Wong. *Nuclear Statistical Spectroscopy*. Oxford University Press, New York, 1986.

[redacted]

Index

* (excited state), 16
3j-symbol, 403
6j-symbol, 405
9j-symbol, 406

actinide series, 244
action, 344
active

[redacted]

  independent particle, 254
  interacting boson, 229–233
  long-wavelength, 172
  random-phase, 271
Argand diagram, 89
astrophysical S-factor, 361
asymmetric fission, 151

big-bang nucleosynthesis, 356–357
binary fission, 151
binding energy, 9
    per nucleon, 10, 155
black hole, 381
Bohr radius, 120
Bonn potential, 98
Born approximation, 286–291, 303
Bose-Einstein statistics, 27
    exchange reaction, 215, 303, 306, 313–314
    form factor, 105, 269
    independence, 72, 81
    number, 29
    radius, 109–111
    symmetry breaking, 72
charged particle capture, 384

[redacted]

core
    collapse, 382
    state, 254
Coriolis force, 228
correlation, two-particle, 351
correspondence principle, 323
Coulomb
    barrier, 361

[redacted]

    electromagnetic, *see* electromagnetic
        transition
    Fermi, 192, 215
    forbidden, 192, 200
    Gamow-Teller, 192
    neutron β^-, 23, 181–183, 356
    quark, weak, 183
    superallowed, 199

direct
    reaction, 286–291, 303
    scattering amplitude, 306
distorted wave Born approximation (DWBA), 291, 303
(d, n) reaction, 290, 315
doorway state, 285
double
    β-decay, 202
    -charge exchange reactions, 314
    transition, 168–181, 306
        quadrupole, 210, 225, 269
        rotational model, 225
        selection rule, 175–177
        vibrational model, 210
electron, 22
    capture, 189, 356, 363, 367
    scattering, 105–120, 391
elementary particle, 21
EMC (European Muon Collaboration)

[redacted]

  diagrams, 96
  path integral, 344
final state interaction, 93
fission, 10, 150–154, 211
  asymmetric, 151
  barrier, 152
  binary, 151
  induced, 151
  isomer, 154
  spontaneous, 150

giant
  dipole resonances, 213
  Gamow-Teller resonance, 215
  resonance, 212 218
Goldberger-Trieman relation, 188
Goldhaber-Teller model, 213
gravitational contraction, 381
grazing collision, 321
Green's function, 286, 430
ground state

[redacted]

  burning, 359, 373–376
($(^3\text{He},t)$)-reaction, 201
hep process, 367
Hermitian conjugate, 401
hexadecapole moment, 127
high-energy nuclear physics, 38, 119
high-spin state, 17, 323, 326–340
Hilbert space, 236, 258
Hill-Wheeler variable, 220
homogeneous equation, 430

intermediate-energy
  nucleon-nucleus scattering, 303–308
  proton scattering, 123
internal
  conversion, 168, 177
  pair
    creation, 168
    production, 177
intraband transition, 225, 226
intrinsic

[redacted]

kaon, 315
    factory, 392
Kelson-Garvey mass formula, 141–143
kinematical moment of inertia, 332
Klein-Gordon equation, 79
K^+-meson, 25, 35, 36, 42, 185
Kronecker delta, 401
Kurie plot, 194

Λ-particle, 36

Majorana
    fermion, 202
    particle, 24
major shell, 240
mass, 10
    defect, 18
    excess, 18
master equation, 324
matrix
    diagonalization, 237

[redacted]

- dynamic, 331
- kinematical, 332
- static, 332

momentum
- dependence, 103
- transfer, 107, 108, 116, 288

$M1$-transitions, 226

Monte Carlo
- calculation, 345
- technique, 394

- -neutron scattering, 80
- number, 7
- prompt, 151
- -proton mass difference, 138
- -rich nucleus, 318, 384
- star, 381, 382
- target, 80
- wave function, 27

neutronization, 383

Nilsson

[redacted]

^{5}B, 357
^{8}B, 363
^{142}Ba, 151
^{7}Be, 190
^{8}Be, 159, 272, 364, 375
^{209}Bi, 273, 324, 325
^{212}Bi, 150
^{82}Br, 202
^{12}C, 18, 160, 204, 269, 304, 312, 364, 365, 375
^{14}C, 313
^{16}C, 138, 139, 159
^{170}Hf, 223
^{180}Hg, 317
^{39}K, 273
^{82}Kr, 202, 203
^{92}Kr, 151
^{5}Li, 273, 375
^{6}Li, 312
^{7}Li, 80, 190
^{24}Mg, 272
^{25}Mg, 233, 273
^{26}Mg, 204
^{12}N, 160, 204

[redacted]

^{41}Sc, 273
^{46}Sc, 16
^{82}Se, 202, 203
^{28}Si, 218
^{152}Sm, 187
^{120,121}Sn, 315
^{132}Sn, 318
^{226}Th, 164
^{48}Ti, 119

  odd-mass, 132, 133, 227, 255
  odd-odd, 133, 134
  proton-rich, 318, 386
  spherical, 65, 218
  superheavy, 244, 318
numerical
  integration, 345
  simulations, 271

[redacted]

-orbit, 76
tensor, 71
time development, 433, 434
two-body spin-orbit, 77
optical
model, 291–303
formal derivation, 292–295
microscopic, 298–302
phenomenological, 295–298

[redacted]

exclusion principle, 38, 44, 60, 90, 96, 99, 155, 399
form factor, 113
matrix, 29, 69
PCAC, 188
pd-scattering, 80
pep process, 367
permutation, 76
operator, 44

  Bonn, 98
  central, 83
  complex, 88, 422
  Coulomb, 79, 426
  density-dependent, 300
  double-hump, 154
  effective, 416
  energy surface, 340
  harmonic oscillator, 102, 240
  nonlocal, 295, 301

[redacted]

QCD, *see* quantum chromodynamics
QGP, *see* quark-gluon plasma
quadratic spin-orbit operator, 76, 78
quadrupole
  interaction, 229
  moment, 224
  transition, 210, 225, 269
  vibration, 207, 232, 267
quantum
  chromodynamics (QCD), 2, 5, 21,

nonresonant, 360–362
(n, p), 303
nuclear, 6
(p, γ), 363, 364
pickup, 17, 286
(p, n), 303
(p, p'), 303
stripping, 17, 286
red giant, 359
reduced

scattering, 428

s
-matrix, 424, 433
operator, 434
-process, 385
Sachs form factor, 113
sampling, 345
saturation
density, 155

[redacted]

    -deuteron, 80
    -proton, 80, 84, 346
  quasi-elastic, 115
  Rutherford, 428
  shape-elastic, 284
Schmidt values, 131
Schrödinger
  equation, 68, 79, 82, 147, 166, 409, 422, 427
  representation, 433

singlet scattering length, 92
Slater determinant, 237
soft pion, 391
solar neutrino problem, 372
Sommerfeld number, 149, 275, 361
space reflection, 397
spectroscopic notation, 245
spherical
  Bessel function, 83, 111, 172, 289, 290, 413, 415

[redacted]

strong interaction, 341
structure function, 116–119
SU_3, 232
    (flavor), 41, 43
Sudbury Neutrino Observatory (SNO), 370
SU_4 symmetry, 11
sum rule, 214
Super

[redacted]

    Fermi distribution, 112, 119
    Gaussian distribution, 112
time
  -dependent
    Hamiltonian, 165
    Hartree-Fock, 325
    perturbation theory, 165–168
    Schrödinger equation, 165

        correlation, 202, 351
        matrix element, 262–267
        spin-orbit operator, 76, 77
    -centered shell model, 272
    -component wave function, 187
    -nucleon system, 57
    -parameter Fermi form, 112, 295
    -particle interferometry, 351

u (atomic mass unit), 18

        universal, 182–187
Weisskopf estimates, 178
Weizacker mass formula, 139–141, 152
Wentzel-Kramers-Brillouin (WKB) method, 148
width, 18, 162, 323
Wigner
    -Eckart theorem, 126, 164, 406
    supermultiplet, 11
Woods-Saxon form, 12, 112, 295

[redacted]